

The University of New South Wales  
School of Mechanical and Manufacturing Engineering

**IN-ORBIT THERMAL ANALYSIS OF BLUEsat**

By

Scott Hansman

Bachelor of Engineering (Aerospace)

Supervisors:      Mr J. Page

Prof. D. W. Kelly

**November 7, 2003**

## Abstract

### Abstract

**BLUESat (Basic Low Earth Orbit UNSW Experimental satellite)** is a multidisciplinary student initiative to design, manufacture, analyse, test, evaluate and successfully launch a microsatellite into low earth orbit (between 500 to 1000 km altitude).

At these altitudes, BLUESat will be susceptible to a multitude of harsh space environments that strongly influence the performance and lifetime of the operational subsystems and structures. The in-orbit thermal environment of BLUESat will present requirements of thermal control system design in order to ensure sound thermal energy balance between the satellite and its hard vacuum environment. To determine the degree of thermal control system implementation required for BLUESat, in-orbit thermal analysis of the satellite is conducted.

Hence this thesis project aimed to determine the temperature distributions of BLUESat over complete, possible orbit profiles in order to determine the level of thermal control system design that needs to be implemented. This was achieved via computational thermal analysis methods accepted within the space industry.

The overall process was divided within two sections:

1. Calculation of the external temperatures due to external heat sources using Finite Difference Method

## Abstract

2. Combining these external temperatures with internal heat inputs using a Finite Element model

The results gave temperature distributions across the entire structure for two orbital scenarios and a selection of initial thermal control design tests such as battery casing materials and specialised thermal control coatings (Optical Solar Reflectors).

Results showed that a 90 Degree Beta angle Sun Synchronous orbita profile is recommended to maintain optimal BLUEsat subsystem and structural performance with an onboard temperature range of 0° C to 20 ° C.

Several other tests were run within the analysis in order to ascertain possible future thermal design for BLUEsat.

Ultimately the in-orbit thermal analysis of BLUEsat successfully provided vast amounts of verified thermal data to assist students with future subsystems implementation in preparation for space qualification.

## Table of Contents

<b>Abstract</b>	<b>1</b>
<b>Table of Contents</b>	<b>3</b>
<b>List of Figures</b>	<b>10</b>
<b>List of Tables</b>	<b>13</b>
<b>1 Thesis Overview</b>	<b>14</b>
1.1 Introduction	14
1.2 Acknowledgments	16
1.3 Nomenclature	17
1.4 Unit Convention	18
1.4.1 Sinda / Nevada	18
1.4.2 Patran	18
<b>2 Background</b>	<b>19</b>
2.1 BLUESat Microsatellite	19
2.2 Thesis Project	21
2.2.1 Objectives of the In-orbit Thermal Analysis	21
2.2.2 Project Planning	22
<b>3 BLUESat Design Outline</b>	<b>25</b>
3.1 Mechanical	25
3.1.1 Trays	25
3.1.2 Bottom Plate	26

## Table of Contents

3.1.3	Top Plate	27
3.1.4	Side Panels	27
3.2	Electrical	28
3.2.1	Communications	28
3.2.2	Flight Computer	29
3.2.3	Solar Modules	30
3.2.4	Batteries	31
3.3	Thermal Requirements	32
<b>4</b>	<b>Theory Review</b>	<b>34</b>
4.1	Orbital Parameters	35
4.1.1	Analysis Parameters	35
4.1.2	Sun Synchronous	37
4.1.3	Orbital Beta Angle	38
4.2	Orbital Thermal Environment	39
4.2.1	Direct Solar Flux	39
4.2.2	Earth Reflected Albedo	40
4.2.3	Earth Infrared	42
4.3	Heat Transfer Theory	44
4.3.1	Convection	45
4.3.2	Conduction	46
4.3.3	Radiation	47
4.4	Passive Thermal Control Systems	49
4.4.1	Thermal Coatings	49
4.4.2	Insulation	50

## Table of Contents

4.4.3	Radiators	51
4.4.4	Conduction Pads	52
4.4.5	Phase Change Materials	53
<b>5</b>	<b>Preliminary Analysis Strategy</b>	<b>55</b>
5.1	Spherical Satellite Analysis	55
5.2	Honeycomb Panel Assumptions	59
<b>6</b>	<b>Finite Differencing Method Analysis</b>	<b>63</b>
6.1	Overview	64
6.2	Finite Differencing Technique	65
6.3	SINDA / ATM Model	67
6.3.1	Geometrical Model	68
6.3.2	Materials and Properties	70
6.3.3	Loads	70
6.4	NEVADA	72
6.4.1	Overview	72
6.4.2	BLUESat Orbital & Planetary Parameters	73
6.4.3	BLUESat Orbital Manoeuvres	74
6.4.4	Flux Loads	76
6.5	Results	76
6.6	Validation of Results	78
<b>7</b>	<b>Finite Element Analysis</b>	<b>85</b>
7.1	Why Patran / Nastran Thermal?	85

## Table of Contents

7.2	BLUESat Model	86
7.2.1	CATIA BLUESat Model	86
7.2.2	Patran Structural Components	87
7.2.3	Modelling Considerations	88
7.2.3.1	Joint Conductance	88
7.2.3.2	Enclosure Radiation	88
7.3	Finite Element Mesh Strategy	90
<b>8</b>	<b>Radiation Analysis of BLUESat</b>	<b>93</b>
8.1	Effects of Internal Radiation	93
8.2	Modelling Enclosure Radiation	94
8.2.1	Optical Properties Comparison	95
8.3	Steady State (SOL 153) Analysis	96
8.4	Steady State Results	97
<b>9</b>	<b>Thermo-Stress Analysis of BLUESat Solar Panels</b>	<b>99</b>
9.1	Solar Panel Design Concerns	99
9.2	Patran Model Representation	102
9.3	Worst Case Temperature Conditions	103
9.4	Analysis Process	105
9.4.1	SOL 153 Temperature Mapping	105
9.4.2	Nastran Structural Analysis	105
9.5	Results	106
9.6	Design Consideration	108

## Table of Contents

<b>10</b>	<b>Transient Orbital Analysis of BLUEsat</b>	<b>110</b>
10.1	SINDA Output Results	110
10.2	Battery Modelling	111
10.2.1	Heat Dissipation	111
10.2.2	Casing Model Representation	112
10.3	BLUEsat Orbital Scenarios	114
10.3.1	Selected Orbital Ranges	114
10.3.2	Fields Function Temp Inputs	117
10.4	Transient (SOL 159) Analysis	118
10.5	Results	119
10.5.1	0 Degree Beta Angle	119
10.5.2	90 Degree Beta Angle	121
10.5.3	Kapton Insulation	127
<b>11</b>	<b>Results Evaluation</b>	<b>130</b>
11.1	Orbital Scenario	130
11.2	Structural Thermal Control Design Considerations	131
11.2.1	External Surfaces	131
11.2.2	Internal Surfaces	132
11.2.3	Joint Conductance	133
11.2.4	Battery Insulation	135
<b>12</b>	<b>Conclusion</b>	<b>137</b>
12.1	FD Analysis	137
12.2	FE Analysis	138

## Table of Contents

12.3	Further Work	139
<b>References</b>		<b>141</b>
<b>A</b>	<b>SINDA G INPUT FILES</b>	<b>147</b>
<b>B</b>	<b>SINDA G OUTPUT FILES</b>	<b>150</b>
<b>C</b>	<b>Calculation of BLUEsat Surface Area and Optical Properties</b>	
C.1	Naked Structure	153
C.2	OSR Coating Structure	154
<b>D</b>	<b>SINDAPLOTS</b>	
D.1	Naked Structure, 0 Degree Beta	156
D.2	Naked Structure, 90 Degree Beta	157
D.3	OSR Structure, 0 Degree Beta	158
D.4	OSR Structure, 90 Degree Beta	159
<b>E</b>	<b>Selected Materials Thermo-Optical Properties</b>	<b>160</b>
E.1	Black Coatings	160
E.2	White Coatings	160
E.3	Conductive Paint	161
E.4	Anodised Aluminium Samples	161
E.5	Metals and Conversion Coatings	162
E.6	Vapour Deposited Coatings	163

## Table of Contents

E.7	Spacecraft Solar Arrays	163
E.8	Misc	164
E.9	Tapes	165
<b>F</b>	<b>BLUESat Material Properties</b>	<b>167</b>
F.1	Aluminium Alloy 7075-T6	167
F.2	Aluminium Alloy 6061-T6	168
F.3	Aluminium Alloy 5052-H39	169
F.4	Kapton K271 One-Sided Thermal Tape	170
F.5	Delrin Acetal homopolymer	170
F.6	Hexweb 5052 Aluminium Honeycomb	171
<b>G</b>	<b>Calculation of Honeycomb Effective Conductivities</b>	<b>173</b>
G.1	L Direction Conductivity	174
G.2	W Direction Conductivity	175
G.3	T Direction Conductivity	176

### **Back Cover IN-Orbit Thermal Analysis CD**

Included on this CD is the following:

- SINDA / ATM / NEVADA Demo Version
- SINDA Input and Output Files
- Patran and Nastran Thermal Files
- Thesis Report (PDF Format)
- Thesis Presentation

## List of Figures

- Figure 2-1: Artist impression of BLUEsat in orbit (courtesy D. Lee)
- Figure 2-2: BLUEsat Thermal Analysis Strategy
- Figure 3-1: CATIA model of BLUEsat Tray
- Figure 3-2: CATIA model of BLUEsat Bottom Plate
- Figure 3-3: CATIA Model of BLUEsat Top Plate
- Figure 3-4: CATIA model of BLUEsat Honeycomb Panel
- Figure 3-5: BLUEsat TX and RX Prototypes
- Figure 3-6: IHU-2 Spaceflight proven flight computer
- Figure 3-7: BLUEsat Bottom (left) and Side and Top Plate (right) Solar Modules
- Figure 3-8: Sanyo HF-A1U NI-MH Rechargeable Batteries
- Figure 4-1: Visual Representation of BLUEsat's Passive Orbit Manoeuvres
- Figure 4-2: Fundamental Orbital Parameter Description
- Figure 4-3: Sun Synchronous orbit
- Figure 4-4: Orbital Beta Angle
- Figure 4-5: Effect of Beta Angle on Flux Loads (Courtesy of Lockheed Martin for Spartnik)
- Figure 4-6: Calculated Albedo Flux used for Thermal Analysis
- Figure 4-7: Earth IR Flux Load used in Thermal Analysis
- Figure 4-8: Diagram Representation of Flux Sources acting upon BLUEsat's External Surfaces
- Figure 4-9: Temperature Gradient across Wall
- Figure 4-10: View Factor Calculation
- Figure 4-11: Typical MLI Cross-Section (Courtesy of NASA)
- Figure 4-12: Usage of a thermal gasket for increased conductivity (Courtesy D. Gilmore [2])
- Figure 4-13: PCM's can be used to maintain onboard temperatures for critical hardware
- Figure 5-1: Direction Definition for Honeycomb Core
- Figure 6-1: Finite Differencing Analysis Process
- Figure 6-2: Six surface cube representation of BLUEsat's external panels
- Figure 6-3: Orbital / Optical Scenarios
- Figure 6-4: Naked Structure Panel Optical Properties
- Figure 6-5: Optical Solar Reflector Panel Optical Properties
- Figure 6-6: Nevada Interface for Planetary and Orbital Parameters. Sun and BLUEsat both have 0 degree RAAN, therefore Maximum eclipse time.
- Figure 6-7: Setup used for 90 Degree Beta Angle. Note Sun is in direct line of the Vernal Equinox, therefore BLUEsat at 90 RAAN will obtain pure sun-lit orbit
- Figure 6-8: PACSAT Temperature Telemetry for a complete Orbit
- Figure 6-9: AO16 Temperature Telemetry including onboard Batteries 1 & 2 Temps
- Figure 6-10: BLUEsat External Panel Temperatures for Naked Structure, 0 Degree Beta

## List of Figures

- Figure 6-11: BLUEsat External Panel Temperatures for Naked Structure, 90 Degree Beta
- Figure 6-12: BLUEsat External Panel Temperatures for OSR Structure, 0 Degree Beta
- Figure 6-13: BLUEsat External Panel Temperatures for OSR Structure, 90 Degree Beta
- Figure 7-1: CATIA assembly of BLUEsat's principal structures prior to simplification for importation into Patran.
- Figure 7-2: Patran solid model of BLUEsat including module trays, battery, and top and bottom plate and side panel mounting blocks.
- Figure 7-3: Conductive effects of surface roughness between joints. (Courtesy Gilmore [2])
- Figure 7-4: Hex Mesh and equivalenced nodes of the battery module tray and interacting structure components.
- Figure 7-5: Hex Mesh of complete BLUEsat structure. Nodes at all interfaces were equivalenced to represent perfect joint conductance.
- Figure 7-6: Tray number allocation used in analysis
- Figure 8-1: Enclosure radiation (orange markers) applied to all tray sides, top, bottom and battery plates.
- Figure 8-2: Battery Module Fringe Plot-no internal radiation
- Figure 8-3: Battery Module Fringe Plot-Bare Aluminium
- Figure 8-4: Battery Module Fringe Plot-Chemglaze Z306
- Figure 9-1: Honeycomb panel dimensional constraints for bolt holes
- Figure 9-2: Shear tear out
- Figure 9-3: Fixed Translational and Rotational boundary conditions for the mirrored half of the panel.
- Figure 9-4: Fixed translations (x,y,z) on one side of the bolt hole. In actual conditions under contraction, the side with same direction as the contraction direction will be free to move.
- Figure 9-5: Peak Stress (Von Mises) due to thermal contraction @ 14.9 ° C
- Figure 9-6: Peak Stress (Von Mises) due to thermal contraction @ -27.9 ° C
- Figure 10-1: Battery Cell dimensions
- Figure 10-2: Battery casing model representation as solid geometry (kapton was modelled as surfaces between battery casing and battery plate)
- Figure 10-3: Battey heat dissipation output with respect to orbital position
- Figure 10-4: Tray temperatures over two orbits (0 Degree Beta)
- Figure 10-5: 6061-T6 Aluminium Battery Casing orbital temperatures
- Figure 10-6: Delrin Battery Casing orbital temperatures
- Figure 10-7: Tray 2 Orbital Temperatures (90 Degree Beta Angle)
- Figure 10-8: Tray 3 Orbital Temperatures (90 Degree Beta Angle)
- Figure 10-9: Tray 4 Orbital Temperatures (90 Degree Beta Angle)
- Figure 10-10: Battery Modules thermal gradient due to lower orbital heating on Side 1
- Figure 10-11: Tray 1 Orbital Temperatures (90 Degree Beta Angle)
- Figure 10-12: Tray 5 Orbital Temperatures (90 Degree Beta Angle)
- Figure 10-13: 6061-T6 Battery Casing Orbital Temperatures
- Figure 10-14: Delrin Battery Casing Orbital Temperatures
- Figure 10-15: Aluminium Battery Casing with Kapton
- Figure 10-16: Aluminium Battery Casing without Kapton

## List of Figures

Figure 11-1: Effective conductance with apparent pressure (Courtesy Gilmore [2])

Figure 11-2: Standard surface roughness for manufacturing processes (Courtesy Gilmore [2])

## List of Tables

- Table 3-1: BLUEsat Operating Temperature Requirements  
Table 4-1: BLUEsat Orbital Parameters as used for Nevada  
Table 4-2: Direct Solar Flux Ranges  
Table 4-3: Effect of Beta Angle on Flux Loads (Courtesy of Lockheed Martin for Spartnik)  
Table 4-4: Effect of Orbital Inclination on Earth Albedo  
Table 4-5: Other forms of Heat Source Considered Negligible  
Table 4-6: Selection of OSR and other Control Coatings  
Table 5-1: Fixed Calculation Values also used in SINDA  
Table 5-2: Absorptivity and Emissivity values as calculated in appendix C  
Table 5-3: Compressive and Shear Properties for Selected Honeycomb Panel  
Table 6-1: Transient sub routines available in SINDA/G  
Table 6-2: Dimension comparison with physical model  
Table 6-3: Specified Flux loads used for analysis. Represent average conditions.  
Table 6-4: PACSAT Orbital Temperature Telemetry  
Table 8-1: Optical properties comparison of bare aluminium and Black paint.  
Table 8-2: Steady State surface temperatures  
Table 9-1: Maximum and Minimum Temperatures for BLUEsat  
Table 9-2: Peak thermal deflection on panel  
Table 10-1: Surface temperatures for 0 Degree Beta Sun Synchronous Naked Structure  
Table 10-2: Surface Temperatures for 90 Degree Beta Sun Synchronous Naked Structure  
Table 10-3: Fields entry times for 0.5 W uniform applied heat of battery dissipation

# 1 Thesis Overview

## 1.1 *Introduction*

BLUESat is a multidisciplinary student microsatellite project at the University of New South Wales. The primary goal of this project is to design, manufacture, analyse, test, evaluate and successfully launch a microsatellite into Low Earth Orbit. Success of this project will also help propel the teams' desire to see an operational and leading Australian university space development centre come to fruition.

Once in orbit, BLUESat will experience a variety of conditions that make up the Space Environment. The in-orbit thermal environment is one such condition which affects the onboard hardware and structural performance of the microsatellite via a combination of internal (electronics heat generation) and external heat fluxes (Direct Solar Flux, Earth Albedo and Earth Infrared). Due to the hard vacuum of space, the heat energy must be managed through conduction and radiation methods of heat transfer. This management must be achieved through a degree of Thermal Control System (TCS) implemented post thermal analysis.

This thesis aims to analyse BLUESat's thermal environment, in particular, to investigate the temperature distributions in-orbit to ascertain what degree of thermal control system design needs to be implemented. This thesis project was to be conducted from a purely analytical approach, using analysis methods

accepted within today's space industry and validated with by comparison to similar microsatellites.

The primary factor to the thermal environment is considered the orbital profile selected for BLUEsat. Certain parameters will determine the exposure levels and durations so two extreme case scenarios were analysed. The objective of this was to ensure BLUEsat will be accounted for extreme temperature ranges since orbit profile selection ultimately rests with the launch provider.

Whist this thesis was not intended to provide detailed thermal control design incorporation for BLUEsat, special focus to thermal control was made of the onboard batteries since it was deemed most critical to the hardware temperature requirement. Similarly, a basic comparison of usage of a standard passive thermal control coating opposed to a naked structure was conducted to gain appreciation of the effects of radiation thermal control that could be utilised.

Structural integrity can be impinged due to the coefficients of thermal expansion of the various spacecraft materials. Misalignment of critical components and stress concentrations at joints can often be obscured due to the complicated nature of heat transfer. The versatility of the finite element analysis software enabled structural analysis of the BLUEsat solar panels under thermal loading. Therefore an evaluation of the current design could proceed, and, if necessary, allow updated design considerations should the result findings be deemed significant.

## **1.2 Acknowledgements**

To Mr J. Page and Prof. D. Kelly, thank you for supervising the topic of my own choice and allowing me to freely choose my path.

On behalf of the BLUEsat team, I would like to thank Ron Behee of Network Analysis Inc. for the sponsorship of SINDA/G Thermal Analysis software which proved vital to my analysis. Similarly Greg Spencer of TAC Technologies for the NEVADA Radiation software and Jadanne Heuchen of Sun Microsystems for awarding BLUEsat a SUNBLADE 2000 Workstation as an academic grant. Their in-kind sponsorship has helped our dream step closer to reality.

Finally to all the team at BLUEsat, I owe much appreciation for your assistance, advice and interest throughout the year.

### 1.3 Nomenclature

$\alpha$	-	absorptivity, is the ratio of energy absorbed by a material to the energy incident on the surface of this material
$\varepsilon$	-	emissivity, is the ratio of the total emissive power of a grey surface to the total emissive power of a black surface at the same temperature
$\rho$	-	material density, $\text{kg/m}^3$
$\beta$	-	Orbital Beta Angle
$Q$	-	Heat Rate, $\text{W}$
$h_c$	-	convection coefficient, $\text{W/m}^2 \text{K}$
$A$	-	Area, $\text{m}^2$
$k$	-	conductivity, $\text{W / m K}$
$\sigma$	-	Stefan-Boltzmann constant, $5.67 \times 10^{-8} \text{ W/m}^2 \text{ K}^4$
$c$	-	specific heat for solid
CTE	-	coefficient of thermal expansion of material
$T$	-	temperature, $^{\circ} \text{C}$ or $\text{K}$
AU	-	Astronomical Unit = 149 598 000 000 meters or Earths mean distance from the sun
$q^s$	-	Direct Solar Flux Constant
$q^A$	-	Earth Albedo
$q^I$	-	Earth Infrared (IR) Emission

## 1.4 Unit Convention

Early analysis was yielding incorrect and often outrageous results due to the improper misuse of units. When applying finite difference and finite element analysis methods via available software, caution must be used particularly when software interfaces exercise different unit defaults with respect to each other.

The following units were used for the respective software codes so as to avoid unit calculation clash.

### 1.4.1 Sinda / Nevada

Length	-	Meters, m
Energy	-	British thermal unit, BTU
Time	-	Seconds, s
Mass	-	Kilograms, Kg
Temperature	-	Degrees Celsius, ° C

$$\text{Stefan-Boltzmann's Constant} = 5.67 \times 10^{-8} \text{ W/m}^2 \text{ K}^4 \times 0.0009486608 \text{ BTU/s} \\ = 5.379 \times 10^{-11} \text{ BTU/s m}^2 \text{ K}^4$$

### 1.4.2 Patran

Length	-	Millimeters, mm
Energy	-	Watts, W
Time	-	Seconds, s
Mass	-	Kilograms, Kg
Temperature	-	Degrees Celsius, ° C

## 2 Background

*"To build a world-class, student-based centre of excellence at UNSW for the sustainable development of Human Resource, Technological, Business and Organizational capabilities for the Exploration and Development of space."*

- Mission Statement of the ULSSD, governing body of the BLUESat Project

### 2.1 **BLUESat Microsatellite**

BLUESat (Basic Low Earth Orbit UNSW Experimental satellite) is a student designed, built and operated microsatellite (10 kg – 100 kg flight mass) based on the original AMSAT-NA modular tray-stack configuration. The primary function of BLUESat is to operate store and forward packet data via PACsat protocol available to amateur radio operators worldwide or commonly known as HAM radio operators. Secondary functions of the microsatellite will include the following:

- Telemetry system to collect spacecraft operational conditions data for experiment and diagnostic purposes
- GPS for accurate determination of satellite orbit position and provision for timing data.
- Side mounted imager for earth still shots

- Coated Lexan experiment to examine the materials' ability to block out Ultra-Violet radiation.

BLUESat will orbit in Low Earth Orbit (LEO) which can range between 500 km to 1000 km. Because the provision of launch is yet to be decided it is not yet determined what orbital parameters will be selected for BLUESat. Hence for the purposes of this thesis an acceptable and most preferred orbit has been assumed. This orbit will involve time varying external heat input environments to the spacecraft due to the periods of direct sunlight and eclipse. It is this cycling which essentially provides the reason for this thesis, that is, how does the thermal environment affect the onboard operational and structural performance of BLUESat in orbit.

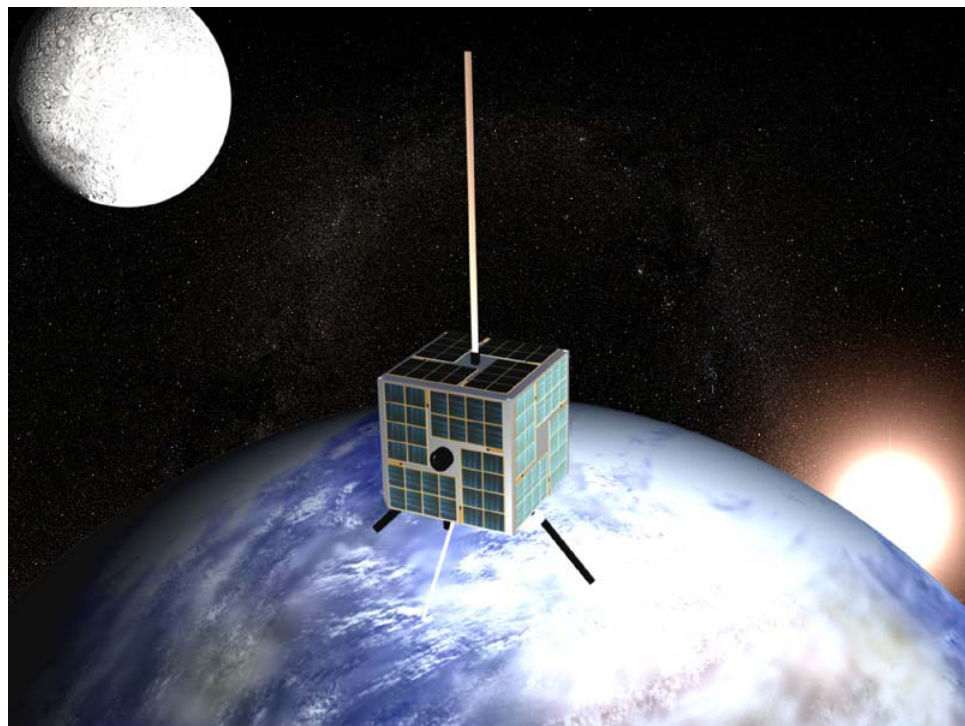


**Figure 2-1: Artist impression of BLUESat in orbit (courtesy D. Lee)**

## 2.2 Thesis Project

### 2.2.1 Objectives of the In-Orbit Thermal Analysis

*Thermal {thûr'môl}*      1. *Pertaining to, determined by, or measured by heat.*

*Elastic {î-las'tik}*      1. *Spontaneously returning to a former size, shape, or configuration after being altered from it*

2. *Capable of expansion and contraction*

Onboard systems require suitable temperature conditions for reliable operation.

For ground based hardware, this is often too easily accounted for by means of free and forced convection (heat sinks and fans), but in the hard vacuum environment of space, a suitable temperature environment must be maintained by a combination of onboard conduction and internal and external radiation exchange. These combinations form what are known as Passive and Active Thermal Control Systems (TCS) designed into the spacecraft.

The role of this thermal analysis was to investigate the temperature distributions across the satellite structure during a period of life, in this case, its orbital or in-orbit thermal environment for determination of thermal control system design implementation.

Orbital parameters also have an influence on the in-orbit thermal environment. For example a Beta angle of 90 degrees will cause a significantly lower Earth

Albedo flux value, because albedo is a factor of reflectivity. Therefore this thesis project sets out to observe the effects of different orbit profiles for BLUEsat.

History of the AMSAT microsatellite design has seen common passive thermal control systems applied. This thesis compares the benefits of passive thermal control systems, in particular the optical manipulation of OSR (Optical Solar Reflector) pressure sensitive adhesive tape, as opposed an entirely naked (no coatings) structure. [1]

Stresses due to thermal expansion and contraction were the final consideration of this thesis. Stress could affect the performance of the satellite structure. Because BLUEsat has a wide variety of metals, each of which has distinctive thermal properties, loading can occur on the fittings thus misalignment and/or stress concentrations at joints. Due to the wide scope theories and concepts this thesis already has, a limited amount of stress analysis was conducted, in particular, the loading on the aluminium honeycomb panel bolts.

As a parallel interest in this topic, another objective was to gain a broader appreciation of:

1. Heat transfer theory for spacecraft applications, fundamental to the research understanding.
2. Orbital mechanics
3. Current Thermal Control Systems Engineering

4. Accepted Thermal Modelling practises currently used in the space industry (e.g. SINDA/G , NEVADA, TRASYS)

### **2.2.2 Project Planning**

The ultimate goal of this project was to analyse the temperature distribution on the satellite structure to verify whether allowable operating temperature conditions of both the structure and hardware are sustained. The major concern was what procedure would be used to model the complex orbital thermal environment.

The first stage in the thesis project was to complete a literature review of the following theories and concepts.

- Heat Transfer Theory
- Spacecraft and Planetary Orbital Parameters
- Orbital Thermal Environment
- Current Spacecraft Thermal Control Systems

Practice into the use of Patran and Nastran Thermal Finite Element software was also conducted early on via 11 online satellite thermal tutorials provided on the support webpage of [www.mscsoftware.com](http://www.mscsoftware.com).

Later in the year, a revision of the analysis procedure was updated to include the use of SINDA/ATM and NEVADA, both of this commercial software is highly

used by the space industry. In effect, the following describes the process used to achieve the temperature distributions on BLUEsat.

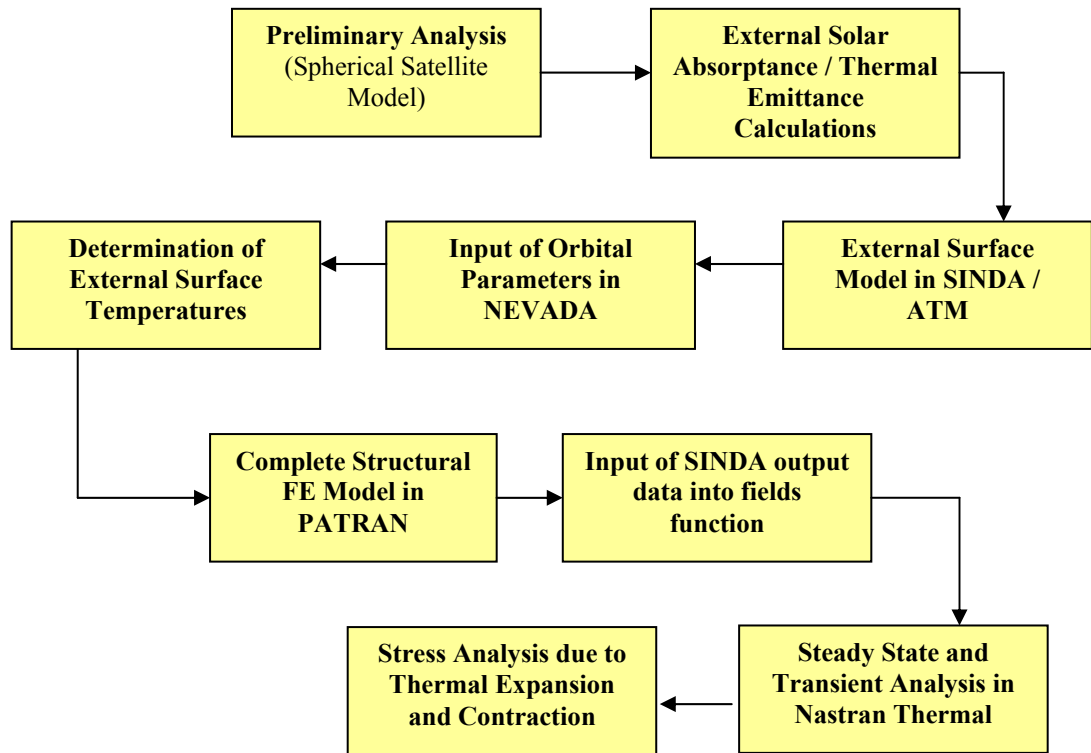


**Figure 2-2: BLUEsat Thermal Analysis Strategy**

Following analysis of the results, recommendations have been made to the level of implementation of thermal control of BLUEsat as well as discussion of possible continuation of research into the thermal analysis of BLUEsat.

## 3 BLUESat Design Outline

Thermal analysis must account for many parameters. The following details the design and material properties of the physical structure that affect thermal analysis as well as brief descriptions of the major hardware components with the structure.

### 3.1 *Mechanical*

A selection of materials is used for the construction of BLUESat. This is a concern for the sound thermal design of BLUESat because each respective material will have their own unique set of mechanical, optical and thermal properties. For example, under significant thermal loading, component misalignment can occur due to the variation of coefficients of thermal expansion. The following describes the major component summaries that were dealt with for the analysis. Please refer to APPENDIX F for material properties.

#### 3.1.1 Trays

BLUESat utilises the flight-proven AMSAT –NA microsatellite design of the 1970's. The purpose of the tray stack configuration was to modularise hardware into a lightweight, economically viable satellite design. Trays were CNC milled from 7075 –T6 Aerospace grade aluminium. Minimum thickness is 2mm per tray which provides an allowable limit to radiation shielding for low earth orbit satellites.

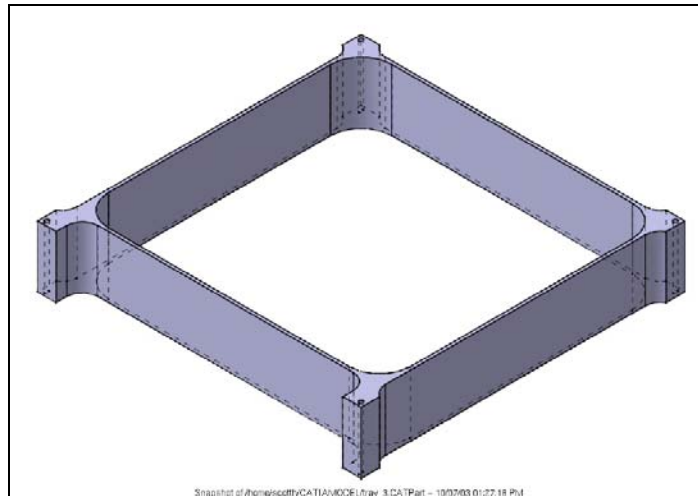


Figure 3-1: CATIA model of BLUESat Tray

### 3.1.2 Bottom Plate

The bottom plate supports the communications transmitters and bottom antennas. At the centre is the spring housing which provides the separation of BLUESat from the launch vehicle. The bottom plate is CNC milled from 7075-T6 Aerospace grade Aluminium with a maximum thickness of 10.5mm. Solar modules are located on the underside of the bottom plate.

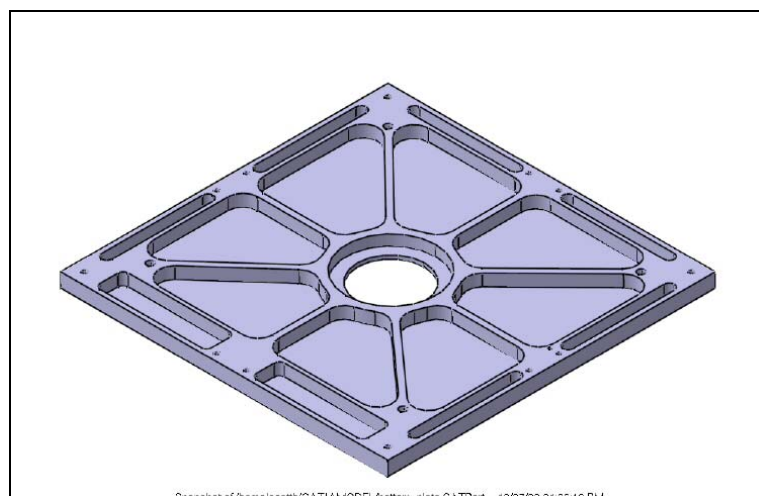


Figure 3-2: CATIA model of BLUESat Bottom Plate

### 3.1.3 Top Plate

The top plate is a 2mm thick 6061-T6 aluminium sheet of dimensions 236 mm by 236 mm. This supports the top receiver antenna mount and the four corner tray stack bolts which also pass thru the trays and bottom plate respectively.

The top plate will also support 4 solar modules.

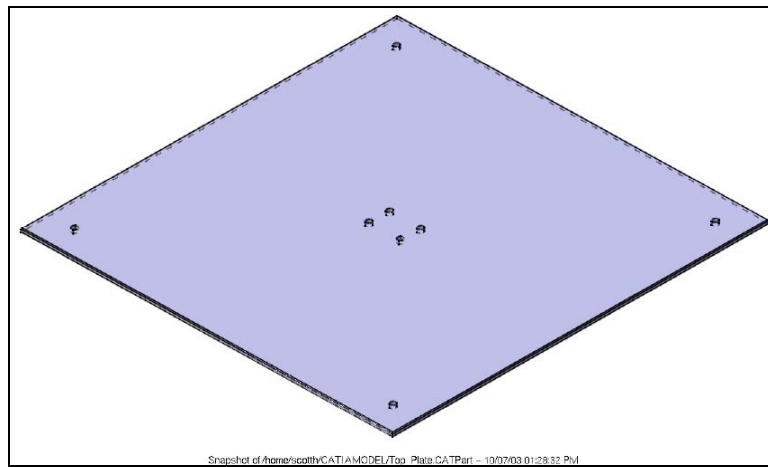
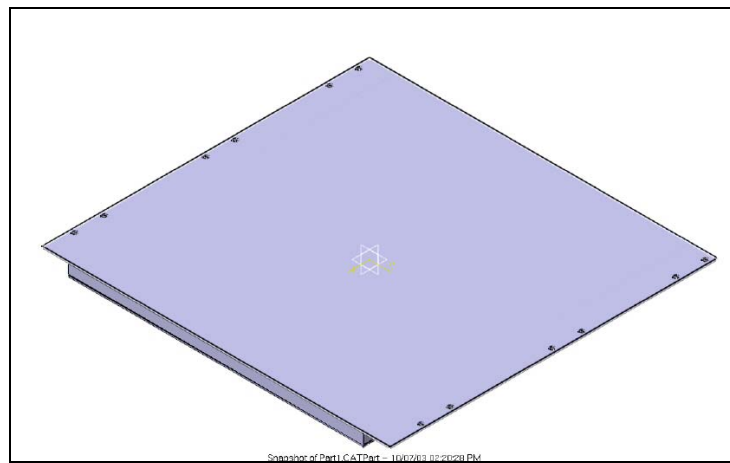


Figure 3-3: CATIA Model of BLUESat Top Plate

### 3.1.4 Side Panels

Prior dynamic analysis of BLUESat recommended the usage of aluminium honeycomb panels for the solar panel side panels to minimise peak deflection and thus prevent failure of the solar modules with cover glass. The selected honeycomb panel is 5052 H39 Alloy Hexagonal Aluminium honeycomb with a core thickness of 7 mm and skin thickness of 1mm per side. Cell size is  $\frac{1}{4}$  in.



**Figure 3-4: CATIA model of BLUESat Honeycomb Panel**

### **3.2 *Electrical***

The role of the thermal analysis is primarily related to the requirement of optimal hardware performance. As a particular component is operational, a percentage of the electrical input will be transformed into heat, light or sound energy.

#### **3.2.1 Communications**

The onboard communications system for BLUESat is the flight proven Hamtronics TA 451 70 cm Transmitter and the Hamtronics R100 2 m Receiver units. Power budget allowable currently for the transmitter is 13.6 V @ 650 mA $\pm$  10 %.

Power output in the form of RF or electromagnetic radiation of wavelength 70 cm is rated at 2.5 W. Therefore the expected thermal dissipation of the unit is considered to be:

$$\begin{aligned}
 (13.6 \times 0.650) - 2.5 \text{ W} &= 8.84 - 2.5 \text{ W} \\
 &= 6.34 \text{ W.}
 \end{aligned}$$

For the purposes of this analysis we assume this is completely in the form of heat loss and in effect will be the largest form of electrical heat dissipation.

For the receiver, heat dissipation has been assumed to be 330 mW based on previous microsatellite data.

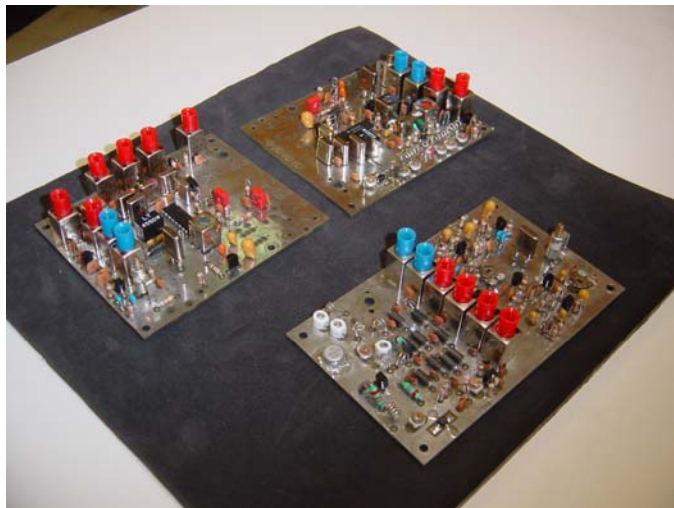


**Figure 3-5: BLUESat TX and RX Prototypes**

### 3.2.2 Flight Computer

Power assumptions for the flight computer are based on the IHU-2, in which earlier version were seen on UoSAT-1 and UoSAT-2 microsatellites. This system has the benefit of built in thermal safety, where the CPU and both memory systems will have heat shunts near the wall casing.

Heat dissipation was assumed to be the maximum run mode power of the StrongARM SA-1100 AA CPU, rated at 400 mW [27].



**Figure 3-6: IHU-2 Spaceflight proven flight computer**

### 3.2.3 Solar Modules

BLUESat's modules comprise of high efficiency buried contact silicon solar cells manufactured at the University of New South Wales' Top Cell laboratories. Efficiency is guaranteed at 18 % for an AM1.5 spectrum at 25 degrees Celsius. [25].

Faber [25] calculates the power budget for a worst case minimum light intensity at 3W. The emissivity and absorptivity coefficients for these modules has been rated at  $\varepsilon = 0.81$  and  $\alpha = 0.69$  according to testing data conducted by Spectrolab [28] for fused Cilica Solar Cells which are of similar characteristics and include cover glass.

Areas and optical properties of the constituent components for both types of solar modules were calculated to determine the panel average  $\varepsilon$  and  $\alpha$  values (refer APPENDIX C). Approximations were made for the connecting tab

surface areas however due to their minimal coverage; optical properties will have minimal impact to the overall calculations.



**Figure 3-7: BLUESat Bottom (left) and Side and Top Plate (right) Solar Modules**

### 3.2.4 Batteries

BLUESat's power system will consist of 4 strings of Sanyo HF-A1U NI-MH (10 cells per string) rechargeable batteries. Battery life will be dependant on the ambient temperature conditions. The power system will be positioned within Tray 3 and on a 5 mm thick plate. This plate will provide direct-conduction coupling to radiate waste heat from the batteries and maintain them between 0 to 20 Degrees Celsius.

For the ecliptic orbit profile that was analysed, a battery casing of large thermal mass was designed in patran to maintain allowable temperature conditions.



**Figure 3-8: Sanyo HF-A1U NI-MH Rechargeable Batteries**

### 3.3 ***Thermal Requirements***

The definitive constraint to this thesis project is the thermal requirements of both the mechanical structure and electrical hardware. A parametric analysis of selected microsatellites and texts was completed to obtain acceptable upper and lower temperature limits that must be maintained for components to perform most efficiently and effectively in orbit. This range is the *Operating Temperature Range*. Should have a particular component been outside the limits, thermal control techniques need to be implemented (such as heat pipes, an active thermal control system). Note the Absolute upper and lower limits are still acceptable limits the components can reach, but never can exceed for all mission phases based on worst case scenarios. [31]

From this data we can deduce that the critical component will be the flight battery cells. [17]. It is stated that the batteries are not to be charged or discharged at temperatures below 0 degrees Celsius ambient. [18] Hence consideration must be made to acquire temperature-voltage on orbit of each of the battery cell modules. Not illustrated in the Operating temperature range but of equal importance is that for multiple modules, temperature difference should be less then or equal to  $\pm 5$  degrees Celsius.

BLUESat Operating Temperature Ranges for Selected Components						
Temperature Limits in Degrees Celsius						
System	Equipment	Absolute Lower	Operational Lower	Operational Upper	Absolute Upper	
Structure	Top Plate (Non-Alignment Critical)	-100	-45	65	100	
	Bottom Plate (Non-Alignment Critical)	-100	-45	65	100	
	Side Panels (Alignment Critical)	-100	-30	30	100	
	Antenna	-100	-65	95	100	
Computer	Flight Computer	-20	0	50	70	
Power	Battery Cell	-5	0	20	25	
	Regulator	-20	0	25	55	
	Solar Module	-105	-10	85	110	
Payload	Lexan Experiment	-40	-10	50	80	
	CMOS Imager	-20	0	40	60	
Telecommunications	Transmitter	-40	-10	50	90	
	Receiver	-40	-10	50	90	
Passive Stabilisation	Bar Magnets	-40	-20	30	50	
	Hysteresis Rods	-100	-20	30	100	

Table 3-1: BLUESat Operating Temperature Requirements

## 4 Theory Review

### 4.1 Orbital Parameters

Finalising the decision on what orbit BLUEsat will have ultimately depends on the launch provider. What is certain is that BLUEsat will have:

- Low Earth orbit between 500 km to 1000km altitude
- Solar Induced Spin Stabilisation
- Magnetic Flip twice per orbit at the equator

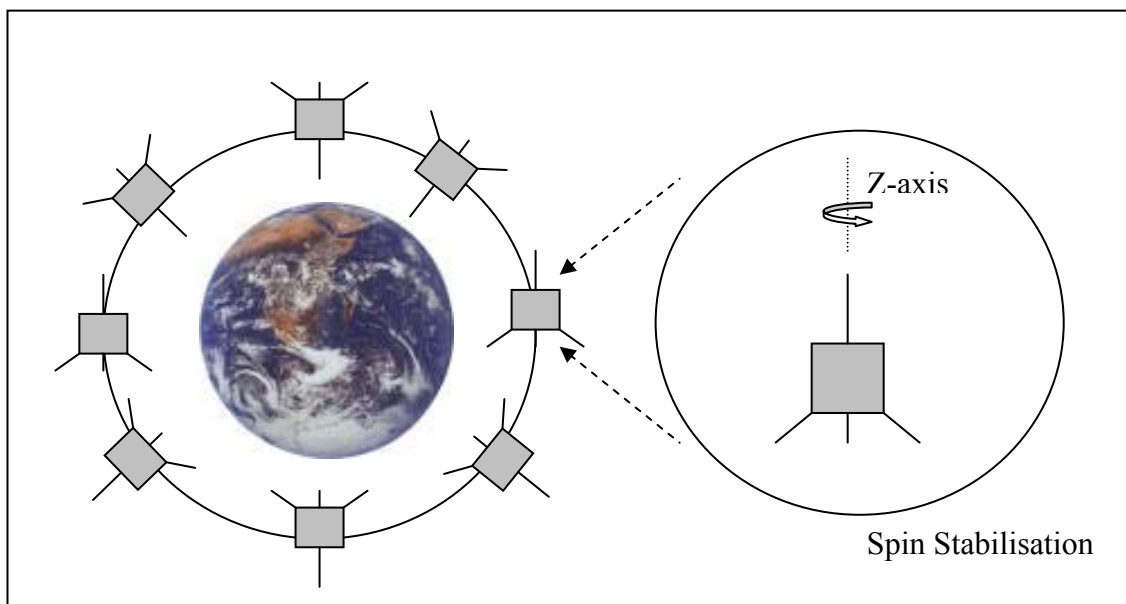


Figure 4-1: Visual Representation of BLUEsat's Passive Orbit Manoeuvres

Low earth orbits are generally at high inclinations to allow large coverage of the earth's surface. The inclinations can vary from 0 to 90 degrees with respect to the orbital plane and the equatorial plane.

### 4.1.1 Analysis Parameters

Thermal Analysis will hold a large factor on determining the most recommended orbit. Orbital Inclination, Beta Angle, Argument of Ascending Node (sun day angle), Orbital Period etc all affects the amount of Solar Flux, earth albedo, and Earth IR.

The following table describe the orbital elements taken into account for the NEVADA orbital flux analysis. Figure 4-2 provides a visual description of some of these parameters.[6]

Orbital Parameter	Symbol	BLUESat Analysis Value
Orbit Semi-Major Axis (Km)	AA	7067
Orbit Eccentricity	EE	0
Orbit Period (Hours)	P	1.642
Orbit Inclination (Degrees)	RI	98.7 (Refer “Sun Synchronous”)
Argument Of Ascending Node (Degrees)	Q	0 and 270 (Refer “Orbit Beta Angle”)
Argument Of Apogee	$\alpha$	0
Sun Angle (Measured From Vernal Equinox) (Degrees)	$\psi$	0
Inclination of Equatorial Plane (Degrees)	$\delta$	23.4
Planet Radius(Km)	$R_p$	6367
Orbit Altitude (Km)	$R_A$	700

Table 4-1: BLUESat Orbital Parameters as used for Nevada

Where

$$AA = \left( \frac{R_{APOGEE} + R_{PERIGEE}}{2} \right)$$

$$EE = \frac{1 - R_{PERIGEE}}{AA}$$

$$P = 1.658669 \times 10^{-4} \times AA^{\frac{3}{2}} \quad [5]$$

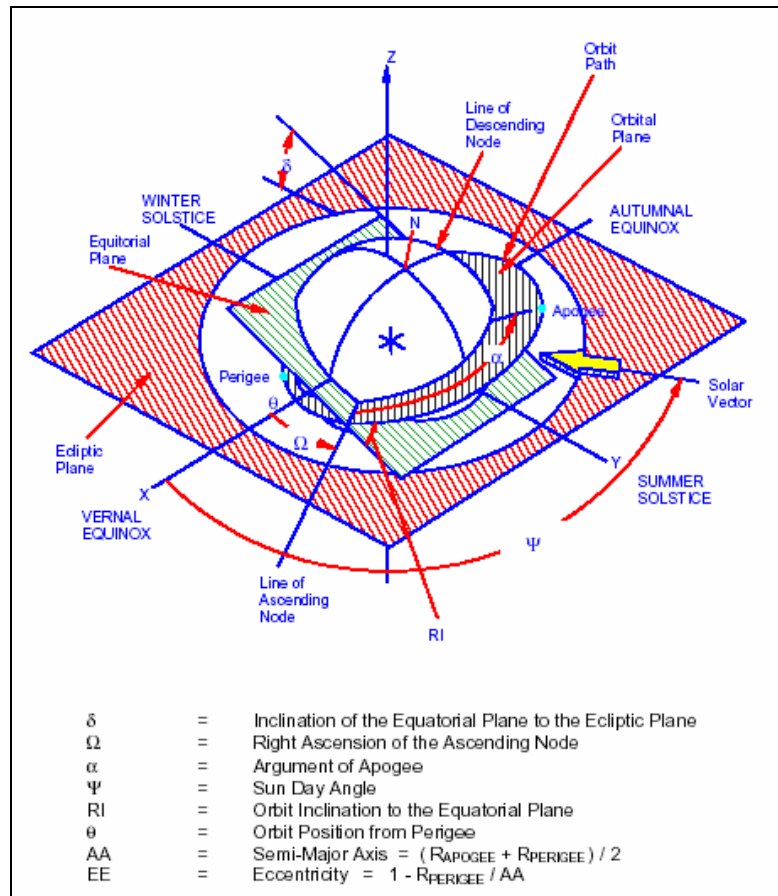


Figure 4-2: Fundamental Orbital Parameter Description

This analysis had selected two of the most common orbital parameter setups for microsatellites currently used. Both these configuration use the same earth orbit type, a *Sun Synchronous* orbit.

#### 4.1.2 Sun Synchronous

A sun synchronous orbit maintains the orbital plane at nearly a fixed angle relative to the sun throughout the earth's orbit. This means a nodal precession rate of 0.9856 deg/day, which is earth's rotation rate around the sun. [3] Hence this orbit must be retrograde with an orbital inclination of 98.7 degrees above the equatorial plane.

The satellite then passes over points on earth at the same local time during its orbit. BLUEsat will then eventually see a different swatch of the earth's surface each revolution due to the earth's rotation. [2]

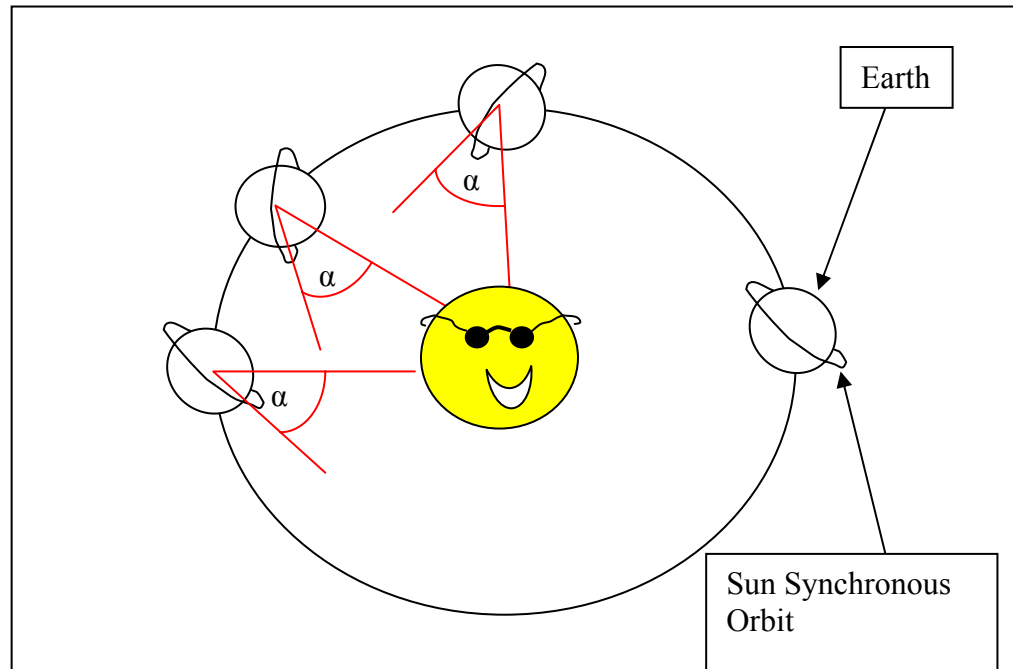


Figure 4-3: Sun Synchronous orbit

### 4.1.3 Orbit Beta Angle

The orbit beta angle ( $\beta$ ) is the primary factor when selecting strength of exposure and duration of direct solar flux, the greatest form of external heat input. The orbit beta angle of an orbit is the minimum angle measured from the solar vector to the plane orbital plane. An orbit Beta angle of 0 degrees gives maximum earth shadowing where as an angle of 90 degrees will ensure BLUEsat orbits in a full sunlit orbit as it continually passes over the umbra. An analysis was conducted for both cases by a manipulative approach. An orbit Beta angle is not provided for input into the VEGAS deck but since a beta angle can vary for an orbiting satellite over a year (even sun-synchronous has a small amount of beta angle change, but is assumed near constant in this analysis), beta angle was fixed by adjusting the Argument of Ascending Node for angles 0 and 270 degrees. This corresponds to beta angles 0 (actually near maximum eclipse time but not actual) and 90 degrees (pure sunlit) respectively.

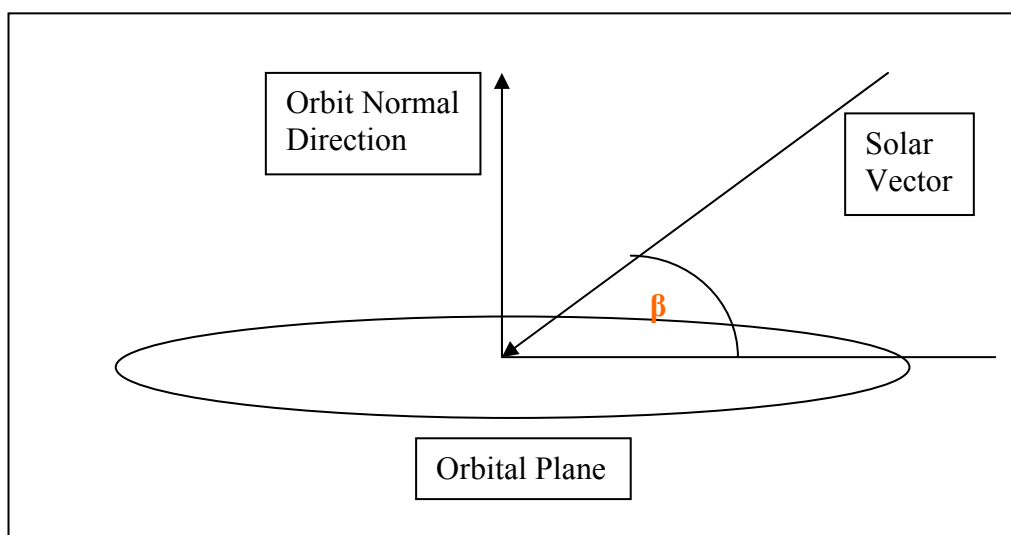


Figure 4-4: Orbital Beta Angle

## 4.2 Thermal Environment

One of the microsatellite hard specifications was that it will operate within a low earth orbit to achieve an orbital period of approximately 100.6 mins [REFER Appendix A]. This coincides with an assumed altitude of 700 km. For this Earth orbit type the principal forms of heat loading is:

1. Direct Sunlight
2. Sunlight reflected off earth (Albedo)
3. Infrared (IR) energy emitted from earth

### 4.2.1 Direct Solar Flux

Particularly for a microsatellite, direct solar input is the greatest form of heat generation onto a spacecraft structure. For this research, the solar constant,  $q^s$ , is used and is equal to  $1367 \text{ W/m}^2$  for a distance of 1 AU. Below is the solar flux range observed for earth and is universally accepted to with 0.4 % accuracy. [2]

Earths Distance From Sun	Direct Solar Flux
Closest (Winter Solstice)	$1414 \text{ W/m}^2$
Solar Constant	$1367 \text{ W/m}^2$
Farthest (Summer Solstice)	$1322 \text{ W/m}^2$

Table 4-2: Direct Solar Flux Ranges

Due to the vast distance of the Sun from Earth, it is safe to consider that the solar vector is in parallel rays by the time they bombard the surfaces of BLUEsat.

### 4.2.2 Earth Reflected Albedo

Earth Albedo,  $q^A$ , refers to the reflection of direct solar off Earth back towards BLUEsat. This is highly variable especially for LEO's where continual passing of geographic features such as seas, clouds snow and polar ice caps vary the strength of albedo. Hence as a general rule the Earth albedo tends to increase with latitude. Since this source is a function of reflectivity, positioning of BLUEsat' for a 90 degree Beta angle will yield an Earth Albedo tending towards zero. For better appreciation of the effects of the Beta angle and its effects of Albedo, Lockheed Martin completed the following data for the Spartnik microsatellite. The highlighted beta angle shows minimum Earth Albedo which suggests the inability for reflected sunlight at the umbra.

Beta Angle	Irradiation Sources: Function of Beta Angle (Watts)				
	Solar	Albedo	Earth IR	Total	Solar + Albedo
0	145.7786	25.1954	48.0115	218.9855	170.974
30	158.9916	21.9239	48.0369	228.9524	180.9155
60	188.9073	12.93433	48.0159	249.85753	201.84163
64	219.6072	11.10916	48.6882	279.40456	230.71636
90	161.578	3.361258	48.0579	212.997158	164.939258
116	219.6072	11.10916	48.6882	279.40456	230.71636
120	188.9073	12.93433	48.0159	249.85753	201.84163
150	158.9916	21.9239	48.0369	228.9524	180.9155
180	145.7786	25.1954	48.0115	218.9855	170.974
210	158.9916	21.9239	48.0369	228.9524	180.9155
240	188.9073	12.93433	48.0159	249.85753	201.84163
244	219.6072	11.10916	48.6882	279.40456	230.71636
270	161.578	3.361258	48.0579	212.997158	164.939258
296	219.6072	12.93433	48.6882	281.22973	232.54153
300	188.9073	12.93433	48.0159	249.85753	201.84163
330	158.9916	21.9239	48.0369	228.9524	180.9155

Table 4-3: Effect of Beta Angle on Flux Loads (Courtesy of Lockheed Martin for Spartnik)

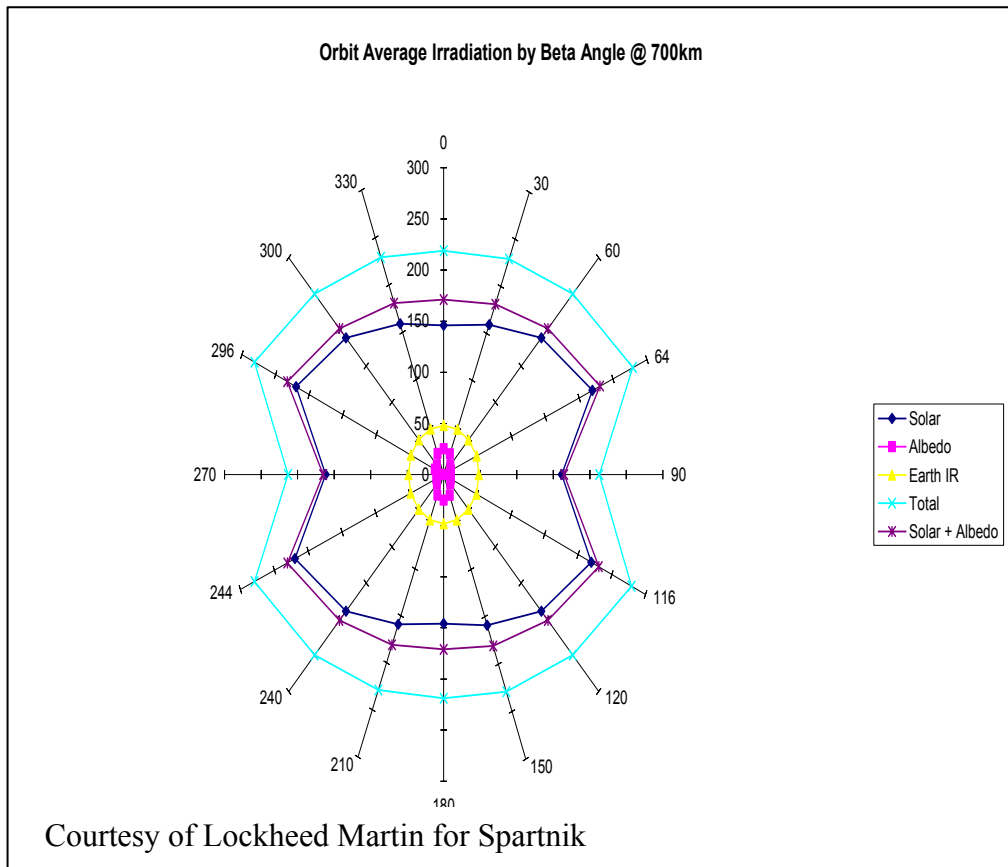


**Figure 4-5: Effect of Beta Angle on Flux Loads (Courtesy of Lockheed Martin for Spartnik)**

Likewise Earth Albedo is a function of orbital inclination. As a general rule, Earth albedo is assumed to be 30 % of the Solar Flux. KARAM [3] states that the following table should be used based on NASA statistics.

Albedo % (NASA TM-82478)			
Orbit Inclination	minimum	average	maximum
±90	0.38	0.42	0.46
±80	0.34	0.38	0.42
±70	0.3	0.34	0.38
±60	0.26	0.3	0.34
±50	0.22	0.28	0.32
±40	0.19	0.25	0.29
±30	0.2	0.24	0.28
±20	0.2	0.24	0.28
±10	0.2	0.24	0.28

Table 4-4: Effect of Orbital Inclination on Earth Albedo

For the purpose of this analysis, Earth Albedo was assumed to be 30 % of Solar Flux.

$$\begin{aligned}
 \text{Earth Albedo} &= 30\% \text{ of Solar Constant} \\
 &= 0.3 \times 1367 \text{ W/m}^2 \\
 &= 410.1 \text{ W/m}^2
 \end{aligned}$$

Figure 4-6: Calculated Albedo Flux used for Thermal Analysis

### 4.2.3 Earth Infrared (IR)

Earth IR is the reemitted energy from the incident sunlight that doesn't get reflected as earth albedo. This amount will vary also and depends very much on the earth's surface temperature. In effect this means high values of Earth IR,  $q^I$ , will be present near equatorial regions. Cloud cover is also a factor and will decrease the amount of passable IR. Thermal control coatings cannot reflect IR

due to the similarity in wavelengths of earth IR to spacecraft IR emission. As opposed to BLUEsat's tendency to be affected by its absorptivity of external heat fluxes, the fraction of Earth IR absorbed by BLUEsat is a function of its emissivity.

Orbit average Earth IR is taken as  $236 \text{ W/m}^2$ , which is equivalent to the wavelength of a blackbody at  $-20^\circ\text{C}$  (average effective Earth temperature).

$$\text{Earth IR} = 236 \text{ W/m}^2$$

**Figure 4-7: Earth IR Flux Load used in Thermal Analysis**

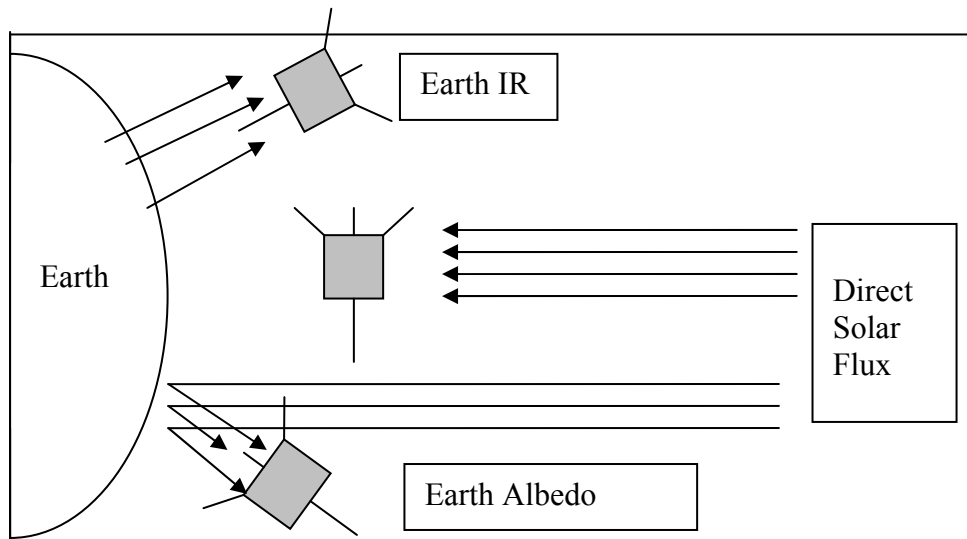


**Figure 4-8: Diagram Representation of Flux Sources acting upon BLUEsat's External Surfaces**

In summary these three external sources of heat are the primary external heat loads that must be balanced on BLUEsat depending on the orbital parameters.

Figure 4-8 summarises the satellite thermal environment. Other heating sources that are neglected for this analysis are included in Table 4-5.

<b>Negligible forms of Heat Source</b>
Moon Albedo
Moonshine
Solar Wind (Positively Charged Particles)
Atmospheric Drag
Starlight
Gamma Rays
Cosmic Thermal Radiation
Free Molecular Heating
Thermal Radiation exchange with other

**Table 4-5: Other forms of Heat Source Considered Negligible**

### **4.3 Heat Transfer Theory**

Understanding of the principal of heat transfer common to a spacecraft orbital environment is necessary for appreciation of analysis and verification of the BLUEsat thermal model. With the exception of convection, these principals are the same as what we expect on earth's surface.

The following describes the mechanisms of the three forms of heat transfer.

1. Convection
2. Conduction
3. Radiation

### 4.3.1 Convection

Convective heat transfer requires a fluid medium to pass across the material/substance either as a function of density differences in a gravitational field (*free convection*) or as a function of a pressure difference (*forced convection*). Convection is based on Newton's Law of Cooling [7]:

$$Q = h_c A \Delta T$$

$$= h_c A (T_2 - T_1)$$

Where  $Q$  = Power  
 $h_c$  = the convection coefficient  
 $A$  = area  
 $T_2, T_1$  = Temperature differential

Convection is seldom used for satellite thermal analysis unless launchpad cooling is a concern. Out of interest, Soviet spacecraft design utilised sealed, pressurised spacecraft with fans to achieve a more constant temperature distribution. [8]

### 4.3.2 Conduction

Conduction is the transfer of heat across a solid due to a temperature differential without displacement of matter. Conduction is the primary mode of heat transfer within BLUEsat (although enclosure radiation has significance if inner trays are painted black). Fourier's law describes one-dimensional heat conduction.

$$Q = -kA \frac{dT}{dx}$$

Where  $Q$  = power (energy per unit time)  
 $k$  = thermal conductivity of material  
 $A$  = Area which conduction passes thru material  
 $dT/dx$  = difference in temperature across incremental length  $x$

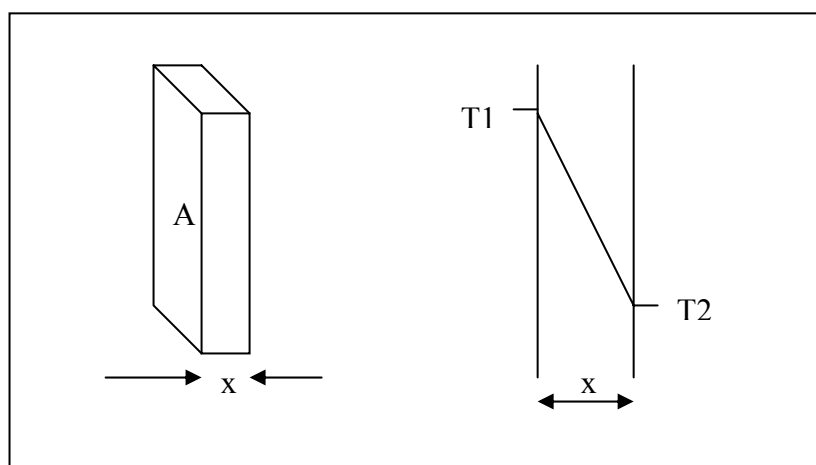


Figure 4-9: Temperature Gradient across Wall

Note that the negative sign indicates a heat flow from a higher to lower temperature. For BLUEsat analysis, we consider conduction in terms of conduction heat rate per unit area or flux where:

$$q \equiv \frac{Q}{A}$$

#### 4.3.3 Radiation

While the transfer of heat energy by convection and conduction requires the presence of a material, radiation does not. Radiation is the transfer of heat energy via electromagnetic energy and is the most complex of forms. For a non black surface, the transfer of heat energy via radiation is based on the Stefan Boltzmann Law for blackbody radiation. A blackbody is considered a perfect emitter.

$$Q = \varepsilon \sigma A T^4$$

$\varepsilon$  = ratio of energy emitted from a non black surface to a blackbody emitter

$\sigma$  = Stefan-Boltzmann constant (5.670 E-08 W/m<sup>2</sup>K<sup>4</sup>)

A = radiating area

Thermal radiation occurs only within a particular range of the electromagnetic spectrum. For the purposes of thermal analysis, we are only concerned with radiation between the wavelengths 0.1 to 100 microns.

The complication lies with the geometrical dependence of the radiating surface. This is often described as the view factor and is the fraction of radiation leaving a surface which is intercepted by another. Calculation of view factors is best explained by the following model used by Karam. [15]

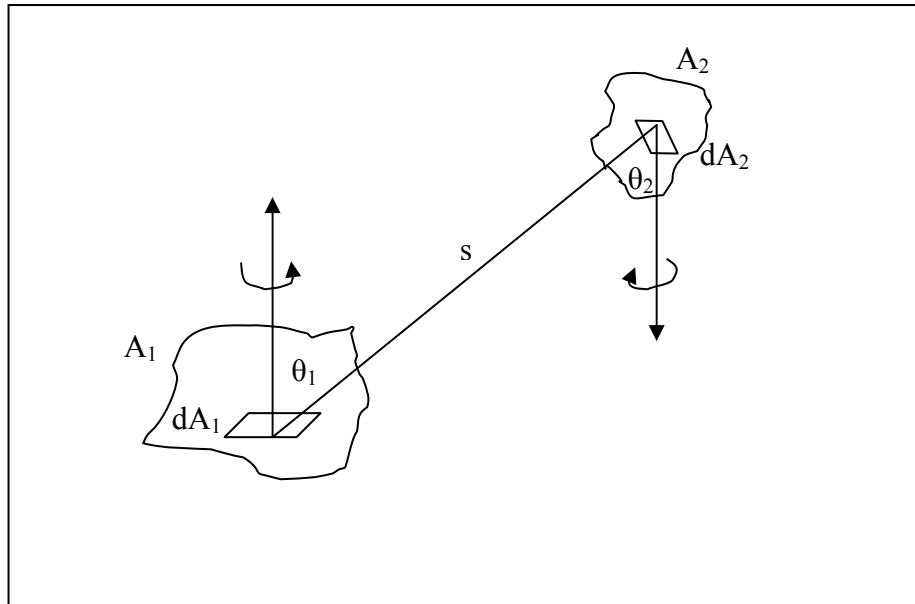


Figure 4-10: View Factor Calculation

Calculation of the fraction of total radiated energy from surface 1 that is intercepted by surface 2 can be related as:

$$F_{12} A_1 = \iint_{A_1 A_2} \frac{\cos \theta_1 \cos \theta_2}{\pi s^2} dA_1 dA_2$$

Most radiation analysis codes can calculate these interchange factors between surfaces.

## 4.4 **Passive Thermal Control Systems**

The role of this thermal analysis was to deduce what level of thermal control systems should be implemented. The simplicity of BLUEsat's design and limited power output really only permits the use of Passive Thermal Control Systems. This is a beneficial system for BLUEsat because it:

- Has no moving parts
- Does not require power input

Prior AMSAT microsatellites have successfully functioned with only the use of specialised paints and tapes to optically manipulate the  $\epsilon$  and  $\alpha$  property of the external and internal surfaces. Such microsatellites include PACSAT, LUSAT, DOVE and WEBERSAT which utilised the use of OSR and VDA (Vapour Deposited Aluminium). [1]

The following summarises the techniques used for passive thermal control systems since active measures are not related to the design of BLUEsat.

### 4.4.1 **Thermal Coatings**

The role of thermal coatings such as Optical Solar Reflectors (OSR) and Vapour Deposited Aluminium (VDA) is to minimise solar absorbed energy and infrared emission while emitting dissipated satellite heat energy. Other coatings can be used to improve absorptivity such as black paint, commonly used internally to assist temperature averaging via radiation. [10]

Surface Coating	$\alpha$ – Solar Absorptivity	$\epsilon$ - Emissivity
8-mil quartz mirrors (OSR)	0.005 to 0.008	0.8
Diffuse quartz mirrors (OSR)	0.11	0.8
2-mil silvered Teflon (OSR)	0.05 to 0.09	0.66
5-mil silvered Teflon (OSR)	0.05 to 0.09	0.78
2-mil aluminized Teflon (OSR)	0.1 to 0.16	0.66
5-mil aluminized Teflon (OSR)	0.1 to 0.16	0.78
Chemglaze Z306 (Black Paint)	0.92 to 0.98	0.89
3M Black Velvet	0.97	0.84

Table 4-5: Selection of OSR and other Control Coatings

#### 4.4.2 Insulation

Multilayer insulation (MLI) is often used to insulate the internals of a satellite from the environmental effects on the external surface. Manned spacecraft and Astronaut space suits are examples that use MLI.

Its construction consists of multiple layers of thin Mylar sheets with a vacuum deposited aluminium finish on one side. The sheets provide a low contact area to reduce heat transportation. [11]

Degradation is an issue for LEO spacecraft because of the interaction between the MLI and atomic oxygen. This results in the oxidation of the polymers within the thermal blanket. [12]

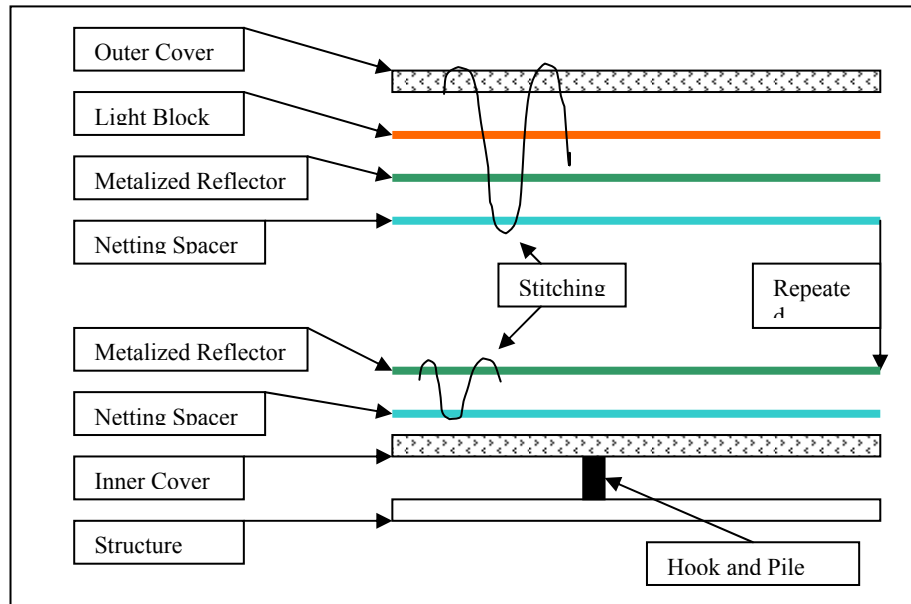


Figure 4-11: Typical MLI Cross-Section (Courtesy of NASA)

#### 4.4.3 Radiators

All heat dissipation from BLUEsat is radiated into space. Types of radiators include spacecraft panels, mounted flat plat radiators and deployable panels.

Aluminium Honeycomb acts as a passive form of radiator. Its benefits are the lateral spread of heat across the face sheets and core conductivity. The implantation of heat pipes into the aluminium honeycomb core can also assist for high heat dissipation hardware.

#### 4.4.4 Conductive Pads

Joints where components are fixed to one another (usually by bolts) exhibit rather poor thermal conduction. Conductive pads are generally made of silicon filled with silver or carbon particles in order to increase the conductivity.

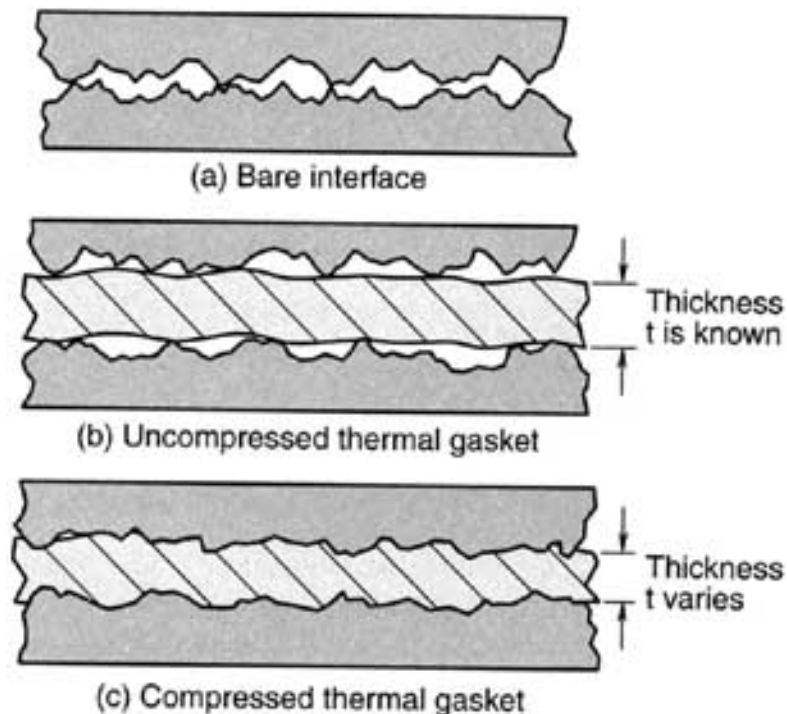


**Figure 4-12: Usage of a thermal gasket for increased conductivity**  
(Courtesy D. Gilmore [2])

CHO-THERM is a particular thermal gasket available on the market, producing good thermal conduction and poor electrical conduction.

#### 4.4.5 Phase Change Materials

Phase change materials absorb thermal energy by transforming from solid to liquid in its simplest form. These are commonly used on electrical components via thermal straps. The use of these systems is recommended for use with components that typically operate an on-off cyclic basis. This is so that the phase change material can refreeze via radiation thus preparing it for another cycle.

Phase change materials can be used smartly by linking a central phase change material to a system of heat pipes. These are then linked to a number of electrical circuits. As the circuits heat up and transfer the heat to the phase change material, it will store the heat energy via melting. For times when the circuits are off and need some “non-operating” temperature requirement, the phase change material will solidify and thus transform heat energy back to the circuit. This is known as Phase Change Material Thermal Energy Storage (PCM-TES).[13]

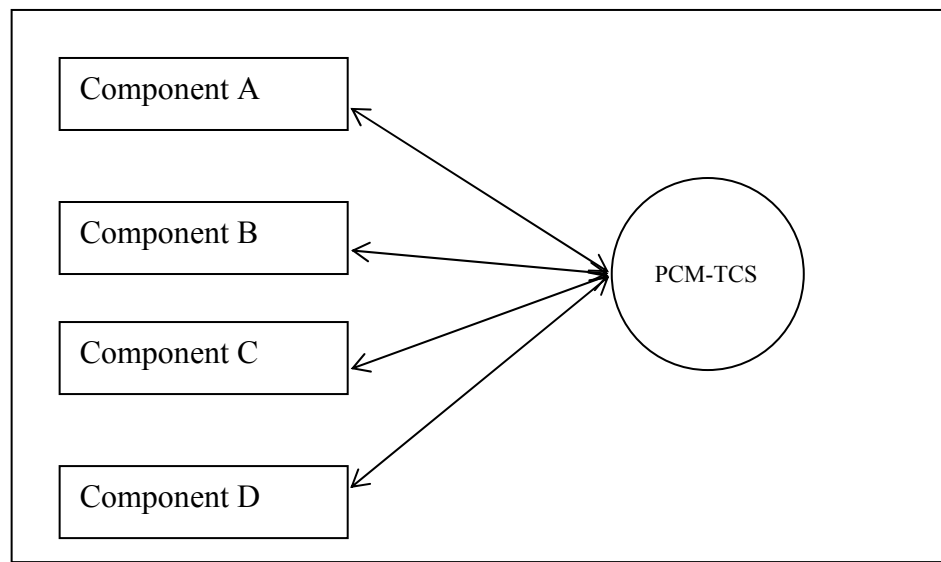


**Figure 4-13: PCM's can be used to maintain onboard temperatures for critical hardware**

## 5 Preliminary Analysis Strategy

### 5.1 Spherical Satellite Analysis

Prior to the computational analysis of SINDA and NEVADA software, a simple model must be calculated to estimate the temperature ranges expected in orbit. This simple calculation takes advantage of an isothermal spherical representation of BLUEsat in orbit under the influence of the energy balance:

$$Q_{absorbed} + Q_{dissipated} - Q_{emitted} = 0$$

Where

$$Q_{absorbed} = Q^S + Q^A + Q^I$$

$$= A_C q^S \alpha + AFq^I \varepsilon + AFq^S a \alpha K_a$$

$$Q_{dissipated} = hardware\_power$$

$$Q_{emitted} = \sigma \varepsilon A T^4$$

The use of a sphere to represent BLUESat is beneficial to its simplicity because the view factors can remain constant even if we assume the sphere is spinning and polar flipping like the actual satellite will in orbit.

Using this relationship the worst case maximum and minimum temperatures were calculated via the following steps. [3]

1. Determine the total surface area.

- TOP PLATE =  $0.238 \text{ m} \times 0.238 \text{ m} = 0.056644 \text{ m}^2$
- SIDE PANELS =  $0.236 \text{ m} \times 0.222 \text{ m} = 0.052392 \text{ m}^2$
- BOTTOM PLATE =  $0.2 \text{ m} \times 0.2 \text{ m} = 0.04 \text{ m}^2$

Therefore the total surface area equals

$$A = 0.056644 + 4 \times 0.052392 + 0.04 = 0.306212 \text{ m}^2$$

2. Sphere Diameter

$$D = \sqrt{A/\pi} = 0.312202349 \text{ m}$$

3. Using the same orbital parameters, solar flux, earth albedo and earth IR as is the SINDA analysis we have the following:

Altitude (H)	700 km
Radius of Earth ( $R_E$ )	6367 km
Angular Radius of Earth ( $\rho = \sin^{-1}(R_E/(H+R_E))$ )	1.122 rad
Direct Solar Flux ( $q^S$ )	1367 W/m <sup>2</sup>
Earth Albedo ( $q^A$ )	30 % of Solar Flux
Earth IR ( $q^I$ )	236 W/m <sup>2</sup>

**Table 5-1: Fixed Calculation Values also used in SINDA**

4. At any particular time, the Solar Flux will be loaded onto half the sphere in orbit. We account for the total cross-sectional area to determine the amount of solar flux energy absorbed. Therefore, the cross sectional area is:

$$A_C = \pi \times (0.3122)^2 / 4 = 0.076552 \text{ m}^2$$

5. Panetti [3] includes an earth albedo correction factor,  $K_a$ , which accounts for the reflection of collimating incoming solar energy off a spherical earth. And similarly  $F$ , the view factor of an infinitesimal sphere viewing a finite sphere.

$$K_a = 0.664 + 0.521\rho - 0.203 \rho^2 = 0.993$$

$$F = (1 - \cos \rho) / 2 = 0.283$$

6. The optical properties of the satellite in this calculation are for a ‘naked’ satellite without any thermal coatings. An excel spreadsheet was used to determine all the exposed surface areas of each material for the top plate, side panels and bottom plate. This was then interpolated to determine the

average emissivity and absorptivity per panel. For this calculation we make another average for the total spacecraft optical properties.

Panel	Absorptivity $\alpha$	Emissivity $\varepsilon$
Top Plate	0.574864495	0.6603965
Side Panel	0.585788417	0.6978979
Bottom Plate	0.530298519	0.5227838
<b>TOTAL S/C AVG</b>	<b>0.57472</b>	<b>0.66246</b>

**Table 5-2: Absorptivity and Emissivity values as calculated in appendix C**

7. The total internal heat generation via electrical components (heat dissipation) is expected to have a minimum to maximum range of 2 to 7 W.

Therefore  $Q_{dissipated} (\text{Min}) = 2 \text{ W}$

$Q_{dissipated} (\text{Max}) = 7 \text{ W}$

8. Thus solving for T into the energy balance equation we get for worst case hot and worst case cold:

$$T_{MAX} = \left[ \frac{A_C q^S \alpha + AFq^I \varepsilon + AFq^E a \alpha K_a + Q_{dissipated} (\text{max})}{A \sigma \varepsilon} \right]^{1/4}$$

$$= 306.09 \text{ K}$$

$$= 33.09 \text{ }^{\circ}\text{C}$$

$$T_{MIN} = \left[ \frac{AFq^I \varepsilon + Q_{dissipated}(\min)}{A\sigma\varepsilon} \right]^{1/4}$$

$$= 191.74 \text{ K}$$

$$= -81.25 \text{ }^{\circ}\text{C}$$

These results provide insight to the expected temperature ranges for the SINDA analysis. Note that this calculation holds many assumptions, one in particular being that it was solve as a steady state (time independent) calculation. It would be expected that transient effects due to thermal capacitance should exhibit lower maximum temperatures and higher minimum temperatures. [3].

## 5.2 *Honeycomb Panel Assumptions*

At this point it is important to discuss the honeycomb panel assumption used within the entire analysis. That is, that the core conductivity of the aluminium core is considered negligible in relation to the skin lateral conductivity.

The aluminium honeycomb used on BLUEsat is HEXCEL 4.3-1/4-20 5052 Aluminium designation. [14]

Honeycomb Designation	Stabilised Compression		Plate Shear				Maximum Thickness mm
	Strength (MPa)	Modulus (MPa)	Strength "L Direction" (MPa)	Modulus "L Direction" (MPa)	Strength "W Direction" (MPa)	Modulus "W Direction" (MPa)	
1.8-3/4-25	0.95	215	0.74	182	0.46	96	150
2.3-1/4-10	1.35	310	0.96	220	0.58	112	150
3.0-3/8-20	2.10	485	1.35	295	0.85	145	150
3.1-3/16-10	2.30	517	1.45	310	0.90	152	150
3.4-1/4-15	2.60	620	1.60	345	1.10	166	150
3.7-3/8-25	2.95	725	1.80	380	1.17	180	150
3.9-1/2-40	3.30	820	1.94	405	1.25	190	150
4.3-1/4-20	3.75	965	2.20	455	1.45	205	150
4.4-3/16-15	4.10	1000	2.25	470	1.48	210	150
4.5-1/8-10	4.20	1034	2.30	483	1.50	214	150
5.2-1/4-25	5.20	1310	2.80	565	1.80	245	150
5.4-3/8-40	5.35	1380	2.90	590	1.95	250	150
5.7-3/16-20	5.80	1520	3.15	620	2.05	265	150
6.9-3/16-25	8.00	1965	4.04	785	2.50	320	75
7.9-1/4-40	10.00	2345	4.80	896	2.90	364	75
8.1-1/8-20	11.00	2414	5.00	930	3.00	372	50

**Table 5-3: Compressive and Shear Properties for Selected Honeycomb Panel**

This designation represents 5052 H39 grade aluminium with a hexagonal cell profile. The cell size is  $\frac{1}{4}$  inch and nominal sheet thickness of 0.002 inch. The core density is 4.3 pounds per cubic foot which translates to be  $68.87 \text{ Kg/m}^3$ . The table above also specifies the shear properties in bot the L and W directions which are illustrated below.

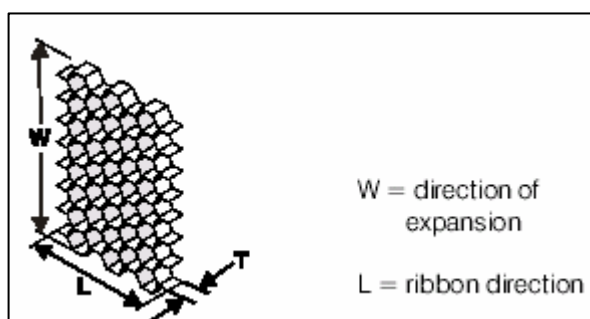


**Figure 5-1: Direction Definition for Honeycomb Core**

The conductivity of heat through the core is largely reduced due to the void of solid material. The thinness of the core sheets also makes the lateral core conductivity negligible in comparison (refer to APPENDIX G).

Karam [15] states that heat conduction between the skins (core conductivity,  $k_c$ ) can be estimated from the relationship:

$$k_c = k_m \left( \frac{\rho_c}{\rho_m} \right)$$

Where  $k_m$  = material conductivity (5052 H39)  
 $= 132 \text{ W/m K}$   
 $\rho_c = 68.87 \text{ kg/m}^3$   
 $\rho_m = 2680 \text{ kg/m}^3$

$$\text{Therefore } k_c = 3.392 \text{ W/m K}$$

This is a reasonable sized core according to Karam: “For aluminium honeycomb,  $k_c$  ranges from about 1 W/m K (very light core) to 5 W/m K (heavy core)”.[15]

Although not completely insignificant (approximately 2.47 % of skin conductivity) it has been neglected for ease of analysis where setting up complex 3D orthotropic material properties proved time consuming and erroneous to the initial BLUESat thermal analysis.

Modelling of honeycomb in both the SINDA and Patran model was however considered as a primary recommendation concluding this thesis. For a more accurate calculation of core lateral and transverse directions refer APPENDIX G.

## 6 Finite Differencing Method Analysis

The following presents in order the procedure used to determine the temperature distributions across the entire satellite structure. Initial efforts were to conduct the entire analysis via the Finite Element Analysis software Msc PATRAN and NASTRAN THERMAL solver.

However the complexity of the orbital relationships of the satellite, earth and sun present difficulties in determining the flux exposure to BLUEsat's external surfaces.

This thesis project then set out to use current TMM (Thermal Mathematical Model) Computer codes used in the space industry. SINDA/G, written by J. Gaski, was used to determine the temperatures across the external panels of BLUEsat in orbit.

Once these temperatures were gathered (refer APPENDIX B) a selected range of temperatures (one complete orbit range) was input into a more detailed Finite Element Model using Msc Patran. Results were calculated using Msc Nastran Thermal (an included analysis package using SOL 153 (steady state) and SOL 159 (transient) solvers.)

This finally displayed the required temperature distributions across the entire satellite structure, providing insight into the level of Thermal Control System implementation.

The use of a finite element code such as Patran and Nastran, also allowed us to conduct stress analysis.

## **6.1 Overview**

SINDA/G stands for Systems Improved Numerical Differencing Analyser (G for Gaski, the creator of the software). SINDA/G is separated into two parts:

1. Pre-processor
2. Library

The pre-processor reads in the problem and constructs a program executable using FORTAN language. The user then can select a pre-written subroutine from the SINDA library to obtain temperatures. [16]

For the analysis, only the transient sub-routine SNDUFR was used because it is the “best overall transient subroutine which balances accuracy and speed and requires the analyst to specify the time step” [23]

The following lists the available transient sub-routines of SINDA that are still in use in the space industry.

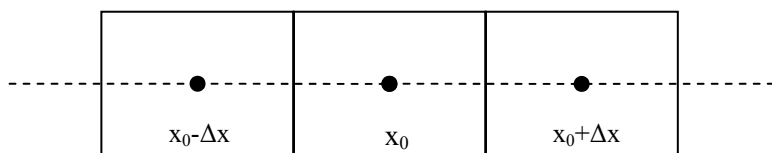
Long Pseudo-Compute Sequence		Description
SNFRDL		Explicit forward differencing, block iteration
FWDBKS		Quartic or linear equation, implicit finite differencing
FWDBCK		Similar to FWDBKL but no local double precision calculations
FDBKCD		Same as FWDBKL with connect and disconnect capabilities
SNAE		Alternating direction explicit finite differencing
SNDUFR		Modified Dufort-Frankel explicit finite differencing
ATSDUF		Automatic time step selection, like SNDUFR otherwise
ATSF BK		Automatic time step selection, like FWDBCK otherwise
SNTSM		Taylor series with weighted average, automatic time step

Table 6-1: Transient sub routines available in SINDA/G

## 6.2 Finite Differencing Technique

In its simplest description, the finite differencing technique uses a discrete network of nodes (or sub volumes) representing the capacitance of the system. These are interconnected by conductors. Taylor Series approximation is then used to calculate the temperatures. Gilmore [2] describes the following finite differencing method.

Consider the one dimensional mesh:



The Taylor Series about  $x_0$  for the temperature  $T$  is

$$T(x_0 + \Delta x) = T(x_0) + \left. \frac{\partial T}{\partial x} \right|_{x=x_0} \cdot \Delta x + \left. \frac{\partial^2 T}{\partial x^2} \right|_{x=x_0} \cdot \frac{\Delta x^2}{2!} + \left. \frac{\partial^3 T}{\partial x^3} \right|_{x=x_0} \cdot \frac{\Delta x^3}{3!} + \dots$$

Where the first and second derivatives can be derived with an associated truncation error of  $O(\Delta x)$  and  $O(\Delta x^2)$  respectively.

The heat conduction equation for a one dimensional heterogeneous, anisotropic solid is then

$$\rho C_p \frac{\partial T}{\partial t} = \frac{\partial}{\partial x} \left[ k_x(T) \frac{\partial T}{\partial x} \right] + Q(T, t)$$

- $\rho$ =density
- $C_p$ =specific heat
- $Q(T, t)$  =source term for input of heat via radiation, conduction and other heat sources ( $\text{W/m}^3$ )

Appling Taylor series therefore yields

$$\frac{\partial}{\partial x} \left[ k_x(T) \frac{\partial T}{\partial x} \right] = \left[ k_x \cdot \left( \frac{T_{n+1}(x + \Delta x) - T_n(x)}{\Delta x} \right) - k_x \cdot \left( \frac{T_n(x) - T_{n-1}(x - \Delta x)}{\Delta x} \right) \right] / \Delta x$$

- $n$ =node number where Taylor series is applied

We now have a relationship of the heat equation in Taylor Series formation as a function of temperature on a 1 dimensional example. Next step is to incorporate the conductors of the Finite Differencing system.

Now apply the volume ( $\Delta x \cdot A$  where  $A = \Delta y \cdot \Delta z$ ) represented by the node to the above equation.

$$A \cdot k_x \cdot \frac{(T_{n+1} - T_n)}{\Delta x} - A \cdot k_x \cdot \frac{(T_n - T_{n-1})}{\Delta x}$$

SINDA translates the terms  $A \cdot k_x$  into the parameter  $G$  which is the conductance. This is called from the conductance block from the SINDA input file (refer APPENDIX A). Therefore from the above equation, the partial differential equation of heat transfer can now be solved for as a set of finite difference equations.

### 6.3 **SINDA /ATM Model**

The initial BLUESat model was developed with SINDA/ATM (Advanced Thermal Modeller). ATM is a FEM mesh generator similar to the interface of Patran. SINDA uses this software to develop more sophisticated satellite models and then converts the information to a Finite Differencing input file (SIN file). For this thesis project, a 300 node demo version of the software was made available along with full versions of SINDA/G solver and NEVADA radiation

software. SINDA / ATM allow the user with the ability to conduct orbital thermal analysis by an interactive procedure [24]:

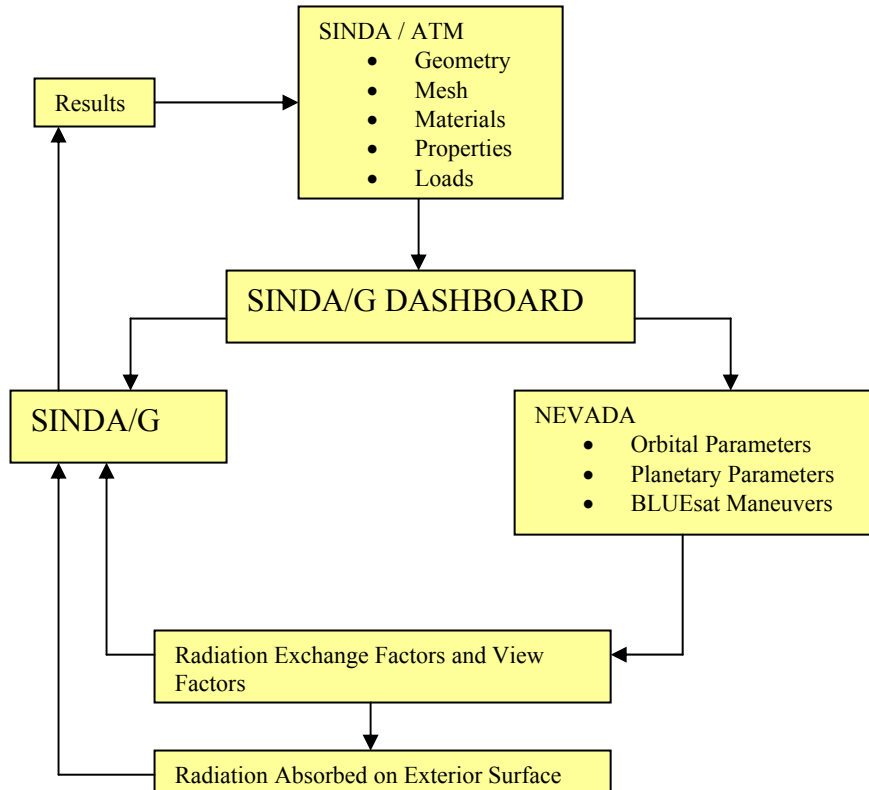


**Figure 6-1: Finite Differencing Analysis Process**

### 6.3.1 Geometrical Model

The objective of the SINDA model was to obtain temperature distributions across all the external surfaces of the BLUEsat structure. This includes the top plate, side panels and bottom plate. The modelling strategy used was to create a six surface cube of representative dimensions to the actual BLUEsat design.

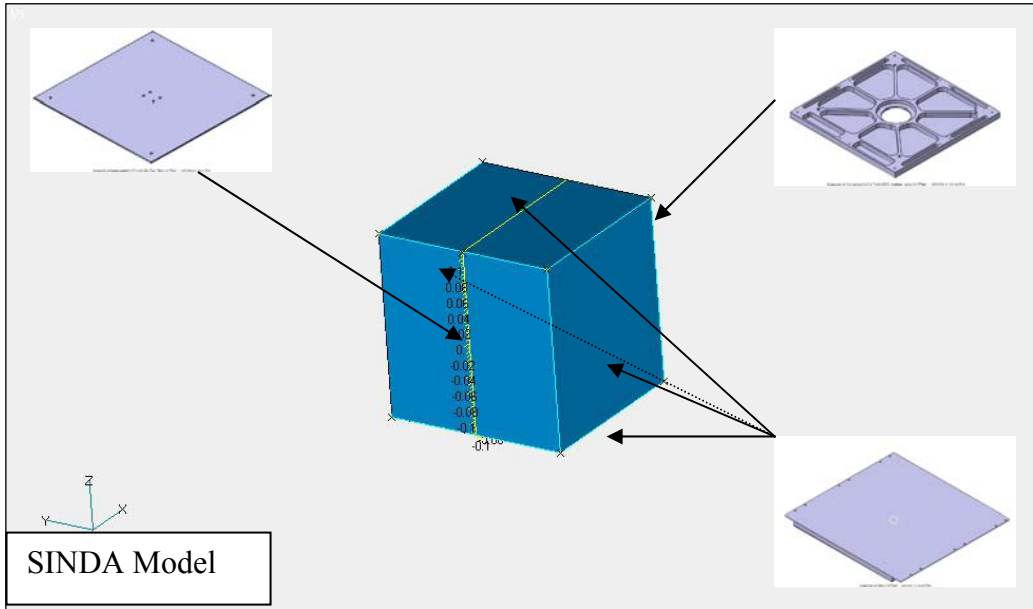


**Figure 6-2: Six surface cube representation of BLUEsat's external panels**

Each surface is connected via its eight nodes generated for the mesh. The dimensions used in this model were tabulated below as well as a comparison to the actual model.

DIMENSIONS	ATM Model (m)	Actual Model (m)
Top Plate	$0.236 \times 0.236$	$0.236 \times 0.236$
Side Panels	$0.236 \times 0.222$	$0.236 \times 0.222$
Bottom Plate	$0.236 \times 0.236$	$0.200 \times 0.200$

**Table 6-2: Dimension comparison with physical model**

This over-representation of the bottom plate means that there will be a greater surface area modelled for the analysis. It would be expected that the results would show temperatures slightly higher (almost negligible due to the vast variety of other significant factors) than the actual model since BLUEsat's heat dissipation is a function of surface area.

### 6.3.2 Materials and Properties

Each surface was assigned the materials relevant to the actual model (refer APPENDIX F). As mentioned earlier, the aluminium honeycomb core has been neglected for the purposes of this thesis project. Therefore the back facing skin was also neglected. The representative honeycomb surfaces in this model are given 1 mm thicknesses with is the skin thickness of the actual honeycomb panel.

### 6.3.3 Loads

For orbital analysis the loads condition was set up for radiation. The surface optical properties that were set up were based on surface average absorptivity and emissivity values calculated in Excel (refer APPENDIX C). This process involved calculating the individual components exposed surface area and compiling that with their respective optical values. An equivalent surface  $\epsilon$  and  $\alpha$  values were then determined for both a naked structure (no external thermal control coatings) and an OSR coated structure (commonly used on previous microsatellites).

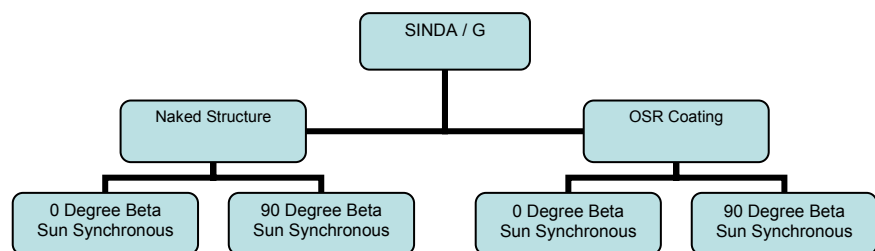


Figure 6-3: Orbital / Optical Scenarios

FIG 6-4 and 6-5 provide a visual representation of these load properties on each surface.

It was expected that for the OSR model, lower overall temperatures would be present because of the higher emissivity properties which mean the spacecraft will emit more heat energy to space.

Naked Optical Properties			
<b>Top Plate</b>			
$\alpha=0.57$ $\varepsilon=0.66$			
Side 3 (-Y)	Side 2 (+z)	Side 1 (+y)	Side 4 (-z)
$\alpha=0.59$ $\varepsilon=0.70$	$\alpha=0.59$ $\varepsilon=0.70$	$\alpha=0.59$ $\varepsilon=0.70$	$\alpha=0.59$ $\varepsilon=0.70$
<b>Bottom Plate</b>			
$\alpha=0.53$ $\varepsilon=0.52$			

Figure 6-4: Naked Structure Panel Optical Properties

				Top Plate
				$\alpha=0.57$ $\epsilon=0.80$
Side 3 (-Y)	Side 2 (+z)	Side 1 (+v)	Side 4 (-z)	
$\alpha=0.60$ $\epsilon=0.80$	$\alpha=0.60$ $\epsilon=0.80$	$\alpha=0.60$ $\epsilon=0.80$	$\alpha=0.60$ $\epsilon=0.80$	
				Bottom Plate
				$\alpha=0.46$ $\epsilon=0.79$
OSR Optical Properties				

Figure 6-5: Optical Solar Reflector Panel Optical Properties

## 6.4 NEVADA

### 6.4.1 Overview

NEVADA uses the program VEGAS-Verified Earthshine and Geometric Albedo and Solar to calculate the external heat inputs on a set of surfaces. Its capabilities include determination of direct and reflected solar, albedo and Earth IR under orbital parameter conditions. The user also has the ability to input spacecraft orientation modes in orbit. The program also considers planetary eclipses and other shadowing effects.

### 6.4.2 BLUESat Orbital and Planetary Parameters

BLUESat was analysed for two orbital types, one with maximum eclipse time of half the orbital period (1.642 hours) known as a 0 degree beta angle, and the other providing BLUESat with a pure sun-lit orbit at 90 degree beta angle. It is fair to say these angles don't remain perfectly in position, low earth orbit spacecraft will exhibit some change in the beta angle during earths orbital period about the sun. [2] It is also interesting to note that a sun-lit or dusk-dawn orbit will only be achieved with the correct RAAN with respect to the sun. To model the spacecraft for a 0 degree beta angle, the suns position was simply place in line of the Vernal Equinox, such that both the Sun angle from Vernal Equinox and RAAN were both 0 degrees. For the 90 degree beta angle, the argument of the ascending node was place 90 degrees, hence also 90 degrees in relation to the sun. The orbital parameters used in NEVADA were as follows:

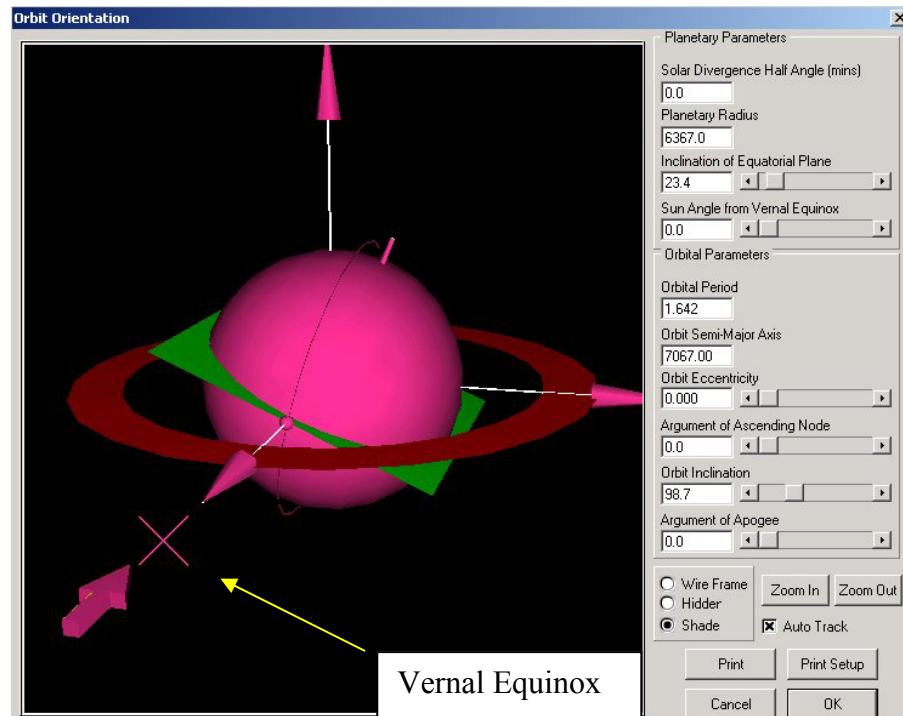


Figure 6-6: Nevada Interface for Planetary and Orbital Parameters. Sun and BLUESat both have 0 degree RAAN, therefore Maximum eclipse time.

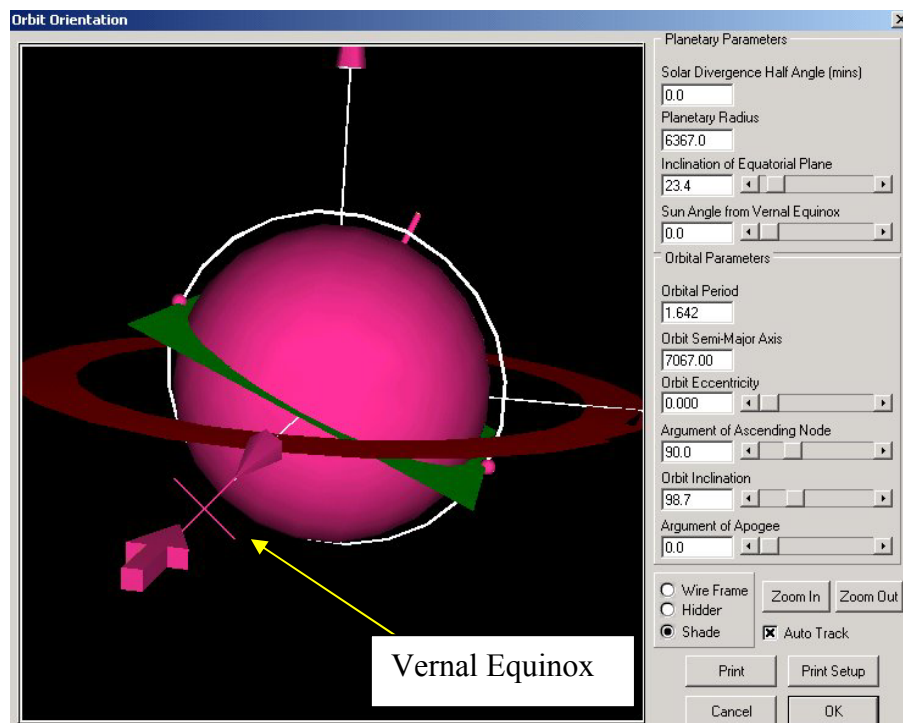


Figure 6-7: Setup used for 90 Degree Beta Angle. Note Sun is in direct line of the Vernal Equinox, therefore BLUEsat at 90 RAAN will obtain pure sun-lit orbit

#### 6.4.3 BLUEsat Orbital Manoeuvres

BLUESat uses passive magnetic attitude stabilisation based on the original AMSAT microsatellite. Four bar magnets with very strong dipole moments provide two flips of BLUESat per orbit; hence the thick bottom plate will either be exposing towards earth or away for majority of the orbit period (but not all). BLUESat's four bottom transmitter antennas provide a slow z-axis spin primarily for minimising harsh thermal gradients on the exterior panels.

These in-orbit manoeuvres were input into NEVADA via angle input into pitch, roll and yaw tables. NEVADA ran the orbital simulation for a total of 24 stages per orbit. Therefore at each 15 degrees about this orbit, the updated position of

BLUESat had to be input. Taking the initial orbit position in the analysis to have the bottom plate facing earth and a spin angle change of 0 degrees, the new spin angle was determined for each of the 24 stages per orbit. The following shows the calculation to determine this angle:

1. Telemetry of similar microsatellites shows a tendency for the spin rate to vary from 0.25 seconds to 2.5 minutes per revolution. This analysis has assumed BLUESat will achieve a 2 minutes per revolution z-axis spin.
2. BLUESat has an orbital period of 1.642 hours for 700km, which is equivalent to 5911.2 seconds per orbit.
3. For 15 degree intervals, BLUESat will take  $5911.2 / 24 = 246.3$  seconds
4. This equals exactly  $246.3 / 120 = 2.525$  revolutions, or 738.9 degrees of rotation.
5. Hence the new angular position could be assumed to be  $738.9 - 720$  degrees = 18.9 degrees

For this analysis we assume an angle change of **15 degrees** (735 degrees) for simplicity to the arduous task of manually inputting updated spacecraft positions per analysis stages.

This process was not entirely correct as the satellite should actually have completed 2 orbits by the time one angle change is done however a bug within the software when applying advanced manoeuvre positions prohibited the use of constant roll rate with respect to time. In effect, the combination of 15 degree spin steps with the perfect equatorial flip has resulted in the disappearance of sun exposure to a BLUESat side during the

orbit (Side 1). This situation meant lower panel temperatures as described later in chapter 10.

#### 6.4.4 Flux Loads

Flux loads were assumed constant over the orbital period. In the actual environment, we would expect near negligible earth albedo for a sun-lit orbit since the albedo is a function of reflectivity and at the umbra, albedo will simply just reflect at an angle past BLUEsat. Hence the analysis was going to provide a decent worst case hot temperature scenario. The values used were the same as what is documented under the chapter Orbital Thermal Environment.

Flux Type	Flux Load
Direct Solar	1367 W / m <sup>2</sup>
Earth Albedo	410 W / m <sup>2</sup>
Earth IR	236 W / m <sup>2</sup>

Table 6-3: Specified Flux loads used for analysis. Represent average conditions.

NEVADA then proceeded to determine the radiation exposed to the external surfaces and passed the results back into the Source and Array Data cards of the SINDA input file.

#### 6.5 Results

Results of the external temperatures for all four cases were then examined in SINDAPLOT and SINDA / ATM. All SINDAPLOTS have been included in APPENDIX D.

Initial comments on these plots would be that the analysis performed correctly due to the sinusoidal thermal variation of the nodal temperatures. Note the data evident at -273 degrees Celsius represents the space node. This is automatically input into the .SIN file by SINDA and is required for the determination of the panel temperatures (since the spacecraft will emit heat energy by radiation to space).

The orbital behaviour of the ecliptic orbit shows a rather large temperature cycle range (-30 to + 20 degrees Celsius) for both the naked and OSR BLUEsat's. Whilst this minimum temperature is a cause for concern (since the battery's require an absolute minimum temp of -5 degrees Celsius), it is still feasible when considering the only heat input during the eclipse periods is the  $236 \text{ W/m}^2$  Earth IR. It is also important to note that internal heat generation was neglected for this stage, so temperatures are expected to be higher for the Patran analysis.

The higher emissivity levels of the OSR satellite clearly show reduced maximum temperatures in both orbital cases as expected.

The sun-lit orbit shows a rather pleasing temperature range of between 0 to 20 degrees Celsius which is absolutely perfect for the onboard thermal environment. The usage of OSR seems to have translated this range down 10 degrees Celsius entirely.

This data has been collected for specific complete orbits where the transient effects have settled down and compiled in excel for determination of each panels temperatures over the orbital period.

## 6.6 **Validation of Results**

Data of both previous thermal analysis and current satellite telemetry was assessed to verify the feasibility of these results. Dick Jansson [1] conducted thermal analysis of the original AMSAT microsatellite. His results showed for a single node representation of LUSAT (also an AMSAT based design like BLUEsat) will experience orbit average temperatures -8.4°C to + 2.6 °C. However, King [4] establishes that the actual temperature results from PACSAT showed the following:

Temperature Point	Minimum	Maximum
Battery	-1.3 °C	+2.0 °C
+z (Top) Array	-19 °C	+21 °C
Receiver Module	-7 °C	+11 °C

Table 6-4: PACSAT Orbital Temperature Telemetry

LUSAT telemetry was also downloaded showing temperature ranges of approximately -23 °C to +30 °C which compares favourably to these results. This telemetry is also beneficial for its battery operating conditions which are perfectly placed between 0 and 10 °C.

Baturkin, [9] mentions “For spinning satellites with perpendicular position of rotation (x and y axis) and Sun light axes the external sides can be used as thermal sink, at emissivity /solar absorbance  $\alpha_s/\epsilon < 1$  the wall temperature will trend to the level of 10°C to 20°C.”

Hence there is strong enough evidence that the SINDA results of BLUEsat are acceptable. From these results, it would be recommended that BLUEsat be aimed at establishing a full sun-lit orbit profile due to its promising temperature ranges.

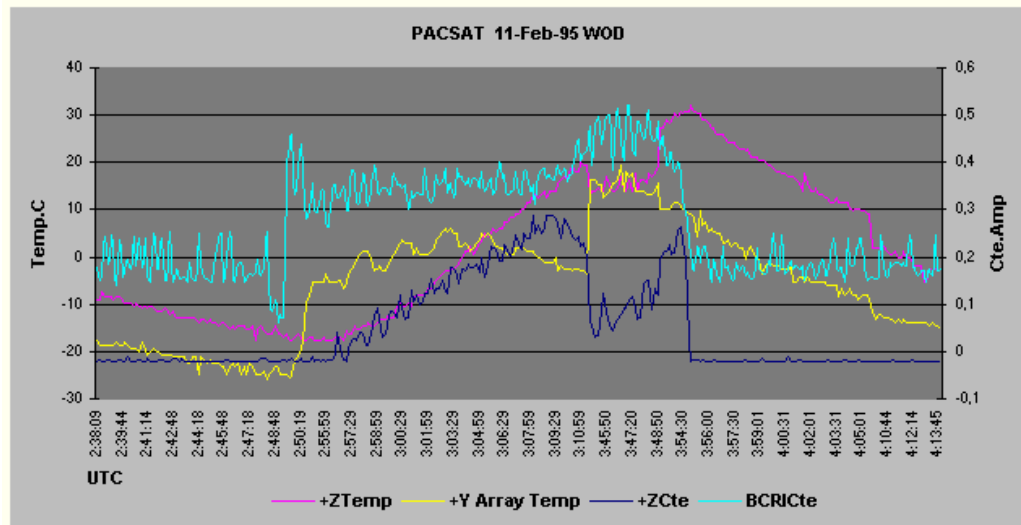


Figure 6-8: PACSAT Temperature Telemetry for a complete Orbit

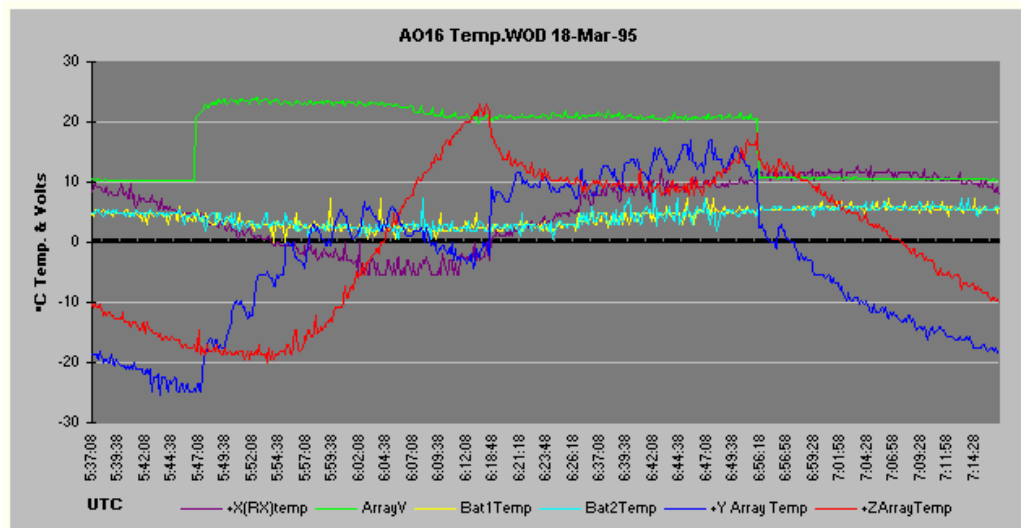


Figure 6-9: AO16 Temperature Telemetry including onboard Batteries 1 & 2 Temps

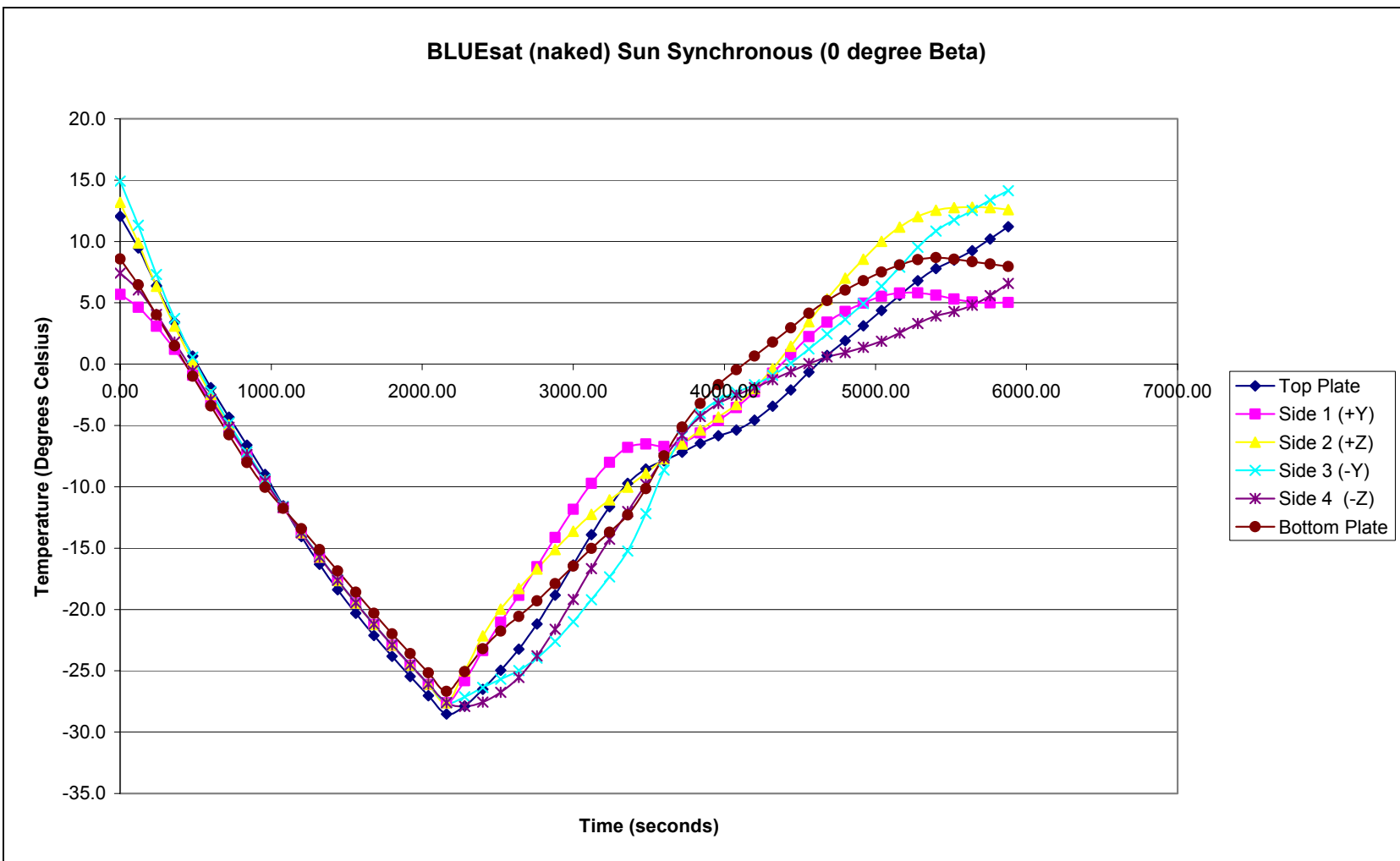


Figure 6-10: BLUESat External Panel Temperatures for Naked Structure, 0 Degree Beta

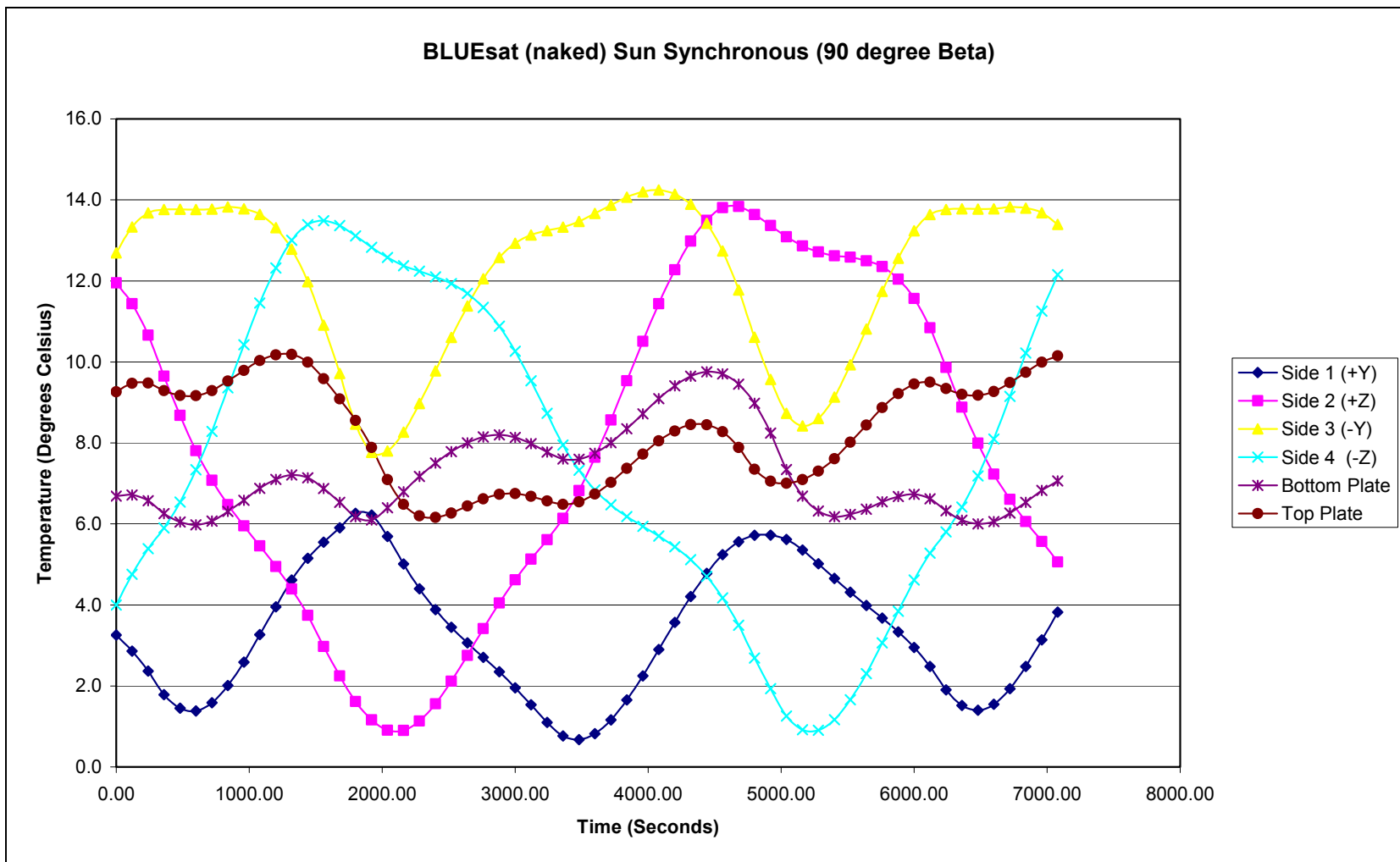


Figure 6-11: BLUESat External Panel Temperatures for Naked Structure, 90 Degree Beta

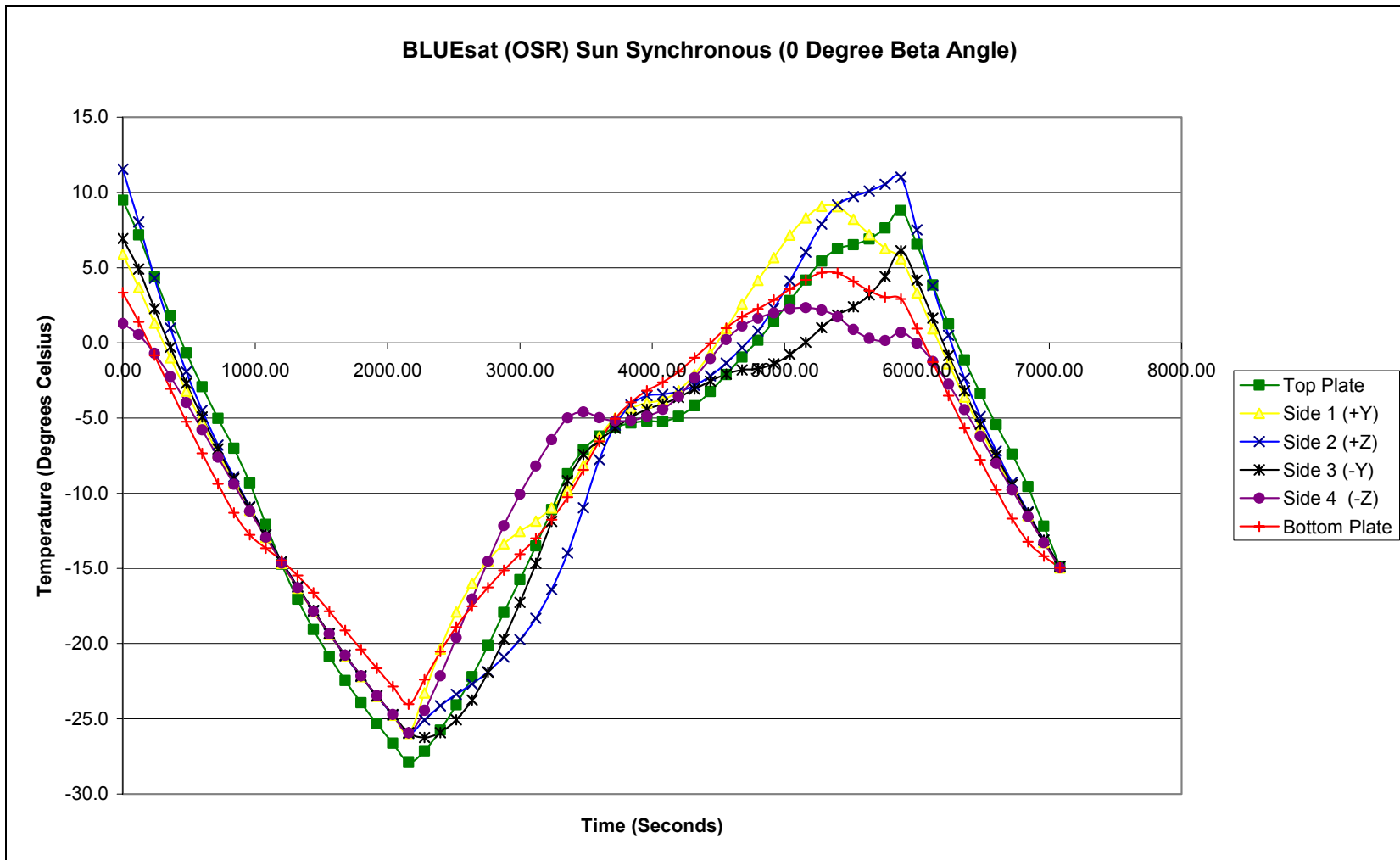


Figure 6-12: BLUESat External Panel Temperatures for OSR Structure, 0 Degree Beta

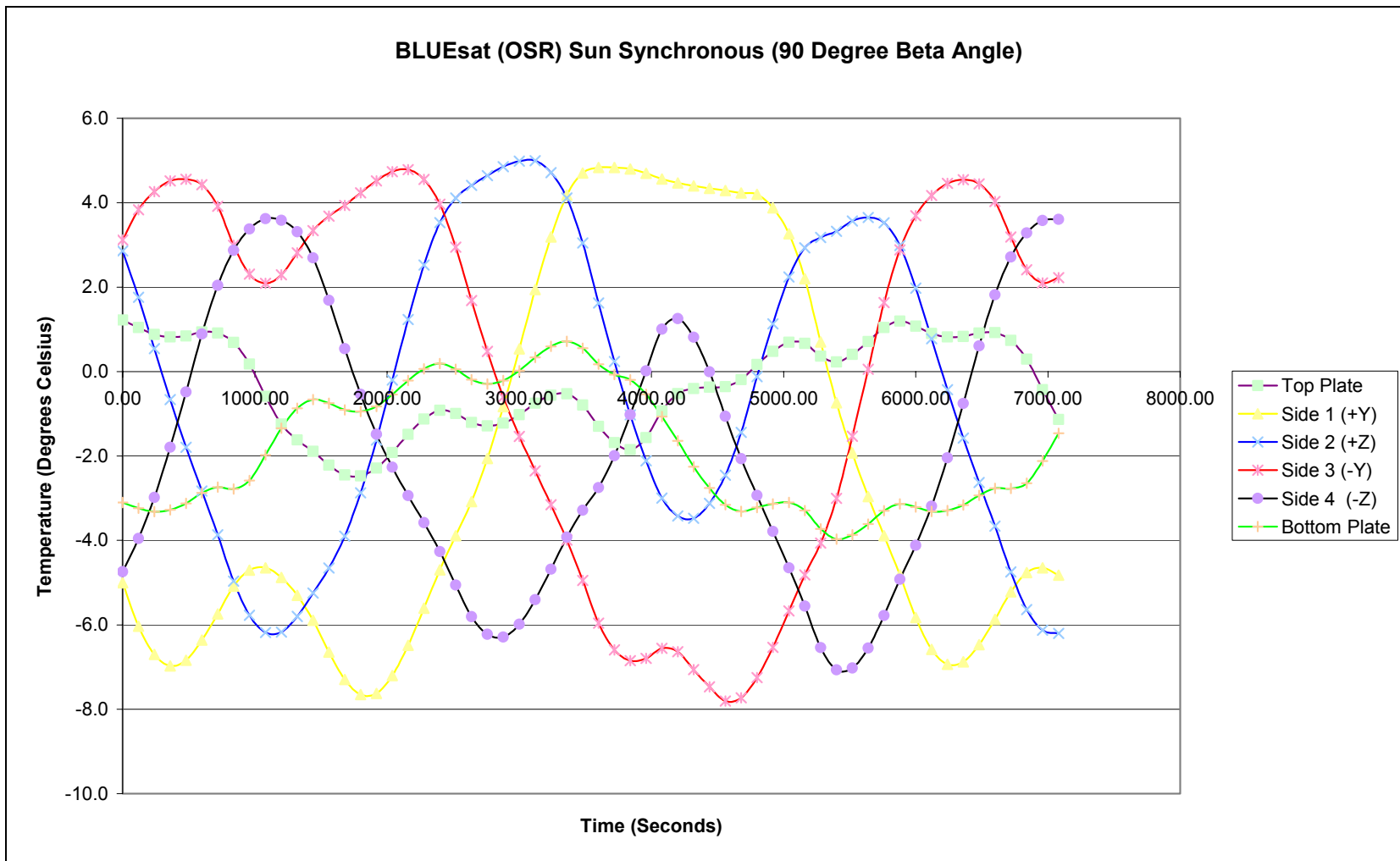


Figure 6-13: BLUESat External Panel Temperatures for OSR Structure, 90 Degree Beta

## 7 Finite Element Analysis

### 7.1 *Why Patran / Nastran Thermal?*

Generally a satellite thermal analysis is conducted entirely through means of finite differencing software such as SINDA/G. Usage of a large number of nodes for a more sophisticated model representation will provide the analyst with a substantially larger temperature results output, perhaps specifying transient temperatures for a given internal platform where electrical subsystems are mounted upon.

Due to the 300 node demo licence of SINDA / ATM and our desire to conduct thermal stress analysis, Patran along with Nastran Thermal Solver was selected. The versatile model importing and mesh seeding capability [2] of Patran allowed us to then build a highly representative model of the physical structure, hence we could analyse local temperature behaviours and ranges to determine the applicability of subsystems interfacing.

Once temperature distributions are mapped on the finite element model, structural analysis can be conducted to analyse structural misalignment and stress concentrations due to the effects of material thermal expansion and contraction.

## 7.2 **BLUESat Model**

The purpose of the five stack tray configuration is to modularise each of the main subsystems. Therefore a particular subsystem can be easily accessed simply by removing the affected tray.

The changing temperatures on each of BLUESat's 6 surfaces also mean that local and average temperatures within each particular tray subsystem will not be the same. Therefore we need to create a model of certain detail so as to monitor temperature behaviour for each tray.

It was considered that BLUESat should be modelled complete with the five tray stacks, battery plate, top plate, bottom plate, solar panel mounting blocks and the 4 side panels to achieve a fair representation of the actual flight model.

These are also the major load carrying and temperature conduction paths. The following describes the Patran modelling process.

### 7.2.1 **CATIA BLUESat Model**

Due to the complexities of many of BLUESat's component designs, it was considered modelling in CATIA would be the best option. Each component was redesigned in CATIA based on the original Pro-Engineer designs and verified with accurate Vernier Calliper measurements of the actual structure.

A level of simplification was applied to these components which were believed not to affect the analysis results. All holes were removed from the components to help the meshing of the structure later, as well as removing all webs from the bottom plate.

Each component was saved and exported as a B-Rep solid IGES file.

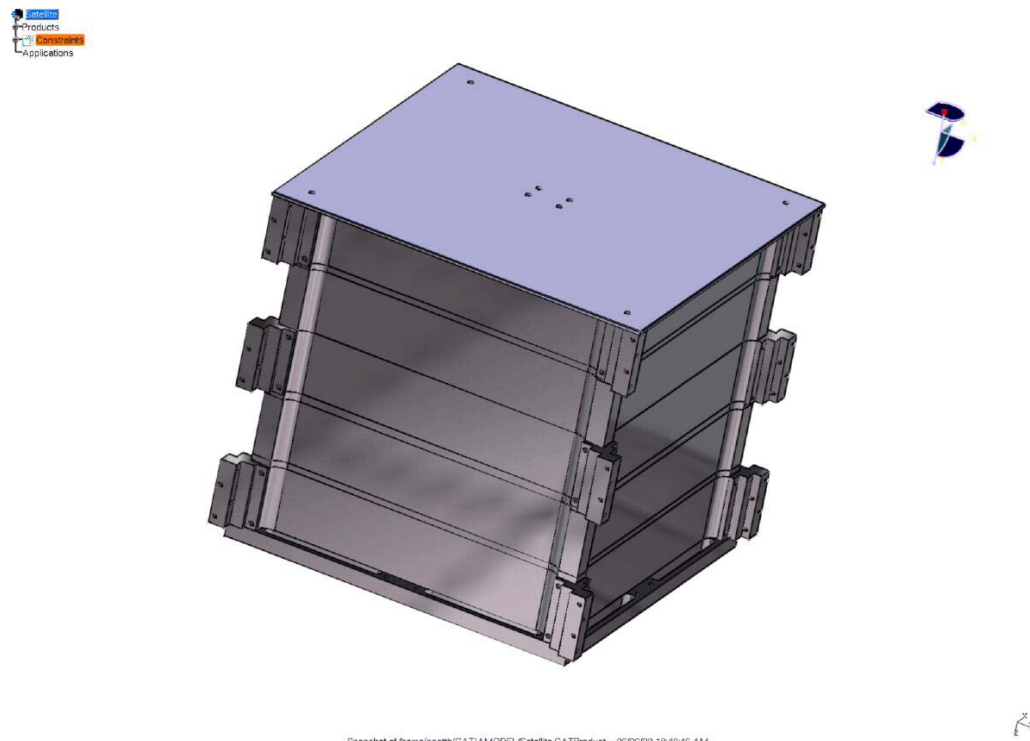


**Figure 7-1: CATIA assembly of BLUEsat's principal structures prior to simplification for importation into Patran.**

### 7.2.2 Patran Structural Model

Importing IGES components meant that points, curves and surfaces are created to represent the component. Therefore solids were extracted using the B-Rep function and all non solid geometries were removed.

The reason for deciding only to use solids for the thermal model was that earlier trials of combining shell elements with solids resulted in irregular output results.

Each component was then translated into correct position in preparation for meshing.

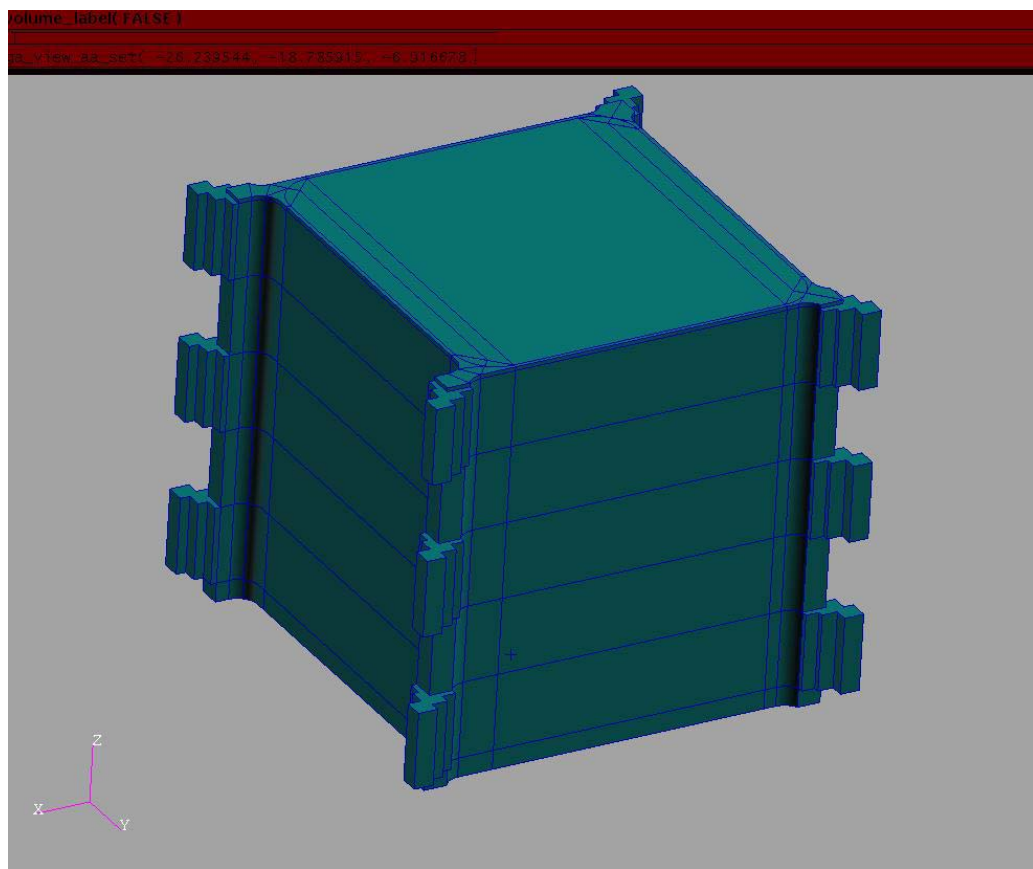


**Figure 7-2: Patran solid model of BLUEsat including module trays, battery, top and bottom plate and side panel mounting blocks.**

### 7.2.3 Modelling Considerations

#### 7.2.3.1 Joint Conductance

In reality, conduction of heat energy across the structure is unpredictable. Machining tolerances, surface finishes and other unforeseeable consequences

will mean that interfaces will exhibit a degree of thermal contact resistance.

Added to the fact the systems is in hard vacuum, it can be expected heat will only travel through a percentage of contacting area of the mating surface.

Hence with the uniformities of the mesh design for each component, it is assumed BLUEsat will have perfect joint conductance. For the physical structure to behave as a near perfect joint conductor, materials such as thermal gaskets, foils and increase torques should be considered.

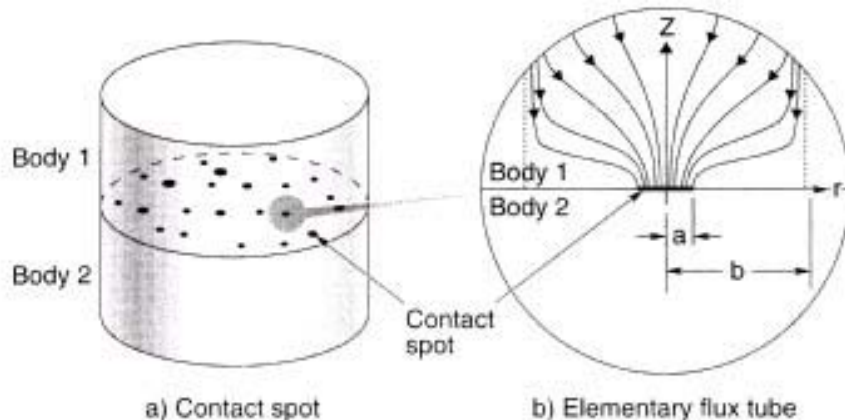


Fig. 8.6. Microcontacts and constricted heat flow. (Courtesy F. Milanez)

Figure 7-3: Conductive effects of surface roughness between joints. (Courtesy Gilmore [2])

### 7.2.3.2 Enclosure Radiation

As for the earlier SINDA analysis, radiation was applied to the external surfaces so calculation of the temperatures can be achieved. All surfaces within the structure will also radiate heat energy into one another, albeit to a lesser degree than conduction.

One capability of Nastran Thermal is its Enclosure Radiation function. It assumes normal linear radiation paths so each surface opposite of each other will interact. Therefore each of the sides of the trays were modelled as individual solids from the corners and meshed separately so an inner side enclosure radiation condition can be applied.

It was assumed only the flat surfaces of the trays will emit radiation is complexity of radiation of curved surfaces will tend to cause failed solution convergence.

### **7.3 *Finite Element Mesh Strategy***

Early attempts to use an auto-TET10 mesh of a near accurate structural model proved disastrous due to failed solution convergence. For thermal analysis, it became evident that the desire for intricate and large mesh maps was not necessary and a level of simplification yet not over assumption needed to be balanced. Cook [21] states that “a thermal FE model may be dictated less by thermal considerations than by an anticipated stress analysis based on the same mesh.”

Using the simplified BLUESat model created by pure solids, a mesh seed generated HEX mesh. Each tray was input the same mesh seed along with the top plate, bottom plate and battery plate (Tray 3 Plate) so the model could be equivalenced. Hence the assumption of perfect joint conductance.

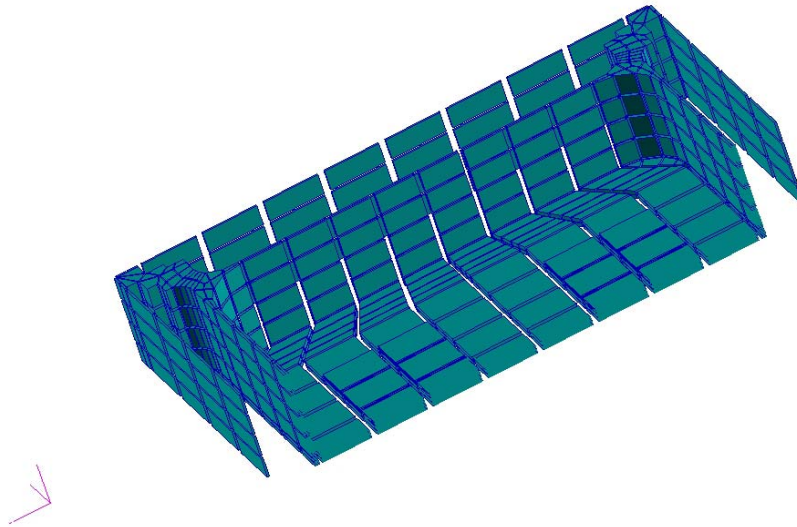


**Figure 7-4: Hex Mesh and equivalenced nodes of the battery module tray and interacting structure components.**

The prismatic design of BLUESat proved ideal for the mesh design as the number of curved surfaces is kept to a minimum. Therefore the total number of elements decreasing from an original TET mesh to a HEX mesh model was significantly lower.

Again the complexities of the webbed bottom plate proved difficult for a HEX mesh to be applied. Time permitting, a detailed bottom plate could have been incorporated but was not deemed essential to the desired thermal results.

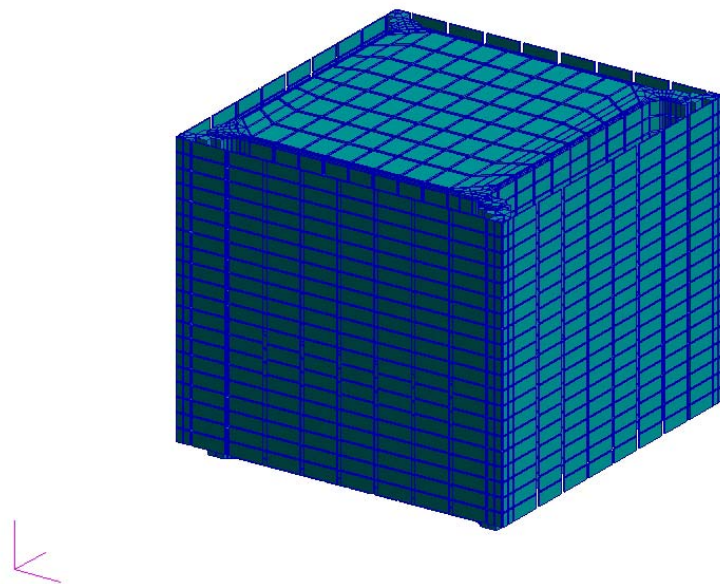


**Figure 7-5: Hex Mesh of complete BLUESat structure. Nodes at all interfaces were equivalenced to represent perfect joint conductance.**

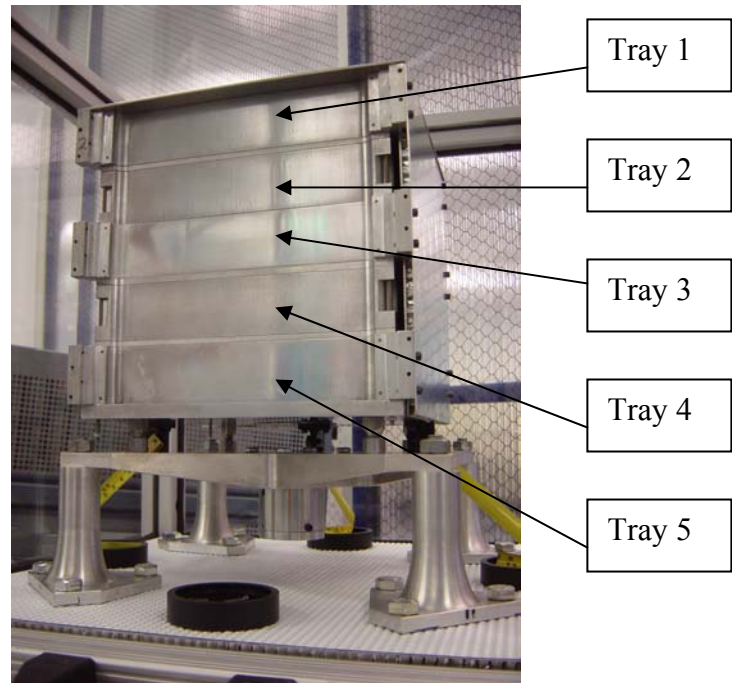


**Figure 7-6: Tray number allocation used in analysis**

## 8 Radiation Analysis of BLUEsat

### 8.1 *Effects of Internal Radiation*

Naturally it is easy to assume internal radiation negligible in relation to the responsiveness of thermal conduction, especially via metals which have by far the highest properties of thermal conduction and heat capacity than most other materials. However to achieve thermal control of such narrow margins when it comes to spacecraft, internal radiation must be considered.

Often satellites will use the art of radiative optical properties to facilitate radiant heat transfer of internal subsystems. Spartrnik, along with many other spacecraft, utilise the high absorptivity, high emissivity properties of black paint on all inner surfaces of the satellite structure to enhance heat sharing through radiation.

High computational demands are often associated with applying internal radiation so the feasibility of neglecting internal radiation for the transient orbital analysis runs needed to be verified.

Hence three steady state analysis tests were run to account for the affect neglecting internal radiation has to the overall temperature distribution.

## 8.2 Modelling Enclosure Radiation

Enclosure radiation was applied to the inner tray side walls (excluding the inner corner walls) and also both sides of the battery plate, inner top plate and inner bottom plate. Enclosure between the solar panel and the external tray sides were not included for this analysis.

Specifying a view factor of 1 implies the direction of radiation acts in a direction normal to the surface. Therefore we are assuming the radiation is not diffuse.

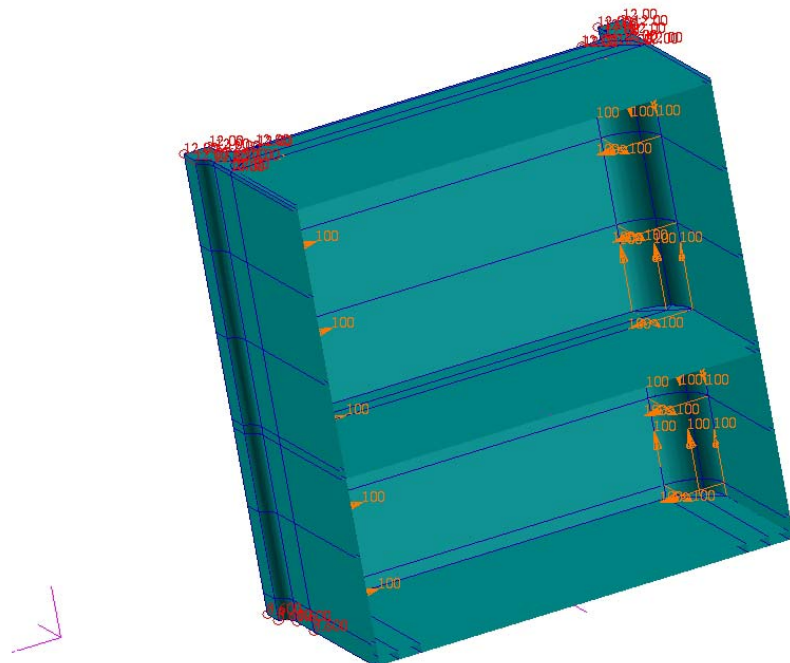


**Figure 8-1: Enclosure radiation (orange markers) applied to all tray sides, top, bottom and battery plates.**

### 8.2.1 Optical Properties Comparison

The three steady state cases included the following:

- Steady State , No Internal Radiation
- Steady State, Bare Aluminium Radiation
- Steady State, Chemglaze Black, Z306

Ideally we are only interested in the comparison of no internal radiation to what effects the bare aluminium has. Chemglaze Black Z306 is a typical internal paint with high emissive and absorptive properties.

The following describes the optical properties for both materials.

Material	Absorptivity	Emissivity
<b>Bare Aluminium</b>	0.09	0.03
<b>Chemglaze z306</b>	0.98	0.89

Table 8-1: Optical properties comparison of bare aluminium and Black paint.

### 8.3 Steady State (SOL153) Analysis

Because we are only concerned with the ultimate steady state solution for each of these cases, external surface temperatures at any specific time for any one of the four SINDA temperature plots would be necessary. The only constraint to the time selection was that the external panel temperatures should provide a range of temperatures rather than be of similar value.

The selected temperatures used were for the Naked, sun synchronous case at time = 3000 seconds:

Top Plate	6.7 °C
Side 1	2.0 °C
Side 2	4.6 °C
Side 3	12.9 °C
Side 4	10.3 °C
Bottom Plate	8.1 °C

**Table 8-2: Steady State surface temperatures**

## **8.4 Steady State Results**

As expected, the low emissivity and absorptivity of bare aluminium results in no observable variation in the overall temperatures as illustrated with the fields values for the battery module tray. For this reason, the following transient analysis was conducted without internal radiation under the assumption that the effective temperature differences it provides is minimal as compared to the relatively large ranges associated with pure conduction. It is important though to recognise that not all surfaces were applied the radiation condition (curved surfaces) which would have contributed to the overall result. To include all radiating surfaces under a transient case may have resulted in failed convergence due to heavy computations.

Applying a typical satellite internal coating such as Chemglaze Z306 to the inner walls of the structure did show a change in the temperature distribution. It is evident a reduction in temperature exists as the added radiation factor helps facilitate the transfer of heat energy. For satellites with high internal heat dissipation, this control would certainly be advised due to its relative easiness in application and low demand from the thermal mass budget.

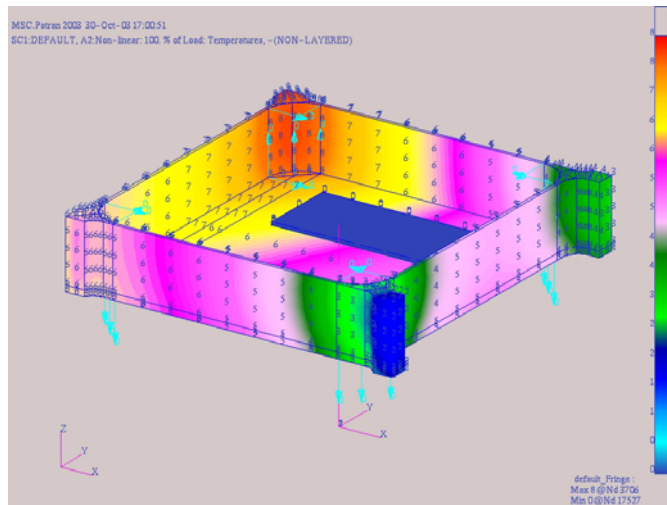


**Figure 8-2: Battery Module Fringe Plot-no internal radiation**

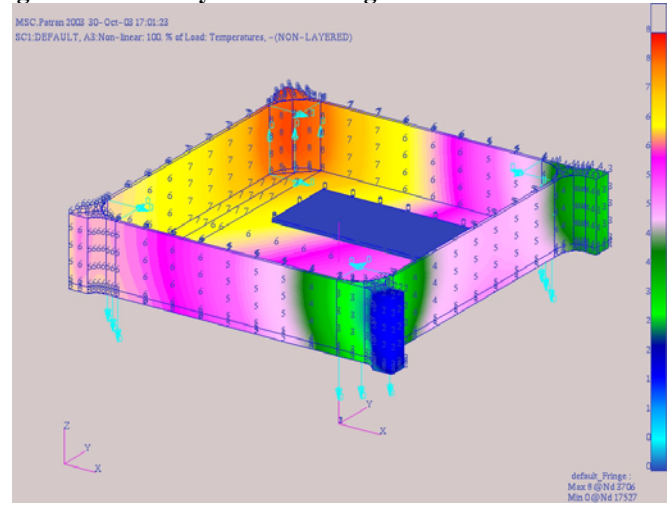


**Figure 8-3: Battery Module Fringe Plot-Bare Aluminium**

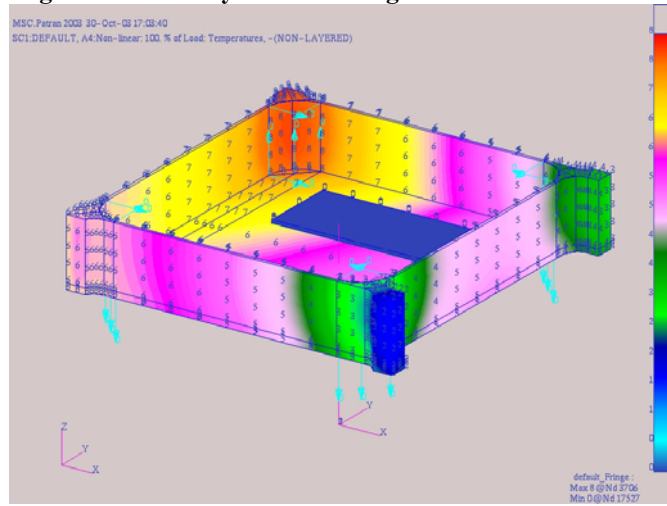


**Figure 8-4: Battery Module Fringe Plot-Chemglaze Z306**

## 9 Thermo-Stress Analysis of BLUEsat Solar Panels

### 9.1 Solar Panel Design Concerns

Recent dimensional constraints to the side mounted solar panels on BLUEsat have meant redesign on the panel mounting method. The updated panel design utilised an aerospace style edging technique to eradicate the usage of fitting inserts into the honeycomb core. These inserts often require the use of resins injected into the core to help fix the insert in place. With the negative effects of vacuum out gassing, application of resin would produce concern.

Since this design has not been previously used in space before, this thesis set out to verify structural integrity of it prior to its testing and evaluation stage.

In effect to the tight dimensional constraints, fitting locations of the honeycomb panel edges had to be positioned as close to the edge as possible.

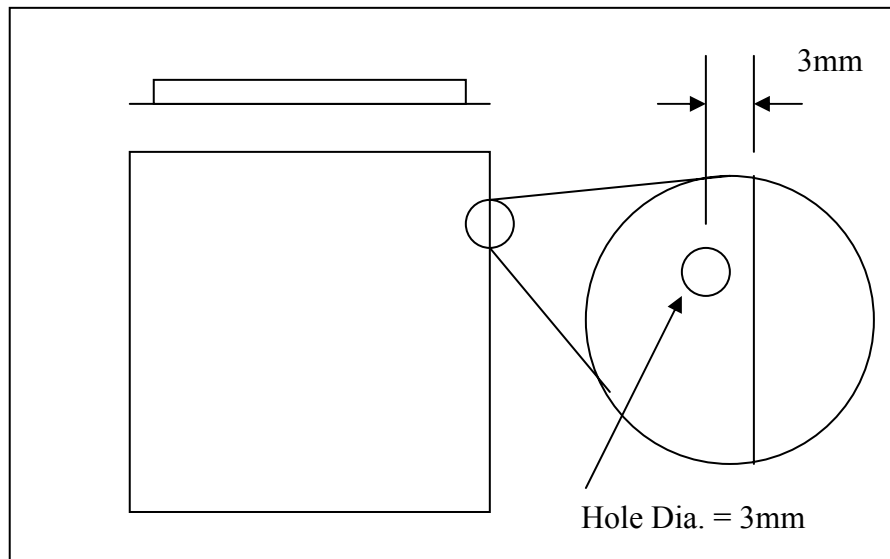


**Figure 9-1: Honeycomb panel dimensional constraints for bolt holes**

Lateral restraint of the honeycomb core and back side skin helps resist shear tear out of the small amount of skin area between the bolt hole and the edge for static and dynamic loads. However the contraction and expansion effects on the panel will cause shear tear out as well as significant stress particularly about the  $12 \times 3\text{mm}$  diameter bolt holes.

Since the edge-distance  $e/D$  ratio is less than 1.5 ( $3 / 3 = 1$ ) the shear tear out failure mode must be considered. [30]

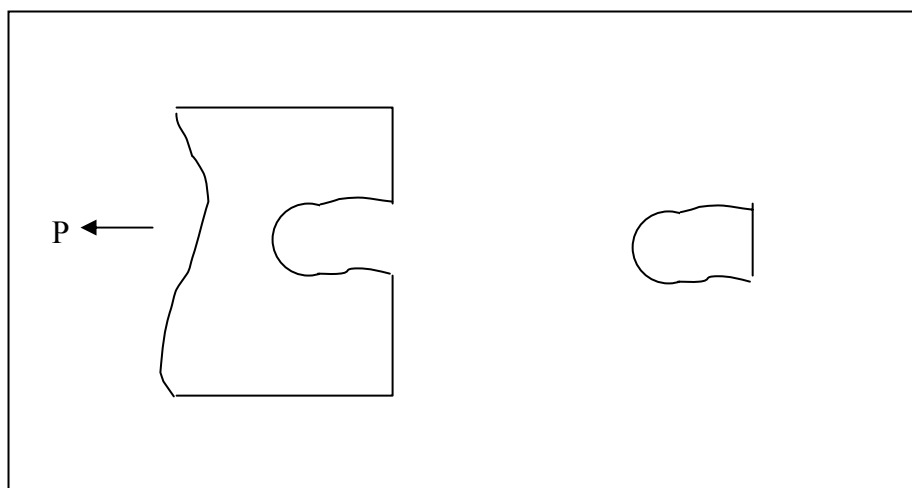


**Figure 9-2: Shear tear out**

Therefore, considering only the compressive effects on the solar panel (skin only, since there is no core or back skin at the hole locations), the peak bearing load on the fitting can be determined.

Calculation of peak load conditions arises from the relationship:

$$f_s = \frac{P_{br}}{A_s}$$

Where  $f_s$  = shear stress

$P_{br}$  = bearing load

$A_s$  = shear area

Shear area is calculated by the following:

$$A_s = 2 \times a \times T$$

$$a = e - 0.383 D$$

where  $e = 3$  mm

$D = 3$  mm

$T = 1$  mm

Gives a shear area of  $3.702 \text{ mm}^2$ . Using the Ultimate tensile strength of the material (5052 aluminium) at 290 Mpa we get the peak loading of:

$P_{br} = 357.9 \text{ N}$  (assuming a stress concentration factor of 3 [32] for the hole)

## 9.2 Patran Model Representation

The current complete BLUEsat model could not be used for such analysis since we are concerned with the stress effects about the hole and shear tear out. The complete BLUEsat model only represents the interfacing of mating components and not the fittings.

A separate shell model of one solar panel was created to be dimensionally accurate with respect to the physical design. Using the principals of mirrored geometry, only half the panel is represented and the appropriate boundary conditions applied to fix the surface for stress analysis.

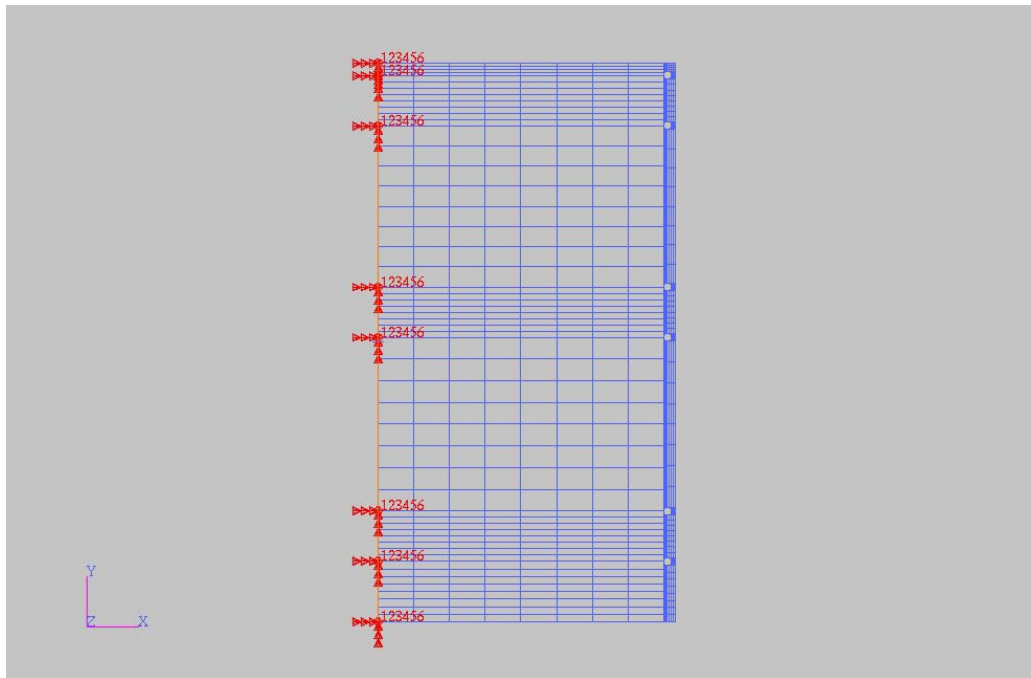


**Figure 9-3: Fixed Translational and Rotational boundary conditions for the mirrored half of the panel.**

When considering the actual behaviour of the bolt holes on the panel under expansion and contraction loadings, the bolt will prevent translation of the panel on the side opposite of the hole to the direction of the loading. Hence for both

cases, contraction will be present (reference temperature is 20 °C), the following load condition is applied.

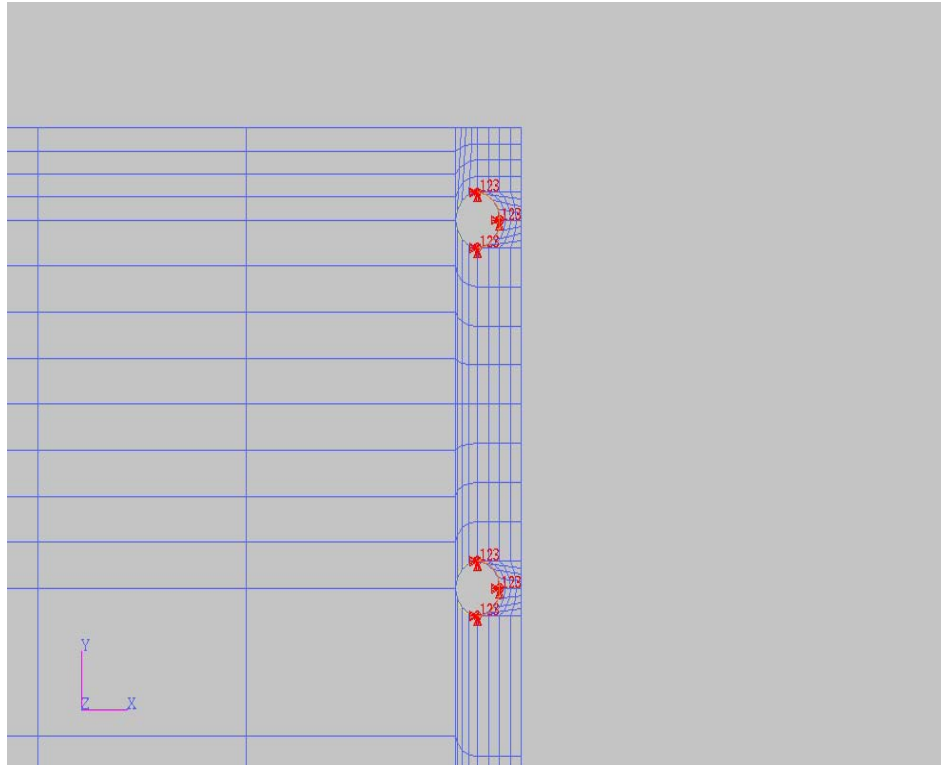


**Figure 9-4: Fixed translations (x,y,z) on one side of the bolt hole. In actual conditions under contraction, the side with same direction as the contraction direction will be free to move.**

### 9.3 **Worst Case Temperature Conditions**

Each of the materials used in BLUEsat each exhibit personal coefficients of thermal expansion (CTE). Although there is a variety of metal coexisting on the structure, they do, albeit, tend to have very close CTE's which, for object of equal dimensions would show similar strains.

What is more of a concern than that of differing CTE's is the varying dimensions and volumes of each component. The thermal expansion of the tray will not be equivalent to the expansion of the panel even if assumed to be at same temperatures.

For this analysis, it was assumed the affected solar panel is isolated from the rest of the structure. Worst case maximum and minimum orbital temperatures were applied to the panel and it was fixed to space related to its reference temperature condition (initial state before expansion). In reality we would expect the structure the panel is fitted to, to also expand relative to the panel. Whether the panel expands at a faster rate to the rest of the structure depends on the transient temperature conditions in-orbit as well as the geometrical constraints.

Therefore, assuming this panel will be fixed to a reference temperature location in space, we achieve a worse case load condition that will be somewhat more significant than what actually occurs.

The worst case temperatures that BLUEsat could be susceptible to are:

Worst Case Cold	-27.9 (naked, 0 Degree Beta)
Worst Case Hot	14.9 (naked, 0 Degree Beta)

**Table 9-1: Maximum and Minimum Temperatures for BLUEsat**

## 9.4 Analysis Process

### 9.4.1 SOL 153 Temperature Mapping

Nastran allows the user to exchange FEM results to and from other result outputs. Therefore the temperature results calculated using Nastran Thermal can then be mapped onto the model for structural analysis using Nastran.

Each case was thus analysed and the analysis code was changed following a results check to ensure the temperatures were uniform across the model.

### 9.4.2 Nastran Structural Analysis

When applying thermal FEM to a new structural analysis, both the materials and properties must be input and assigned respectively. The following thermal properties for 5052 Aluminium were used:

- Elastic Modulus 70 000 Mpa
- Poisson's Ratio 0.33
- CTE (0-20 °C) 0.0000238
- Reference Temp. 0.0°C

Note that the CTE for aluminium is rated with respect to a temperature range of 20 to 100 °C where the effect of expansion becomes significant at high temperatures. Without the availability of experimental data on the CTE of aluminium at cryogenic temperatures (between 0 to 273 K), we have thus used an assumption that this relationship remains linear for temperatures below 20 °C. In actual fact, there would be a reduction in the CTE for temperatures as the atomic kinetic energy reduces with absolute temperature scale.

## **9.5 Results**

The extreme cold condition produces rather large stresses concentrated about all bolt holes as expected. However as stated above we have assumed linear CTE for temperatures below 20 °C which was allocated as the reference temperature for the aluminium in its initial state (room temperature-293K).

For this assumption, the peak stress for minimum temperature is  $1.73 \times 10^3$  Mpa, positioned on the top RHS bolt hole. For the maximum temperature, a contractive force also applies to the panel since the applied temperature is also below its reference temperature of 20 °C. Its peak stress was  $1.91 \times 10^2$  Mpa occurring on the bottom RHS bolt hole.

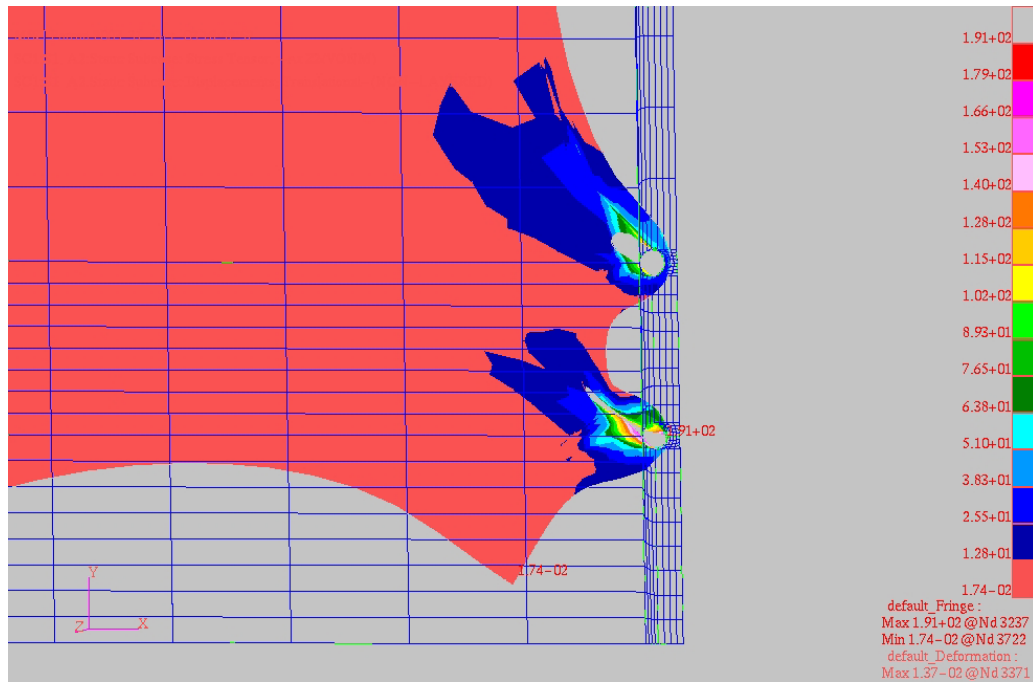


Figure 9-5: Peak Stress (Von Mises) due to thermal contraction @  $14.9^{\circ}\text{C}$

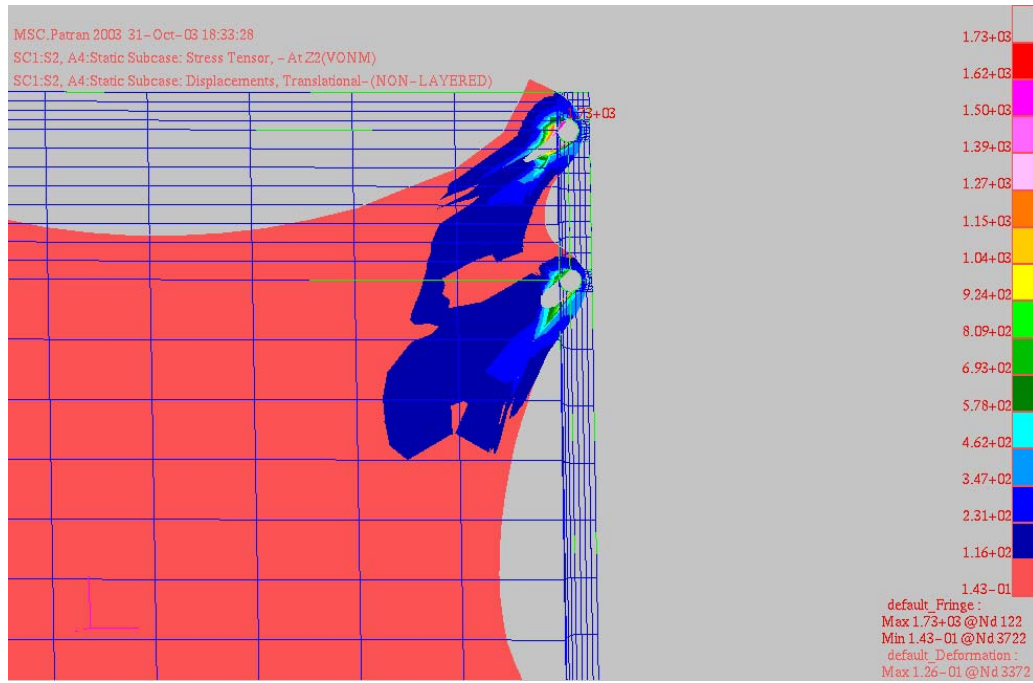


Figure 9-6: Peak Stress (Von Mises) due to thermal contraction @  $-27.9^{\circ}\text{C}$

At 1730 Mpa, the panel will fail not only in shear out, but also due to the stress being greater then the Ultimate tensile stress of 300 Mpa for the material.

At these levels, there is cause for concern to the design of the panel. However, a secondary analysis was performed to determine what the maximum deflection amplitudes were for the panel. For this case, all displacement boundary conditions on the bolt holes were removed to allow free movement of the panel edge. Both temperature cases were analysed, giving the following results.

Temperature / Displacement	X-Direction	Y-Direction
-27.9 ° C	0.01 mm	0.137 mm
+14.9 ° C	0.00107 mm	0.0146 mm

Table 9-2: Peak thermal deflection on panel

These displacements represent the minimum allowable tolerance for machining of the bolt holes. Thus if a perfect dimension was achieved via machining, stresses as significant as above may be present.

## 9.6 *Design Considerations*

The assumption of analysing a thin plate as opposed to the 3D orthotropic thermal properties of an aluminium honeycomb panel has yielded worst case scenarios. Added to this the assumption of perfect positional fixing of the bolt holes in the analysis we can expect lower overall stress on the physical flight model.

The most significant factor of this analysis is the maximum deflections on the panel caused by thermal expansion (or in this case contraction). Accounting for deflections of 0.137mm is easily achieved through a variety of measures.

1. Assign dimensional tolerances that allow 'play' in the structure for thermal effects
2. Use rolling or sliding joints instead of hard fittings [30]
3. Ensure high thermal conductivity at interfaces to minimise thermal gradients and the resulting internal stresses
4. Ensure interacting materials with large temperature ranges have similar CTE's.

## 10 Transient Orbital Analysis of BLUEsat

Ultimately we are concerned with the internal thermal environment that the onboard subsystems must perform within as these are the most important parameter for the thermal engineer [33]. Using the temperature data gained from SINDA, we can analyse BLUEsat throughout complete orbits analytically to ensure sound thermal conditions.

### 10.1 SINDA Output Results

Using the raw temperature data compiled from the SINDA output files (.SOT) we could select a time period that reflects two complete orbits of sinusoidal thermal behaviour. Using excel these ranges were plotted (see pages 78-81) and tabulated to respective surface temperatures approximated to 1 decimal place.

Because the temperature ranges of the OSR coated BLUEsat lie within the ranges of the naked structure, only the naked structure was analysed with Nastran Thermal.

Each case was input as a fields function for 2 complete orbits totalling 1200 individual temperature inputs. Time taken for 2 orbits totalled 11880 seconds for each case.

## **10.2 Battery Modelling**

For the purposes of this thesis, we were concerned with the strict temperature requirements upon the batteries. That is, the batteries are not to charge or discharge at less than 0 °C. During the eclipse period of BLUEsat's orbit, power derived directly from the solar modules will cease and satellite functioning will depend on the stored energy of the batteries. For the systems engineer this will also present some power regulation issues. During the sun-lit exposure period, the batteries will not discharge; instead systems will draw their power again from the modules. Therefore we assume the main period of battery activity will occur during eclipse time, so need to analyse this scenario to control battery ambient temperature.

### **10.2.1 Heat Dissipation**

During peak power operation of BLUEsat during the period of eclipse, three systems could be accounted for to determine the maximum power required for a particular instance of time in-orbit. These include the following and their power demand:

- TX @ 8.84 W (2.5W RF output, therefore 6.34 W dissipated)
- RX @ 0.5 W
- Flight Computer @ 1 W (realistically for a Strongarm CPU: 0.6 W)

This gives a total peak power demand of 10.34 W  $\approx$  10 W. The two battery packs within BLUEsat are connected in parallel hence will each output 5 Watts each for the systems. Assuming a power efficiency of 90 % for the power system, the energy lost to heat dissipation for each battery string is 0.5 Watts.

### 10.2.2 Casing Model Representation

Each cell will be positioned onto a platform of reasonable large thermal mass and secured down. Initial design options include an aluminium bed with machined slots on the top for the cells to sit in. Since the cell will have the insulative coating removed from their external surface, an electrical insulator such as kapton or fibreglass wrapped around to isolate the negative of the cell to the aluminium bed.

Assuming each battery string will be designed such that they will be packaged in two rows of ten formation, each battery casing will require a mounting surface area of  $10 \times 10 \times 42 \text{ mm} = 4200 \text{ mm}^2$  in accordance with the battery dimensions.

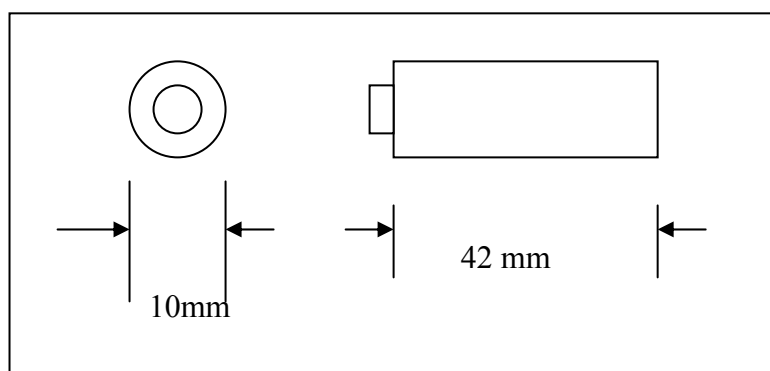
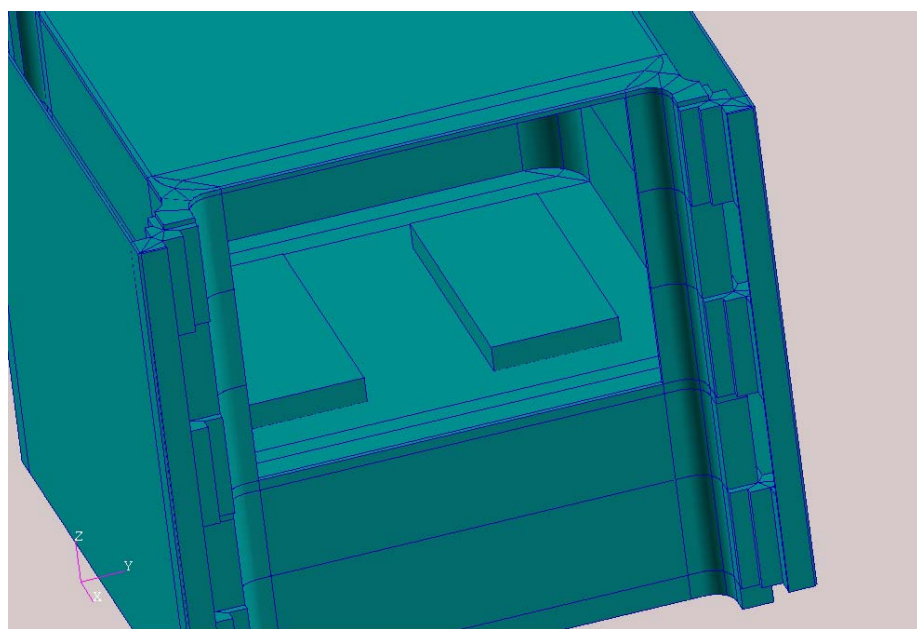


Figure 10-1: Battery Cell dimensions

The casing represented in Patran was created based on certain nodes for the corners so as to ensure proper equivalence to the battery plate. The dimensions of the casing model are  $49 \text{ mm} \times 108 \text{ mm} = 5292 \text{ mm}^2$  per case which is roughly in agreement with the initial casing size estimates.

The casings are each modelled as solid geometries, each with a thickness of 10 mm. The main concern with the casing is the threat of extremely low temperatures during the eclipse period. We aim to ensure that all heat dissipated by the batteries will remain localised, thus providing the correct ambient conditions. Two materials have been selected for the casing. The problem with using an Aluminium casing is the possibility of mating with the negative terminal (battery cell shell) and causing a short. Therefore we want to also analyse the usage of a Delrin casing.



**Figure 10-2: Battery casing model representation as solid geometry (kapton was modelled as surfaces between battery casing and battery plate)**

As an example of thermal control design through analysis, a thermal insulator has been added in between the battery casing and the battery plate. The objective is to isolate the battery heat generated from the subzero structure conditions. The material used for this test is Standard Kapton Tape because of its excellent insulative properties.

- Thermal Conductivity      0.16 W/ m K
- Specific Heat                1.080 J/ g °C

### ***10.3 BLUEsat Orbital Scenarios***

#### **10.3.1        Selected Orbital Ranges**

The two ‘naked’ orbital scenarios were analysed using Nastran Thermal. To allow the transient effects to settle, two complete orbital data ranges were input as a field function into Patran. This allowed the results settle to more sinusoidal temperature behaviour.

Time	Top Plate	Side 1 (+Y)	Side 2 (+Z)	Side 3 (-Y)	Side 4 (-Z)	Bottom Plate	Time	Top Plate	Side 1 (+Y)	Side 2 (+Z)	Side 3 (-Y)	Side 4 (-Z)	Bottom Plate
0.00E+00	12.0	5.7	13.2	14.9	7.4	8.6	6.00E+03	12.0	5.7	13.2	14.9	7.4	8.6
1.20E+02	9.5	4.6	9.9	11.3	6.1	6.5	6.12E+03	9.5	4.6	9.9	11.3	6.1	6.5
2.40E+02	6.4	3.1	6.3	7.3	4.1	4.0	6.24E+03	6.4	3.1	6.3	7.3	4.1	4.0
3.60E+02	3.4	1.2	3.1	3.7	1.8	1.5	6.36E+03	3.4	1.2	3.1	3.7	1.8	1.5
4.80E+02	0.6	-0.9	0.2	0.6	-0.5	-1.0	6.48E+03	0.6	-0.9	0.2	0.6	-0.5	-1.0
6.00E+02	-1.9	-3.1	-2.5	-2.2	-2.9	-3.4	6.60E+03	-1.9	-3.1	-2.5	-2.2	-2.9	-3.4
7.20E+02	-4.3	-5.3	-4.9	-4.8	-5.1	-5.8	6.72E+03	-4.3	-5.3	-4.9	-4.8	-5.1	-5.8
8.40E+02	-6.6	-7.5	-7.3	-7.2	-7.4	-8.0	6.84E+03	-6.6	-7.5	-7.3	-7.2	-7.4	-8.0
9.60E+02	-9.0	-9.6	-9.5	-9.4	-9.5	-10.0	6.96E+03	-9.0	-9.6	-9.5	-9.4	-9.5	-10.0
1.08E+03	-11.6	-11.7	-11.7	-11.6	-11.7	-11.8	7.08E+03	-11.6	-11.7	-11.7	-11.6	-11.7	-11.8
1.20E+03	-14.0	-13.8	-13.7	-13.7	-13.7	-13.4	7.20E+03	-14.0	-13.8	-13.7	-13.7	-13.7	-13.4
1.32E+03	-16.3	-15.7	-15.7	-15.7	-15.7	-15.1	7.32E+03	-16.3	-15.7	-15.7	-15.7	-15.7	-15.1
1.44E+03	-18.4	-17.6	-17.6	-17.6	-17.6	-16.9	7.44E+03	-18.4	-17.6	-17.6	-17.6	-17.6	-16.9
1.56E+03	-20.3	-19.5	-19.5	-19.4	-19.4	-18.6	7.56E+03	-20.3	-19.5	-19.5	-19.4	-19.4	-18.6
1.68E+03	-22.1	-21.2	-21.2	-21.2	-21.2	-20.3	7.68E+03	-22.1	-21.2	-21.2	-21.2	-21.2	-20.3
1.80E+03	-23.8	-22.9	-22.9	-22.9	-22.9	-22.0	7.80E+03	-23.8	-22.9	-22.9	-22.9	-22.9	-22.0
1.92E+03	-25.5	-24.5	-24.5	-24.5	-24.5	-23.6	7.92E+03	-25.5	-24.5	-24.5	-24.5	-24.5	-23.6
2.04E+03	-27.0	-26.1	-26.1	-26.1	-26.1	-25.2	8.04E+03	-27.0	-26.1	-26.1	-26.1	-26.1	-25.2
2.16E+03	-28.5	-27.6	-27.6	-27.6	-27.6	-26.7	8.16E+03	-28.5	-27.6	-27.6	-27.6	-27.6	-26.7
2.28E+03	-27.9	-25.8	-25.0	-27.1	-27.9	-25.1	8.28E+03	-27.9	-25.8	-25.0	-27.1	-27.9	-25.1
2.40E+03	-26.5	-23.4	-22.2	-26.4	-27.6	-23.2	8.40E+03	-26.5	-23.4	-22.2	-26.4	-27.6	-23.2
2.52E+03	-25.0	-21.0	-20.0	-25.7	-26.8	-21.8	8.52E+03	-25.0	-21.0	-20.0	-25.7	-26.8	-21.8
2.64E+03	-23.2	-18.8	-18.3	-25.0	-25.5	-20.6	8.64E+03	-23.2	-18.8	-18.3	-25.0	-25.5	-20.6
2.76E+03	-21.2	-16.5	-16.7	-24.0	-23.8	-19.3	8.76E+03	-21.2	-16.5	-16.7	-24.0	-23.8	-19.3
2.88E+03	-18.8	-14.1	-15.1	-22.6	-21.6	-17.9	8.88E+03	-18.8	-14.1	-15.1	-22.6	-21.6	-17.9
3.00E+03	-16.4	-11.8	-13.6	-21.0	-19.2	-16.5	9.00E+03	-16.4	-11.8	-13.6	-21.0	-19.2	-16.5
3.12E+03	-13.9	-9.7	-12.2	-19.2	-16.7	-15.0	9.12E+03	-13.9	-9.7	-12.2	-19.2	-16.7	-15.0
3.24E+03	-11.6	-8.0	-11.1	-17.3	-14.3	-13.7	9.24E+03	-11.6	-8.0	-11.1	-17.3	-14.3	-13.7
3.36E+03	-9.7	-6.8	-10.0	-15.2	-12.0	-12.3	9.36E+03	-9.7	-6.8	-10.0	-15.2	-12.0	-12.3
3.48E+03	-8.6	-6.5	-8.9	-12.2	-9.8	-10.1	9.48E+03	-8.6	-6.5	-8.9	-12.2	-9.8	-10.1
3.60E+03	-7.9	-6.7	-7.7	-8.6	-7.6	-7.5	9.60E+03	-7.9	-6.7	-7.7	-8.6	-7.6	-7.5
.72E+03	-7.2	-6.4	-6.5	-5.9	-5.8	-5.1	9.72E+03	-7.2	-6.4	-6.5	-5.9	-5.8	-5.1
3.84E+03	-6.4	-5.6	-5.4	-4.0	-4.3	-3.2	9.84E+03	-6.4	-5.6	-5.4	-4.0	-4.3	-3.2
3.96E+03	-5.8	-4.6	-4.3	-2.9	-3.2	-1.7	9.96E+03	-5.8	-4.6	-4.3	-2.9	-3.2	-1.7
4.08E+03	-5.4	-3.5	-3.3	-2.3	-2.5	-0.5	1.0080E+04	-5.4	-3.5	-3.3	-2.3	-2.5	-0.5
4.20E+03	-4.6	-2.2	-2.0	-1.7	-1.9	0.7	1.0200E+04	-4.6	-2.2	-2.0	-1.7	-1.9	0.7
4.32E+03	-3.4	-0.7	-0.4	-0.9	-1.3	1.8	1.0320E+04	-3.4	-0.7	-0.4	-0.9	-1.3	1.8
4.44E+03	-2.1	0.8	1.5	0.1	-0.6	3.0	1.0440E+04	-2.1	0.8	1.5	0.1	-0.6	3.0
4.56E+03	-0.6	2.3	3.4	1.2	0.0	4.1	1.0560E+04	-0.6	2.3	3.4	1.2	0.0	4.1
4.68E+03	0.7	3.4	5.3	2.5	0.6	5.2	1.0680E+04	0.7	3.4	5.3	2.5	0.6	5.2
4.80E+03	1.9	4.3	7.0	3.6	0.9	6.0	1.0800E+04	1.9	4.3	7.0	3.6	0.9	6.0
4.92E+03	3.1	5.0	8.6	4.9	1.4	6.8	1.0920E+04	3.1	5.0	8.6	4.9	1.4	6.8
5.04E+03	4.4	5.5	10.0	6.4	1.9	7.5	1.1040E+04	4.4	5.5	10.0	6.4	1.9	7.5
5.16E+03	5.6	5.8	11.2	7.9	2.5	8.1	1.1160E+04	5.6	5.8	11.2	7.9	2.5	8.1
5.28E+03	6.8	5.8	12.0	9.5	3.3	8.5	1.1280E+04	6.8	5.8	12.0	9.5	3.3	8.5
5.40E+03	7.8	5.6	12.6	10.8	3.9	8.7	1.1400E+04	7.8	5.6	12.6	10.8	3.9	8.7
5.52E+03	8.5	5.3	12.8	11.7	4.3	8.6	1.1520E+04	8.5	5.3	12.8	11.7	4.3	8.6
5.64E+03	9.2	5.1	12.8	12.5	4.8	8.3	1.1640E+04	9.2	5.1	12.8	12.5	4.8	8.3
5.76E+03	10.2	5.0	12.8	13.4	5.6	8.2	1.1760E+04	10.2	5.0	12.8	13.4	5.6	8.2
5.88E+03	11.2	5.0	12.6	14.1	6.6	8.0	1.1880E+04	11.2	5.0	12.6	14.1	6.6	8.0

Table 10-1: Surface temperatures for 0 Degree Beta Sun Synchronous Naked Structure

Time	Top Plate	Side 1 (+Y)	Side 2 (+Z)	Side 3 (-Y)	Side 4 (-Z)	Bottom Plate	Time	Top Plate	Side 1 (+Y)	Side 2 (+Z)	Side 3 (-Y)	Side 4 (-Z)	Bottom Plate
0.00E+00	9.3	3.3	12.0	12.7	4.0	6.7	6.00E+03	9.5	2.9	11.6	13.2	4.6	6.7
1.20E+02	9.5	2.9	11.4	13.3	4.8	6.7	6.12E+03	9.5	2.5	10.8	13.6	5.3	6.6
2.40E+02	9.5	2.4	10.7	13.7	5.4	6.6	6.24E+03	9.3	1.9	9.9	13.8	5.8	6.3
3.60E+02	9.3	1.8	9.6	13.8	5.9	6.3	6.36E+03	9.2	1.5	8.9	13.8	6.4	6.1
4.80E+02	9.2	1.5	8.7	13.8	6.5	6.0	6.48E+03	9.2	1.4	8.0	13.8	7.2	6.0
6.00E+02	9.2	1.4	7.8	13.8	7.3	6.0	6.60E+03	9.3	1.5	7.2	13.8	8.1	6.1
7.20E+02	9.3	1.6	7.1	13.8	8.3	6.1	6.72E+03	9.5	1.9	6.6	13.8	9.1	6.3
8.40E+02	9.5	2.0	6.5	13.8	9.4	6.3	6.84E+03	9.7	2.5	6.1	13.8	10.2	6.5
9.60E+02	9.8	2.6	5.9	13.8	10.4	6.6	6.96E+03	10.0	3.1	5.6	13.7	11.3	6.8
1.08E+03	10.0	3.3	5.5	13.6	11.5	6.9	7.08E+03	10.2	3.8	5.1	13.4	12.2	7.1
1.20E+03	10.2	4.0	5.0	13.3	12.3	7.1	7.20E+03	10.2	4.5	4.5	12.9	12.9	7.2
1.32E+03	10.2	4.6	4.4	12.8	13.0	7.2	7.32E+03	10.0	5.1	3.9	12.2	13.3	7.2
1.44E+03	10.0	5.2	3.7	12.0	13.4	7.1	7.44E+03	9.7	5.5	3.1	11.1	13.5	6.9
1.56E+03	9.6	5.5	3.0	10.9	13.5	6.9	7.56E+03	9.2	5.8	2.4	10.0	13.4	6.6
1.68E+03	9.1	5.9	2.2	9.7	13.4	6.5	7.68E+03	8.7	6.2	1.7	8.7	13.2	6.3
1.80E+03	8.6	6.3	1.6	8.5	13.1	6.2	7.80E+03	8.0	6.3	1.2	7.9	12.9	6.1
1.92E+03	7.9	6.2	1.2	7.8	12.8	6.1	7.92E+03	7.3	5.8	1.0	7.8	12.6	6.3
2.04E+03	7.1	5.7	0.9	7.8	12.6	6.4	8.04E+03	6.6	5.1	0.9	8.2	12.4	6.7
2.16E+03	6.5	5.0	0.9	8.3	12.4	6.8	8.16E+03	6.2	4.5	1.1	8.8	12.3	7.1
2.28E+03	6.2	4.4	1.1	9.0	12.2	7.2	8.28E+03	6.2	4.0	1.5	9.6	12.1	7.4
2.40E+03	6.2	3.9	1.6	9.8	12.1	7.5	8.40E+03	6.2	3.5	2.0	10.4	12.0	7.7
2.52E+03	6.3	3.4	2.1	10.6	11.9	7.8	8.52E+03	6.4	3.1	2.6	11.2	11.8	8.0
2.64E+03	6.4	3.1	2.8	11.4	11.7	8.0	8.64E+03	6.6	2.8	3.3	11.9	11.4	8.1
2.76E+03	6.6	2.7	3.4	12.1	11.3	8.1	8.76E+03	6.7	2.4	3.9	12.5	11.0	8.2
2.88E+03	6.7	2.3	4.0	12.6	10.9	8.2	8.88E+03	6.8	2.0	4.5	12.9	10.4	8.2
3.00E+03	6.7	2.0	4.6	12.9	10.3	8.1	9.00E+03	6.7	1.6	5.0	13.1	9.7	8.0
3.12E+03	6.7	1.5	5.1	13.1	9.5	8.0	9.12E+03	6.6	1.2	5.5	13.2	8.9	7.8
3.24E+03	6.6	1.1	5.6	13.2	8.7	7.8	9.24E+03	6.5	0.8	6.0	13.3	8.1	7.6
3.36E+03	6.5	0.8	6.1	13.3	8.0	7.6	9.36E+03	6.5	0.7	6.7	13.4	7.4	7.6
3.48E+03	6.5	0.7	6.8	13.5	7.3	7.6	9.48E+03	6.7	0.8	7.5	13.6	6.9	7.7
3.60E+03	6.7	0.8	7.6	13.7	6.8	7.7	9.60E+03	7.0	1.1	8.4	13.8	6.5	7.9
3.72E+03	7.0	1.2	8.6	13.9	6.5	8.0	9.72E+03	7.3	1.5	9.3	14.0	6.2	8.3
3.84E+03	7.4	1.7	9.5	14.1	6.2	8.4	9.84E+03	7.7	2.1	10.3	14.2	6.0	8.6
3.96E+03	7.7	2.2	10.5	14.2	5.9	8.7	9.96E+03	8.0	2.8	11.3	14.3	5.8	9.0
4.08E+03	8.0	2.9	11.4	14.2	5.7	9.1	1.0080E+04	8.3	3.4	12.1	14.2	5.5	9.4
4.20E+03	8.3	3.6	12.3	14.1	5.4	9.4	1.0200E+04	8.4	4.1	12.9	14.0	5.2	9.6
4.32E+03	8.5	4.2	13.0	13.9	5.1	9.6	1.0320E+04	8.5	4.7	13.4	13.6	4.8	9.8
4.44E+03	8.4	4.8	13.5	13.4	4.7	9.8	1.0440E+04	8.3	5.2	13.8	12.9	4.3	9.7
4.56E+03	8.3	5.2	13.8	12.7	4.2	9.7	1.0560E+04	8.0	5.5	13.9	12.0	3.7	9.5
4.68E+03	7.9	5.6	13.8	11.8	3.5	9.4	1.0680E+04	7.4	5.7	13.7	10.8	2.9	9.1
4.80E+03	7.3	5.7	13.6	10.6	2.7	9.0	1.0800E+04	7.1	5.7	13.4	9.8	2.1	8.4
4.92E+03	7.1	5.7	13.4	9.6	1.9	8.2	1.0920E+04	7.0	5.7	13.2	8.9	1.4	7.5
5.04E+03	7.0	5.6	13.1	8.7	1.3	7.3	1.1040E+04	7.1	5.4	12.9	8.4	1.0	6.8
5.16E+03	7.1	5.4	12.9	8.4	0.9	6.7	1.1160E+04	7.3	5.1	12.8	8.5	0.9	6.4
5.28E+03	7.3	5.0	12.7	8.6	0.9	6.3	1.1280E+04	7.5	4.7	12.6	9.0	1.1	6.2
5.40E+03	7.6	4.7	12.6	9.1	1.2	6.2	1.1400E+04	7.9	4.4	12.6	9.8	1.5	6.2
5.52E+03	8.0	4.3	12.6	9.9	1.7	6.2	1.1520E+04	8.3	4.0	12.5	10.6	2.2	6.3
5.64E+03	8.4	4.0	12.5	10.8	2.3	6.4	1.1640E+04	8.8	3.7	12.4	11.5	2.9	6.5
5.76E+03	8.9	3.7	12.4	11.7	3.1	6.5	1.1760E+04	9.1	3.4	12.1	12.4	3.7	6.6
5.88E+03	9.2	3.3	12.0	12.6	3.8	6.7	1.1880E+04	9.4	3.0	11.7	13.1	4.5	6.7

Table 10-2: Surface Temperatures for 90 Degree Beta Sun Synchronous Naked Structure

### 10.3.2 Fields Function Temp Inputs

Units of time were maintained at 120 second intervals to keep resemblance to the original SINDA outputs. This allowed a reasonable time period for each temperature step to conduct through the structure under the natural effects of transient thermal lag.

Each NON-Spatial Tabular input function could then be assigned to the respective FE elements for running of the transient cases.

As mentioned earlier, battery discharge rates peak during the eclipse period which only occurs for the 0 Degree Beta angle. This can be represented as a periodic square wave function as follows:

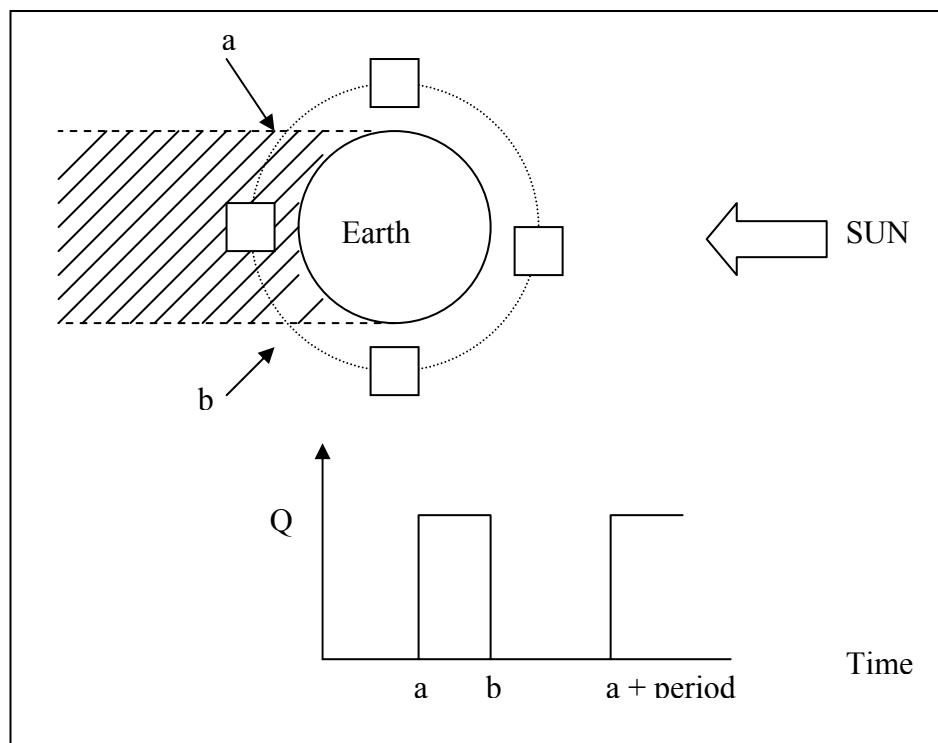


Figure 10-3: Battey heat dissipation output with respect to orbital position

The period between a and b has been assumed to be 50 % of the orbital time. In terms of orbital time, the fields function to represent the battery discharge period is:

Orbital Position	Time in Orbit
Entry into Eclipse (1 <sup>st</sup> Orbit)	480 seconds
Exit from Eclipse (1 <sup>st</sup> Orbit)	4440 seconds
Entry into Eclipse (2 <sup>nd</sup> Orbit)	6480 seconds
Exit from Eclipse (2 <sup>nd</sup> Orbit)	10440 seconds

Table 10-3: Fields entry times for 0.5 W uniform applied heat of battery dissipation

#### 10.4 Transient (SOL159) Analysis

The two load cases (for each orbital scenario) were posted for transient analysis into Nastran Thermal for 100 time steps. This ensures the BLUEsat FE model will orbit twice. From our results of the effects of internal radiation, no internal radiation has been assigned for the transient cases.

The purpose of conducting a transient analysis is so we can deduce a number of behaviours of internal temperatures:

1. Minimum and Maximum Tray Temperatures per orbit
2. Battery Casing Temperatures per orbit
3. Effect of Kapton Insulation

#### 4. Aluminium / Delrin Battery Casing Comparison

NOTE: Ideally we want to ensure that suitable temperatures are maintained in the battery casing for as long as possible. Hence the purpose to objective 4 is to compare the thermal capacitance of both aluminium and Delrin battery casings.

### 10.5 Results

#### 10.5.1 0 Degree Beta Angle

Over the two complete orbits, the thermal gradients of the internal trays remained relatively low. Tray temperatures were based on a selection of 4 nodes per tray, each in the direct inner centre of the tray sides. For the 20 node selections the temperatures for each trays was plotted against time:

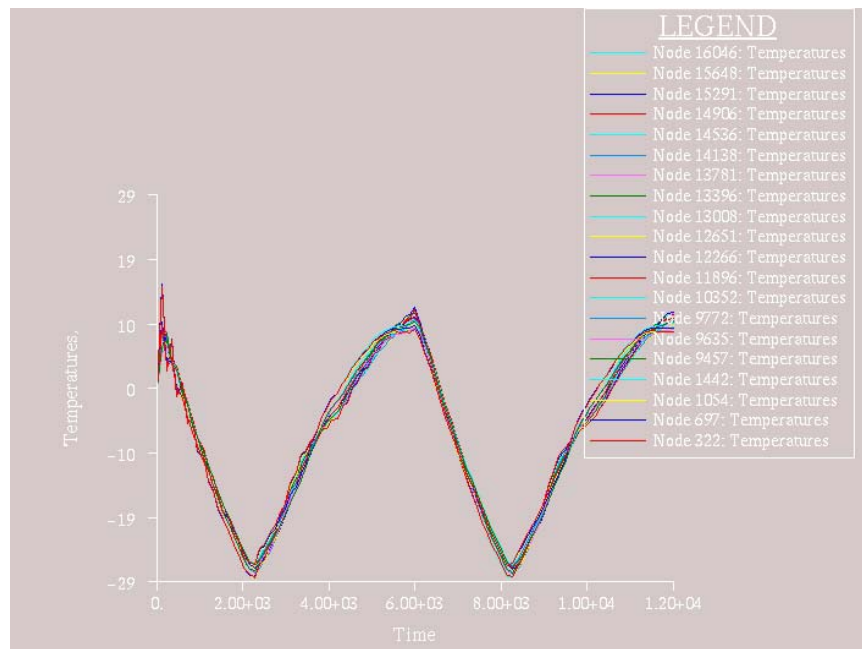


**Figure 10-4: Tray temperatures over two orbits (0 Degree Beta)**

From these results we could deduce that maximum temperature differentials were no more than 3-4 °C, while maximum and minimum temperatures were within the range of:

- + 14 °C
- - 29 °C

The combination of extreme low external heat input during the eclipse period, and the low subsystem heat dissipation, yields an internal spacecraft thermal environment unacceptable for BLUEsat's mission requirement; that onboard and structural components maintain an optimal temperature range of 0 to 20 °C.

Two battery casings were modelled for the same orbit case, one using Delrin, the other aluminium. The aim was to verify the most suitable material, based on minimum temperature.

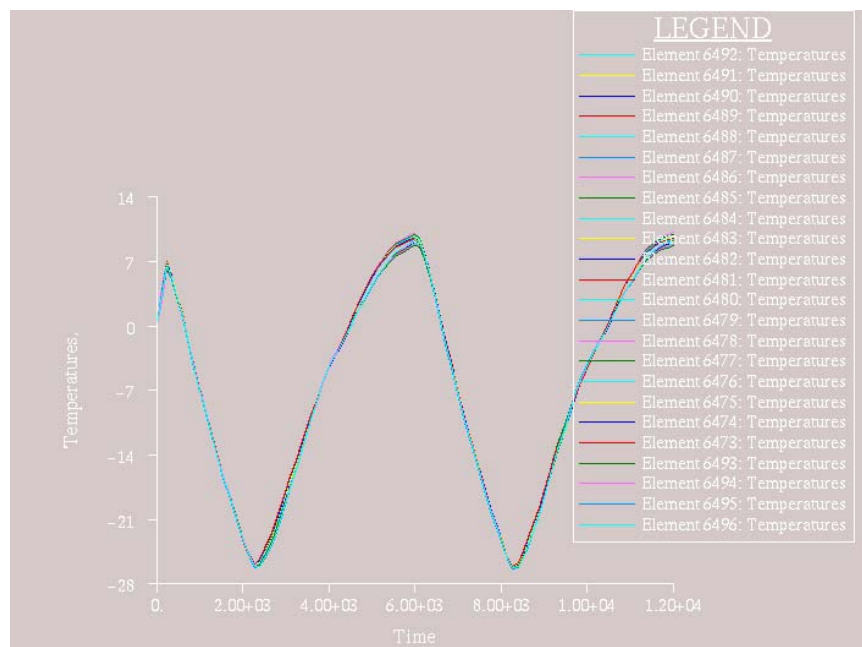


**Figure 10-5: 6061-T6 Aluminium Battery Casing orbital temperatures**

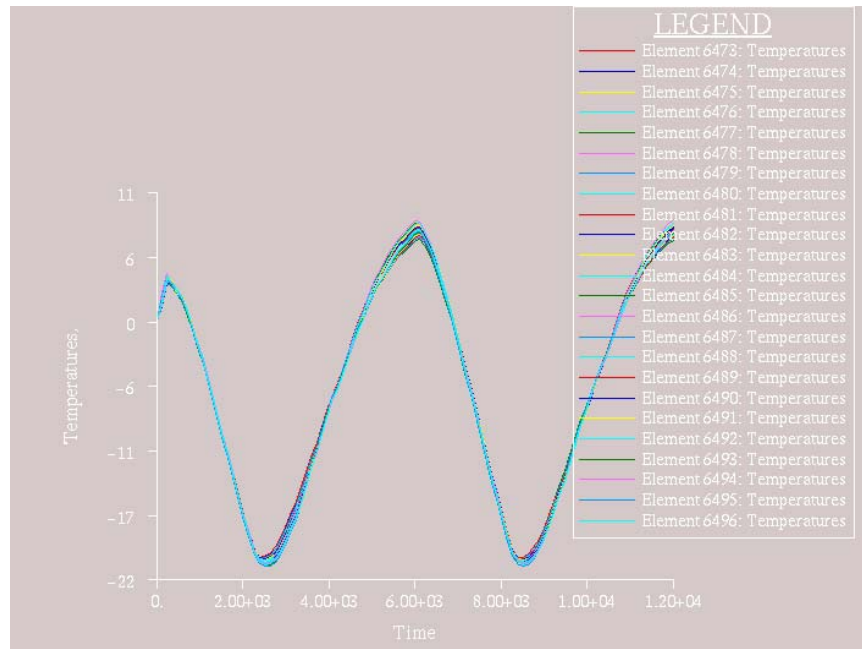
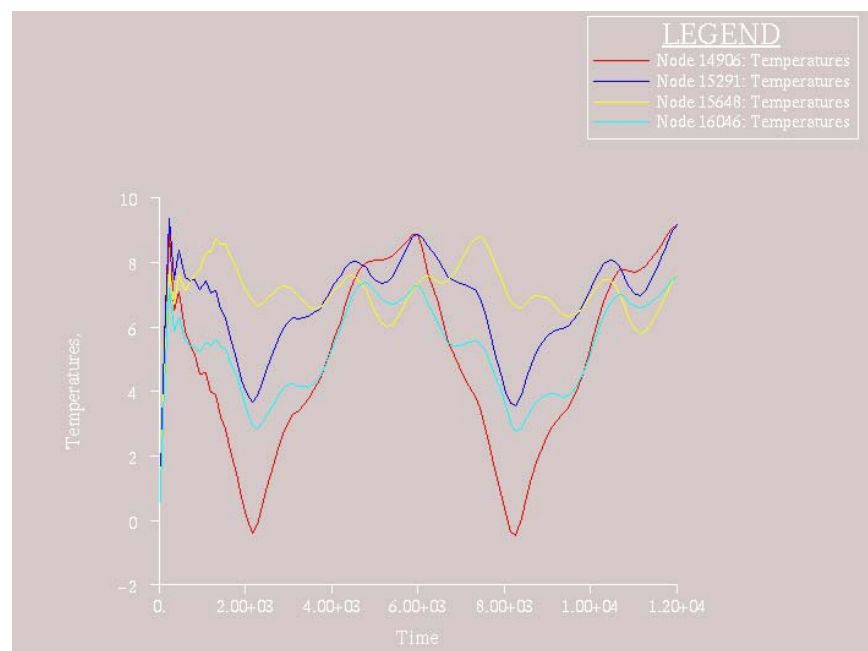
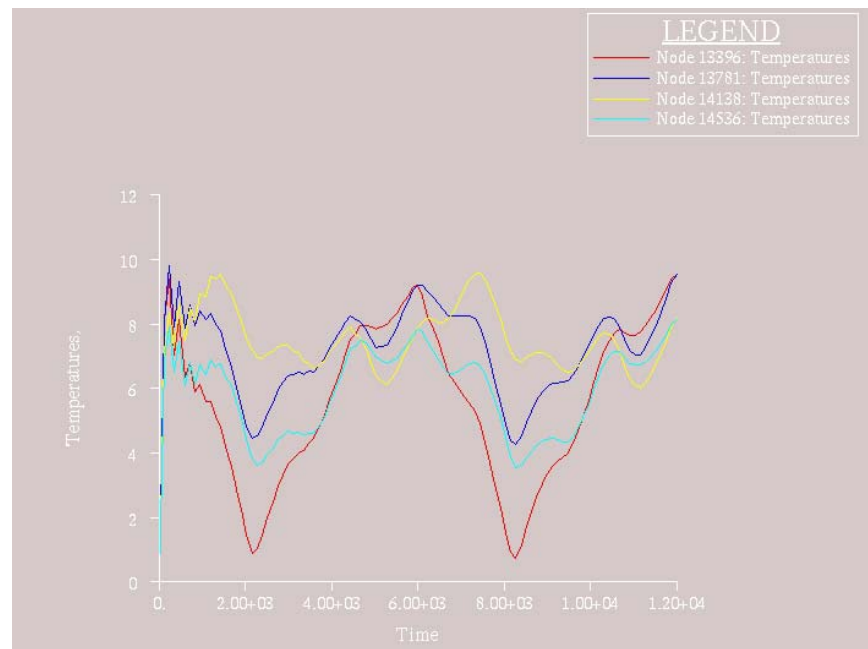


**Figure 10-6: Delrin Battery Casing orbital temperatures**

From these results, it is noticeable that the lower thermal conductance and the relatively high specific heat of the Delrin perform substantially better than the aluminium casing. While the maximum temperatures are similarly around + 10 °C, the Delrin's lowest established temperature is -20 °C; approximately 7 °C higher than the aluminium casing.

### 10.5.2 90 Degree Beta Angle

Whilst the temperature range for BLUEsat in a pure sun-lit orbit is optimal for the onboard subsystems, varying from +1 °C to + 14 °C, the thermal gradient across the trays was shown significant temperature variation. The large variation of temperatures on the side panels contributed to thermal gradients of approximately 5 °C, particularly for the middle three trays.



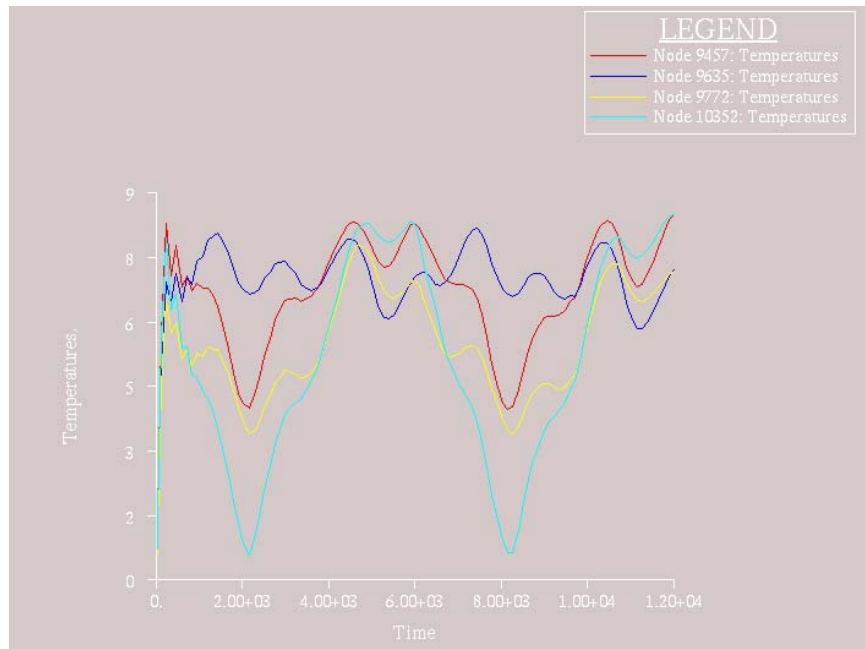


**Figure 10-9: Tray 4 Orbital Temperatures (90 Degree Beta Angle)**

The representative nodes (NODES 13396, 14906 and 10352) for the large temperature drop spikes can be referenced back to the tray side in closest contact to Side 1 of the SINDA analysis. This panel establishes a maximum temperature of no greater than 6.3 °C as opposed to the cyclic maximums of approximately 14 °C for the other 3 panels.

Although not completely critical to majority of the components (as the range still remains within the acceptable 0 to 20 °C band) and the structure, the battery placement location presents a concern since the limit temperature differential between each battery module is  $\pm 5$  °C.

This abnormality can be linked to a unique orbital behaviour of BLUEsat that was configured in NEVADA. The simplification of the orbital manoeuvre inputs meant that, when the z-axis spin rate of BLUEsat combines with the

equatorial flip, Side 1 fails to ever view direct sunlight. Ideally, we could have assumed similar temperatures for Side 1 to the other panels.

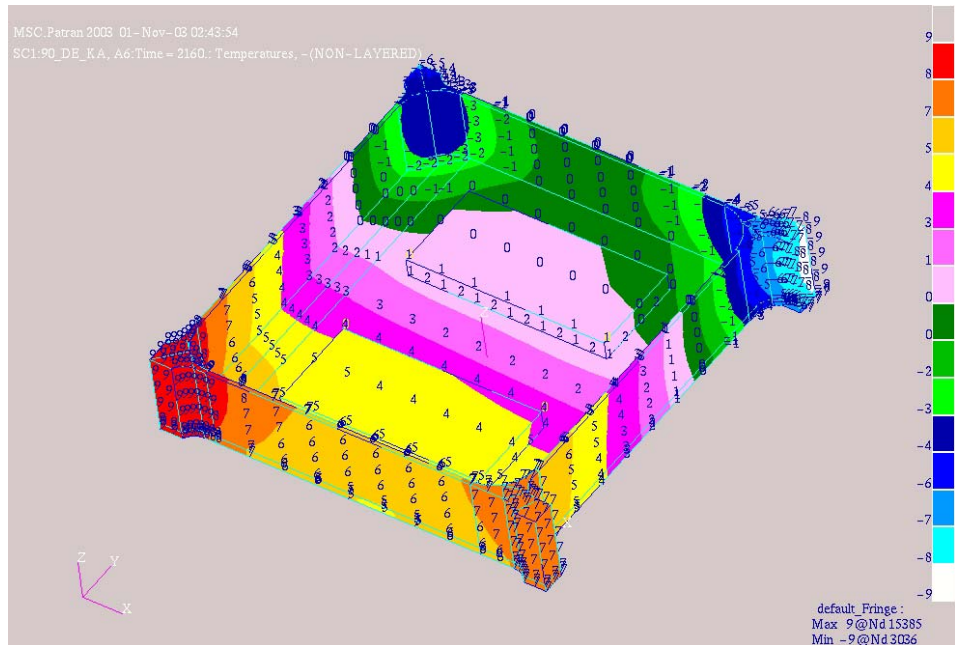


**Figure 10-10: Battery Modules thermal gradient due to lower orbital heating on Side 1**

The direct attachment to the top and bottom plate improved the overall thermal gradient for the Tray 1 and Tray 5 respectively.

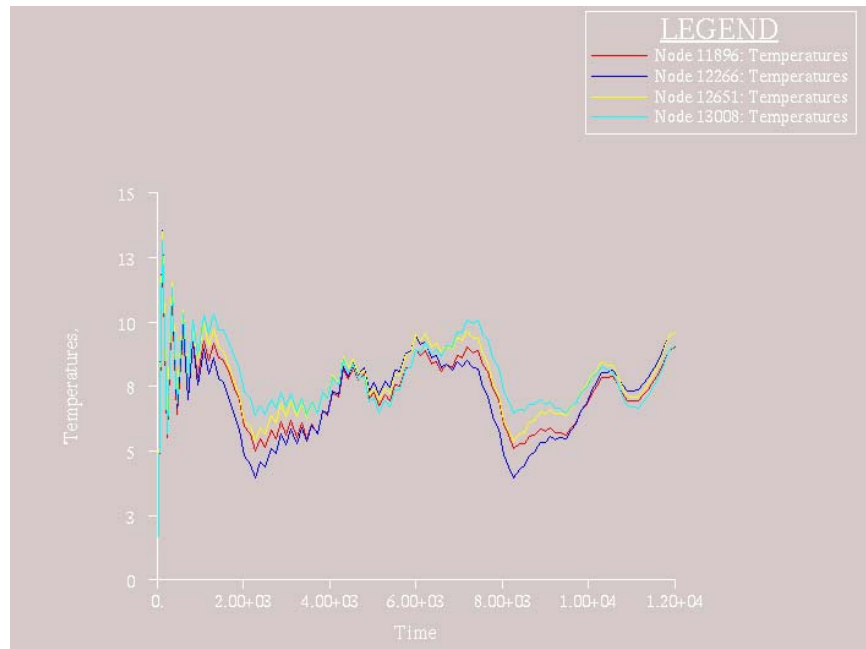


**Figure 10-11: Tray 1 Orbital Temperatures (90 Degree Beta Angle)**

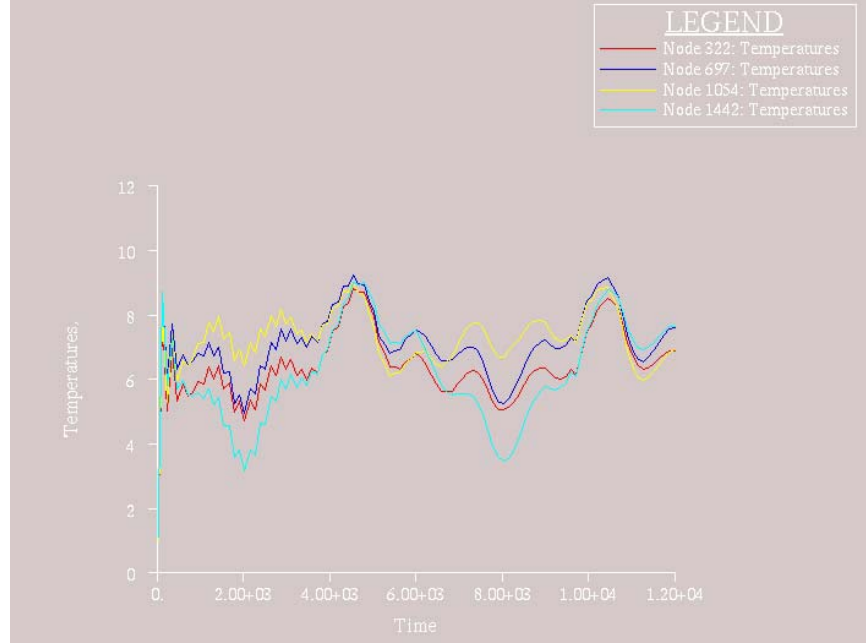


**Figure 10-12: Tray 5 Orbital Temperatures (90 Degree Beta Angle)**

Note the early nodal temperature distortion of the 1<sup>st</sup> orbit reflects the transient response to the impact of 5 temperature inputs (four side panels plus top or bottom plate) and the conductance of heat energy throughout the rest of the

structure. By the 2<sup>nd</sup> orbit, it is evident the thermal conductance behaviour has settled.

The thermal gradient experienced on the middle trays was also evident on the battery casings. Kapton was again installed between the casings and the battery plate. The results for the aluminium casing show a difference in temperatures between the two battery modules greater than 5 °C as it is obvious to recognise the two modules in relation to the element numbers. Therefore, for this analysis, using an aluminium casing would not meet our component thermal requirements.

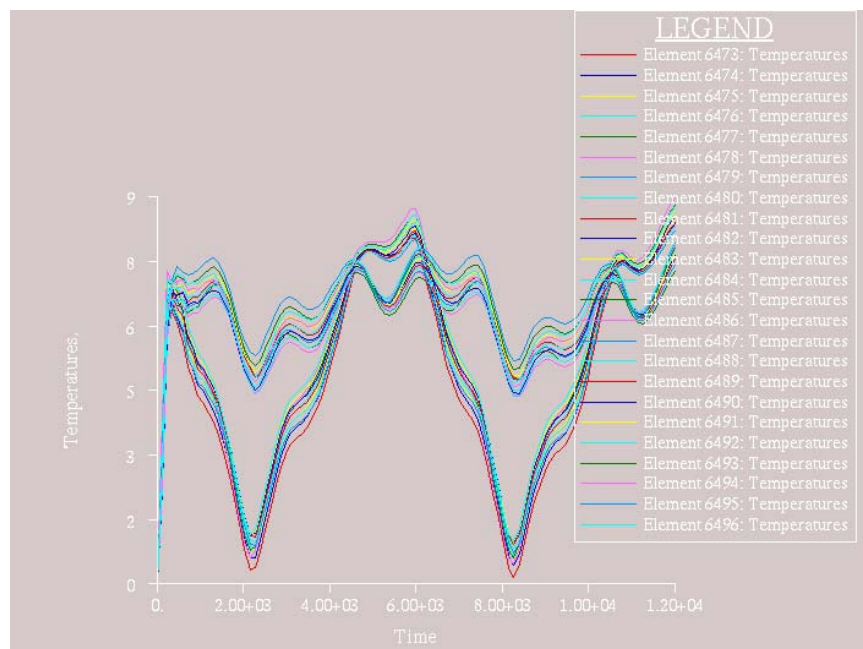


**Figure 10-13: 6061-T6 Battery Casing Orbital Temperatures**

Similarly to the 0 degree Beta angle results, the Delrin performed marginally better to its aluminium counterpart, with slightly lower differences in temperatures for the two modules. However the thermal gradient across each particular module was greater by approximately 0.5 - 1 °C.

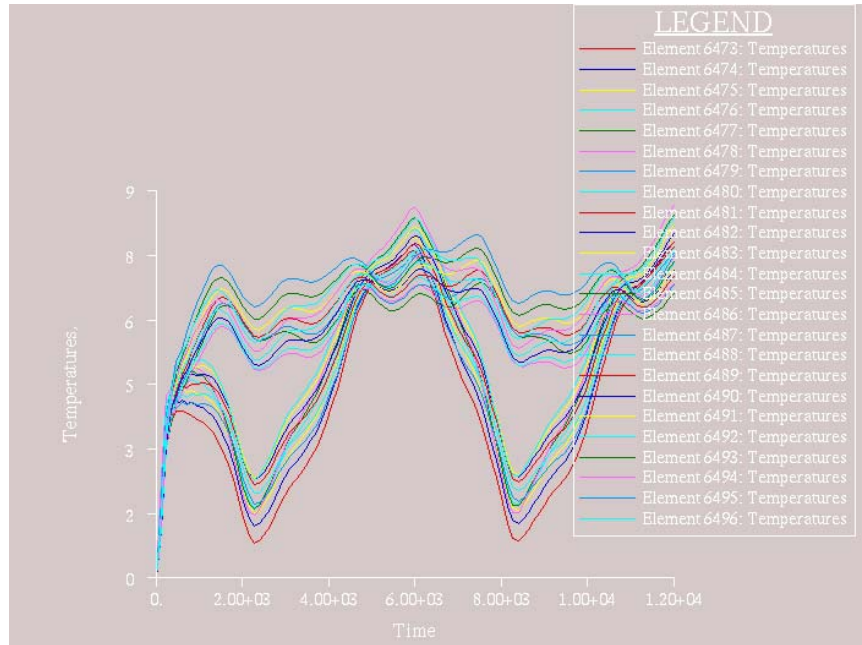


**Figure 10-14: Delrin Battery Casing Orbital Temperatures**

As stated above, the orbital anomaly of Side 1 not viewing the direct solar flux became apparent for the 90 Degree Beta case and thus affects the results for the battery casing analysis as well. If assuming proper heating on all sides in the NEVADA analysis (up to + 14 °C approximately), we could expect both modules to remain within a 5.5 °C to 8.5 °C margin operating condition which would be safe for optimal operating conditions.

### 10.5.3 Kapton Insulation

Kapton was implemented in both analyses as an example of thermal control design via computational analysis. Following from the SINDA results it became clear the 0 degree beta orbital case will yield extremely low onboard temperatures, especially for the batteries. The low specific heat and thermal

conductivity of kapton allows it to be a decent thermal insulator to some level as the flow of heat energy becomes lagged.

Results though, showed that under transient conditions, where each computation was done with 120 second intervals (2 minutes each), the effect of using Kapton had no apparent success in blocking stored heat energy within the casings to the rest of the structure where the temperatures were sub zero.

Therefore, these results show that the implementation of Kapton will not improve the thermal control of the battery modules.

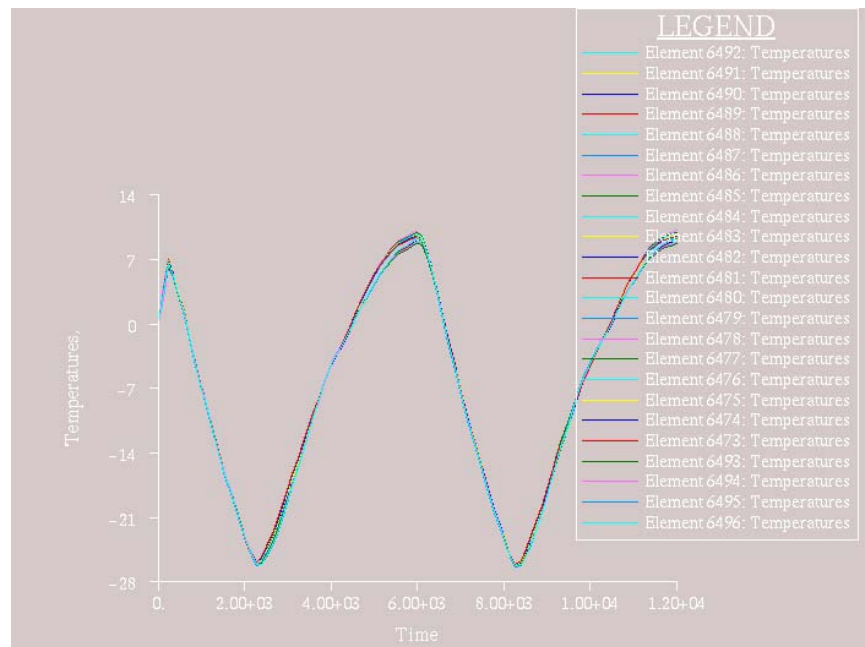


**Figure 10-15: Aluminium Battery Casing with Kapton**

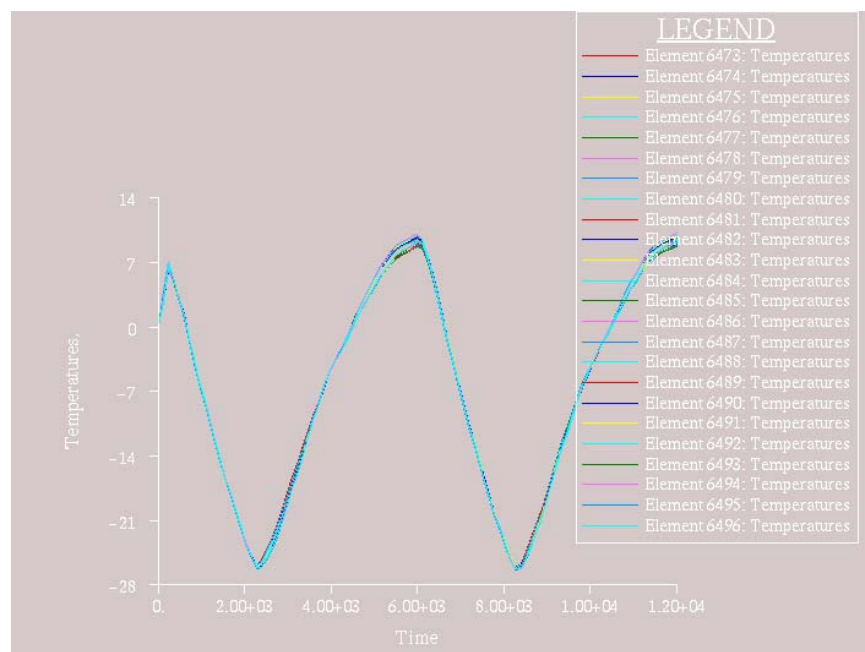


**Figure 10-16: Aluminium Battery Casing without Kapton**

## 11 Results Evaluation

### 11.1 Orbital Scenario

In review of the results from both the SINDA plots and visual representation in Patran, a few concerns are needed to be raised when considering an orbital selection with eclipse time. However it must be recognised that for the 0 Degree Beta angle, this only signifies the worst case cold temperature scenario where approximately 50 % of the orbital period is in eclipse. For the current AMSAT microsatellites launched over a decade ago, the duration of the satellite in darkness was approximately one-third of the orbit.

To select an optimal orbit from a thermal analytical point of view, a pure sun-lit orbit would be recommended for BLUEsat. The temperature range for such an orbit is perfect for the onboard operating condition as well as structurally because of its narrow temperature range and near earth surface-like temperatures.

Another advantage to a 90 Degree Beta orbit is the continuous illumination of sunlight on the solar cells. The orientation of BLUEsat would be ideal for this as the thick bottom plate will not be subjected to direct solar flux hence remain cooler than the 0 Degree Beta orbit. Continual solar illumination also means the batteries will continually be in a cold case condition; not discharging thus heating up.

Should an ecliptic orbit be selected, the major cause for concern is the moderate low temperature conditions with BLUEsat. Relying only on the minimal effect of Earth IR, it is impossible for BLUEsat to maintain optimal operating conditions solely due to the fact its onboard equipment operate at significantly low powers (the trade off for micro technology!). In effect low thermal dissipations cannot compete with the sheer lack of stored structural heat energy.

## ***11.2 Structural Thermal Control Design Considerations***

### **11.2.1 External Surfaces**

When applying the OSR to the external surfaces of BLUEsat for the SINDA analysis, it was assumed that the entirety of the non-covered surfaces would have the OSR applied. In reality, thermal coatings are usually applied in small regions and reanalysed in order to ‘fine-tune’ spacecraft thermal performance.

Therefore taking the 90 Degree Beta angle orbital scenario into account, the amount of OSR could be reduced in order to raise the minimum temperature. Achieving a desired solution is purely based on trial and error, where it might be feasible to utilise the characteristics of several thermal surface coatings. For

example, since the bottom plate has relatively lower temperatures due to its surface normal direction to earth, a coating of higher absorbance might be incorporated.

When considering the SINDA results, maintaining a bare aluminium external surface would be acceptable since the desired temperature range is achieved. Note that the bare aluminium surface condition was assumed to be “as received”. To reduce maximum temperature, thus solar absorptivity, the aluminium should be polished.

### **11.2.2 Internal Surfaces**

The effect of passive thermal control should become significant within the structure rather than on the external surfaces. The predominant aim for thermal control of BLUEsat is to maintain acceptable temperature ranges for all subsystems.

In review of the thermal behaviour according to the transient thermal analysis, there are obviously some significant heat transfer trends occurring where large thermal gradients are spread throughout the trays.

It is recommended to apply Chemglaze Z306 (space qualified) to all inner surfaces to improve the radiation of thermal energy. In effect, temperatures within BLUEsat will become more balanced overall.

High dissipating equipment such as the TX should also be fixed to a plate or casing to act as a thermal doubler: relieving high temperatures off the circuit. The casing should also be painted black to alleviate high temperatures.

### **11.2.3 Joint Conductance**

All regions on BLUEsat that are mated together via fittings will present a significant thermal risk if the machining tolerance is high. The inability for heat energy to conduct through the satellite will create possible misalignment and stress concentrations due to thermal expansion.

The results of this thesis are based on perfect conductance, and, even though in reality can't be achieved; TCS measures are advised to ensure sound thermal transport throughout BLUEsat.

For all components with hard dimensional constraints, such as the mating surfaces of the trays, tray plates, solar panels, top plate and bottom plate, the following options are:

1. machining tolerance should be improved
2. Increase in torque thus contact pressure
3. Interstitial material such as thin foil which is softer then the interacting surfaces.

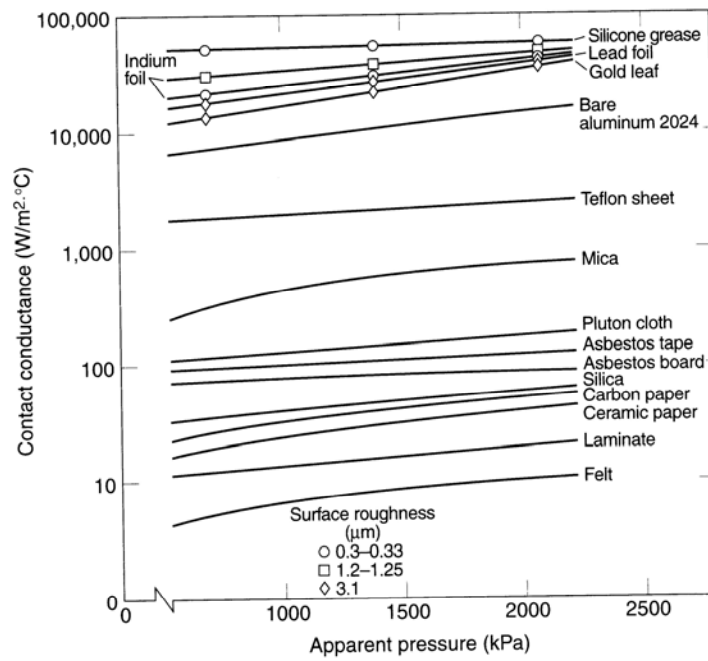


FIG. 8-26 Heat-transfer coefficients of selected interstitial materials.<sup>8,45</sup>

**Figure 11-1: Effective conductance with apparent pressure (Courtesy Gilmore [2])**

**Table 8.1. Surface Roughness Produced by Common Production Methods<sup>a</sup>**

Process	Roughness Average $R_a$ [ $\mu\text{m}$ ( $\mu\text{in}$ )] <sup>b</sup>											
	50 (2000)	25 (1000)	12.5 (500)	6.3 (250)	3.2 (125)	1.6 (63)	0.8 (32)	0.4 (16)	0.2 (8)	0.1 (4)	0.05 (2)	0.025 (1)
Flame cutting	■■■■■											
Snagging	■■■■■											
Sawing	■■■■■											
Planing, shaping	■■■■■											
Drilling	■■■■■											
Chemical milling	■■■■■											
Elect. discharge mach	■■■■■											
Milling	■■■■■											
Broaching	■■■■■											
Reaming	■■■■■											
Electron beam	■■■■■											
Laser	■■■■■											
Electrochemical	■■■■■											
Boring, turning	■■■■■											
Barrel finishing	■■■■■											
Electrolytic grinding	■■■■■											
Roller burnishing	■■■■■											
Grinding	■■■■■											
Honing	■■■■■											
Electro polish	■■■■■											
Polishing	■■■■■											
Lapping	■■■■■											
Super finishing	■■■■■											
Sand casting	■■■■■											
Hot rolling	■■■■■											
Forging	■■■■■											
Perm mold casting	■■■■■											
Investment casting	■■■■■											
Extruding	■■■■■											
Cold rolling, drawing	■■■■■											
Die casting	■■■■■											

<sup>a</sup>*Machinery's Handbook*, Industrial Press<sup>b</sup>The ranges shown are typical of the processes listed. Higher or lower values may be obtained under special conditions.**Figure 11-2: Standard surface roughness for manufacturing processes (Courtesy Gilmore [2])**

#### 11.2.4 Battery Insulation

The affectivity of implementing Kapton to insulate the battery modules from the battery plate was negligible for both scenario cases and thus is not required between the battery casings and the bottom plate.

For the 0 degree Beta orbital case, using a Delrin battery casing showed better thermal performance (temperatures tended closer to 0, with a lower range), than the aluminium casing. Delrin tended to have a greater temperature distribution across each module for the 90 degree beta angle, yet still below the 5 ° C limit.

If the thermal mass budget is low (amount of mass added to satellite for thermal control), in which case for a microsatellite it should, using Delrin battery casings would be recommended due to its lower density:

- Aluminium - 2700 Kg / m<sup>3</sup>
- Delrin - 1410 Kg / m<sup>3</sup>

This reduced the weight to approximately half. Being an electrical insulator as well, Delrin would be more suitable for interaction with naked battery cells.

Usage of aluminium means special preparation of cells where the skins have to be wrapped in either kapton or fibreglass to prevent shorting.

## 12 Conclusion

By conducting the thermal analysis of BLUEsat using a two stage finite difference / finite element approach, feasible results have now been obtained to enable the implementation of thermal control system design. From the results obtained, certain thermal design has been recommended as well as the desired orbital profile.

The variety of factors that contribute to the in-orbit thermal environment can easily be accounted for by this approach. The unique view factor finite difference calculations mean that any orbital scenario can be analysed according to the mission ( only two were accomplished in this case) ,whilst continual design and implementation of systems in BLUEsat can simply be modelled in the existing thermal FE model for reanalyses when required.

### 12.1 FD Analysis

Results from the Finite difference analysis proved to be acceptable when verified with existing similar microsatellites telemetry. From this we can deduce that the software used was essential for sound analysis of the spacecraft in-orbit thermal environment.

These temperature results for the external sides of BLUEsat were established by solving finite difference heat balance equations for six surfaces of simplified representation to the physical model.

One issue with the software was the inability to properly input the correct spin conditions in the orbital manoeuvres card in Nevada. Software problems were apparent when advanced orbital inputs were carried out so a simplified spin model needed to be substituted.

## **12.2 FE Analysis**

The detailed FE BLUEsat model allowed better appreciation of the thermal conditions and behaviour within the structure. Using data gained from the SINDA analysis, temperature distributions from within the satellite were established successfully, albeit under a number of assumptions.

Using Nastran, a thermo-stress analysis on the side solar panels allowed further design improvements for survivability in the harsh space environment.

Battery design and thermal conditions were also analysed, thus the recommendations to the Delrin casing and a sun-lit orbit were advised.

Creation of a finite element model allows subsystem interfacing to be conducted based on the internal thermal environment (such as installing the TX in a region of lower thermal energy to assist heat dissipation via conduction from the hot final stage amplifier).

### 12.3 Further Work

Being the first phase of thermal analysis of BLUESat being completed, much simplification and many assumptions needed to be made in order to achieve acceptable results. With software availability being the largest issue to this thesis, it became apparent that for ease of satellite orbital analysis in the future, selecting specifically designed software is essential. For a better interface between the radiation solver software (Nevada) and a detailed FE model, Patran Thermal would be recommended as it has the ability to perform satellite thermal analysis through specific importing / exporting interfaces with NEVADA [24].

Utilising this interface could then be orchestrated through the use of SINDA / ATM which allows imports of complex Patran FE models, sets up radiation and material properties and then passes to Nevada for radiation analysis.

Other improvements to the thermal model would include the following which predominantly address the many assumption made for this thesis.

1. Modelling aluminium honeycomb with its orthotropic conductivity properties for a more realistic heat transportation behaviour on the model (see Appendix G)
2. Apply temperature dependant material properties for analysis of the non-linear thermal behaviour in the structure
3. Apply internal radiation conditions to all surfaces

4. Apply other subsystems heat flux onto the model (at the time of writing, many subsystems had not yet been finalised)

## References

[1] Dick Jansson

*Microsatellite Thermal Design and Flight Thermal Coatings*

AMSAT – NA Memorandum

[2] David G. Gilmore

*Spacecraft Thermal Control Handbook*

The Aerospace Corporation

[3] J. Wertz & W. Larson

*Space Mission Analysis and Design, 3<sup>rd</sup> Edition*

Space Technology Library, 1999

[4] J. A. King, R. McGwier, H. Price, J. White

*The In-Orbit Performance of Four Microsatellite Spacecraft*

[5] Dean Mackenzie

*Analysis of Solar Panels for the Australis-1 Microsatellite*

UNSW School of Mechanical And Manufacturing Engineering, 1994

[6] TAC Technologies

*VEGAS (Verified Earthshine, Geometric Albedo and Solar) Manual*

Software Manual

## References

[7] D. P. DeWitt

*Fundamentals of Heat and Mass Transfer*

John Wiley and Sons

[8] M. D. Griffen & J. R. French

*Space Vehicle Design*

AIAA Education Series

[9] Volodymyr Baturkin

*Micro-satellites Thermal Control – Concepts and Components*

Kyiv Polytechnic Institute

[10] Spartnik Microsatellite Project

*Thermal Final Design Review*

[11] M. M. Finckenor and D.D. Dooling

*Multilayer Insulation Material Guidelines*

NASA/TP-1999-209263

[12] Matthieu Gasquet

*Solar Orbiter: Thermal Analysis and Design of an Extreme Ultra Violet*

*Spectrometer*

Research Thesis Report, Cranfield University

## References

[13] D. V. Hale, M. J. Hoover and M. J. O'Neill

*Phase Change Materials Handbook*

NASA Contractor Report

[14] *HexWeb Honeycomb Attributes and Properties*

HEXCEL Composites

[15] Robert D. Karam

*Satellite Thermal Control for Systems Engineers*

Progress in Astronautics and Aeronautics

[16] Ron Behee

*SINDA / G Thermal Modelling System Users Guide*

Network Analysis Inc.

[17] Ashley Butterworth

*Conversation*

7<sup>th</sup> October 2003

[18] Sanyo

*Sanyo Cell Type HF-A1U Specifications*

<http://www.master-instruments.com.au>

## References

[19] Matweb

*Material Specifications*

<http://www.matweb.com>

[20] Patran

*Online Example Tutorials*

[http://www.mscsoftware.com/support/online\\_ex/scenario/satellitestructural.cfm](http://www.mscsoftware.com/support/online_ex/scenario/satellitestructural.cfm)

[21] R. D. Cook

*Finite Element Modelling for Stress Analysis*

John Wiley & Sons, USA

[22] European Cooperation for Space Standardisation

*ECSS-E-30 Part 1A Thermal Control*

Requirements and Standards Division

[23] R. Behee

*SINDA / G Library Reference Guide Version 2.3*

Network Analysis Inc.

[24] Dieter Roos & Alan Diner

*Thermal Design of a Satellite with Articulating Solar Panels*

Research Publication

## References

[25] Daniel Faber

*Solar Arrays for a Microsatellite*

UNSW School of Mechanical and Manufacturing Engineering, 2001

[26] K & K Associates

*Thermal Finishes*

<http://www.tak2000.com/data/finish.htm>

[27] Digital

*DIGITAL Semiconductor SA-1100 Microprocessor Data Sheet*

Digital Equipment Corporation

[28] Spectrolab

*Silicon K4702 Silicon Solar Cells*

<http://www.spectrolab.com/DataSheets/K4702/k4702.pdf>

[29] TAK2000

*Thermal Conversions Utility*

<http://www.tak2000.com/thermalconv.htm>

[30] Thomas P. Sarafin

*Spacecraft Structures and Mechanisms*

Space Technology Library

## References

[31] ECSS-E-30

*Space Engineering, Mechanical Part 1 Thermal Control*

European Cooperation for Space Standardisation

[32] Paul Croaker

Design and Analysis of BLUEsat's Solar Panels

UNSW School of Mechanical and Manufacturing Engineering, 2000

[33] M. Mahbubi Fard and M. H. Rahimyan

*Design and Analysis of a Microsatellite Passive Thermal Control System*

*Using Determinants and FEM Methods*

Mechanical Eng. Department, University of Tehran, Tehran, Iran

## A SINDA G INPUT FILES

### SINDA INPUT FILE (SIN)

The following is the complete SINDA Input File (SIN) Generated from both FEMAP (Advanced Thermal Modeller) and NEVADA Radiation Analysis code. Refer to CD for all complete SINDA Input Files used for this thesis.

```

C SINDA/G input file created for problem name: model3_90_n
BCD 3THERMAL LPCS
END
BCD 3NODE DATA
  1, 0.000000 , 0.3040634 $BLUESat model
  2, 0.000000 , 0.3040634
  5, 0.000000 , 0.3040634
  9, 0.000000 , 0.3040634
 10, 0.000000 , 0.3040634
 14, 0.000000 , 0.3040634
 16, 0.000000 , 0.3040634
 23, 0.000000 , 0.3040634
C Boundary nodes created by the translator
 -24, -273.1500 , 0.000000 $Radiation to space
END
BCD 3SOURCE DATA
PER 1,A5008,A5007, 0.2500000 , 0.000000 , 5963.638
PER 1,A5008,A5005, 0.2500000 , 0.000000 , 5963.638
PER 1,A5008,A5003, 0.2500000 , 0.000000 , 5963.638
PER 2,A5008,A5007, 0.2500000 , 0.000000 , 5963.638
PER 2,A5008,A5004, 0.2500000 , 0.000000 , 5963.638
PER 2,A5008,A5005, 0.2500000 , 0.000000 , 5963.638
PER 5,A5008,A5005, 0.2500000 , 0.000000 , 5963.638
PER 5,A5008,A5002, 0.2500000 , 0.000000 , 5963.638
PER 5,A5008,A5003, 0.2500000 , 0.000000 , 5963.638
PER 9,A5008,A5003, 0.2500000 , 0.000000 , 5963.638
PER 9,A5008,A5007, 0.2500000 , 0.000000 , 5963.638
PER 9,A5008,A5006, 0.2500000 , 0.000000 , 5963.638
PER 10,A5008,A5003, 0.2500000 , 0.000000 , 5963.638
PER 10,A5008,A5006, 0.2500000 , 0.000000 , 5963.638
PER 10,A5008,A5002, 0.2500000 , 0.000000 , 5963.638
PER 14,A5008,A5005, 0.2500000 , 0.000000 , 5963.638
PER 14,A5008,A5004, 0.2500000 , 0.000000 , 5963.638
PER 14,A5008,A5002, 0.2500000 , 0.000000 , 5963.638
PER 16,A5008,A5004, 0.2500000 , 0.000000 , 5963.638
PER 16,A5008,A5007, 0.2500000 , 0.000000 , 5963.638
PER 16,A5008,A5006, 0.2500000 , 0.000000 , 5963.638
PER 23,A5008,A5002, 0.2500000 , 0.000000 , 5963.638
PER 23,A5008,A5004, 0.2500000 , 0.000000 , 5963.638
PER 23,A5008,A5006, 0.2500000 , 0.000000 , 5963.638
END
BCD 3CONDUCTOR DATA
C Conductors due to element conduction
  1, 1, 2, 0.3342663E-03
  2, 1, 5, 0.3662082E-03
  3, 1, 9, 0.3342663E-03
  4, 2, 14, 0.3662082E-03
  5, 2, 16, 0.3342663E-03
  6, 5, 10, 0.3342663E-03
  7, 5, 14, 0.3342663E-03
  8, 9, 10, 0.3662082E-03
  9, 9, 16, 0.3342663E-03
 10, 10, 23, 0.3342663E-03
 11, 14, 23, 0.3342663E-03

```

```

12, 16, 23, 0.3662082E-03
C Conductors due to radiation loads
-13, 1, 24, 0.2556148E-01
-14, 2, 24, 0.2556148E-01
-15, 5, 24, 0.2747756E-01
-16, 9, 24, 0.2556148E-01
-17, 10, 24, 0.2747756E-01
-18, 14, 24, 0.2747756E-01
-19, 16, 24, 0.2556148E-01
-20, 23, 24, 0.2747756E-01
END
BCD 3CONSTANTS DATA
DRLXCA=0.1000000E-02
ARLXCA=0.1000000E-02
NLOOP=5000
OUTPUT=120.0000           $Time step
TIMEND=50000.00           $Orbital analysis time duration
SIGMA=0.5379000E-10
TMPZRO=273.1500
END
BCD 3ARRAY DATA
C arrays from orbital radiation solution
5008
 0.000000 , 248.4720 , 496.9800 , 745.4520
 934.7400 , 934.9200 , 993.9240 , 1242.432
 1490.904 , 1739.376 , 1987.884 , 2236.356
 2484.864 , 2733.336 , 2981.808 , 3230.316
 3478.788 , 3727.080 , 3975.840 , 4224.240
 4472.640 , 4721.400 , 4969.800 , 5028.840
 5028.840 , 5218.200 , 5466.600 , 5715.000
 5963.760
END
5002
 1.545700 , 1.545700 , 1.545700 , 1.545700
 1.545700 , 1.545700 , 1.545700 , 1.552200
 1.669500 , 2.047900 , 2.611400 , 3.273300
 3.659300 , 3.908800 , 3.581400 , 3.965000
 3.710400 , 3.308200 , 2.628900 , 2.120000
 1.688100 , 1.552600 , 1.545700 , 1.545700
 1.545700 , 1.545700 , 1.545700 , 1.545700
 1.545700
END
5003
 1.545400 , 1.545400 , 1.545400 , 1.545400
 1.545400 , 37.95600 , 39.38700 , 43.79000
 43.96300 , 44.48000 , 40.61900 , 34.10200
 25.37000 , 14.99500 , 3.416500 , 3.446500
 3.146600 , 2.737600 , 2.071500 , 1.644100
 1.545400 , 1.545400 , 1.545400 , 1.545400
 1.545400 , 1.545400 , 1.545400 , 1.545400
 1.545400
END
5004
 1.510400 , 1.510400 , 1.510400 , 1.510400
 1.510400 , 1.510400 , 1.510400 , 1.510400
 1.510400 , 1.608000 , 2.006800 , 2.748800
 3.182800 , 3.495300 , 3.499500 , 15.46200
 26.25700 , 35.36500 , 42.08000 , 46.09500
 46.05100 , 43.50200 , 39.12400 , 37.70100
 1.510400 , 1.510400 , 1.510400 , 1.510400
 1.510400
END
5005
 0.000000 , 0.000000 , 0.000000 , 0.000000
 0.000000 , 0.000000 , 0.000000 , 0.000000
 0.000000 , 10.54600 , 20.37400 , 28.81300
 35.28800 , 39.35900 , 43.53700 , 42.05400
 37.70500 , 30.78600 , 21.76900 , 11.26800
 0.000000 , 0.000000 , 0.000000 , 0.000000
 0.000000 , 0.000000 , 0.000000 , 0.000000
 0.000000
END
5006
 6.343900 , 6.343900 , 6.343900 , 6.343900
 6.343900 , 30.38500 , 28.08600 , 17.63000

```

```
6.866900 , 8.958900 , 11.23700 , 12.33300
13.71600 , 14.63100 , 15.34400 , 14.65400
13.79300 , 12.42300 , 11.04400 , 9.044300
6.850200 , 17.33200 , 27.50700 , 29.74500
6.343900 , 6.343900 , 6.343900 , 6.343900
6.343900

END
5007
1.072300 , 1.072300 , 1.072300 , 1.072300
1.072300 , 1.072300 , 1.072300 , 1.078400
1.203100 , 1.583200 , 1.957100 , 2.433200
2.741000 , 2.952900 , 3.207700 , 3.178100
2.958300 , 2.609900 , 2.061100 , 1.543200
1.179000 , 1.078800 , 1.072300 , 1.072300
1.072300 , 1.072300 , 1.072300 , 1.072300
1.072300

END
END
BCD 3EXECUTION
  SNDUFR           $Subroutine selected
END
BCD 3VARIABLES 1
END
BCD 3VARIABLES 2
END
BCD 3OUTPUT CALLS
  TPNTSN
  NEUOUT
END
BCD 3END OF DATA
```

## B SINDA G OUTPUT FILES

### SINDA OUTPUT FILE (SOT)

The following is an extract out of the SINDA Output file **model3\_0\_n.SOT**.

(C) COPYRIGHT 1982-2001 J.D.GASKI SINDA/G VERSION-2.20 NETWORK ANALYSIS ASSOCIATES, INC. - PAGE 1

```
*** NOTE *** SNDUFR REQUIRES 35 DYNAMIC STORAGE LOCATIONS OUT OF 87 AVAILABLE ***
TIMEND= 50000. , CSGFAC= 1.0000 , DTIMEI= 0.0000 , NLOOP = 5000
ARLXCA= 0.10000E-02, ATMPCA= 0.0000 , DTMPCA= 0.10000E+09

*****
TIME= 0.00000E+00, DTIMEU= 0.00000E+00, CSGMIN( 0)= 0.00000E+00, ATMPCC( 0)= 0.00000E+00, DTMPCC( 0)=
0.00000E+00
LOOPCT= 0 , ARLXCC( 0)= 0.00000E+00, DRLXCC( 0)= 0.00000E+00

**** OUTPUT TEMPERATURES IN DEGREES ****
T 1= 0.0000 T 2= 0.0000 T 5= 0.0000 T 9= 0.0000 T 10= 0.0000 T 14= 0.0000
T 16= 0.0000 T 23= 0.0000 T 24=-273.1500

*****
TIME= 1.20000E+02, DTIMEU= 1.20000E+02, CSGMIN( 5)= 2.85542E+02, ATMPCC( 0)= 0.00000E+00, DTMPCC( 5)=-
2.35500E+00
LOOPCT= 0 , ARLXCC( 0)= 0.00000E+00, DRLXCC( 0)= 0.00000E+00

**** OUTPUT TEMPERATURES IN DEGREES ****
T 1= -1.7345 T 2= -1.7281 T 5= -2.3550 T 9= -1.7291 T 10= -2.3495 T 14= -2.3486
T 16= -1.7227 T 23= -2.3432 T 24=-273.1500

*****
TIME= 2.40000E+02, DTIMEU= 1.20000E+02, CSGMIN( 23)= 2.85749E+02, ATMPCC( 0)= 0.00000E+00, DTMPCC( 5)=-
2.59721E+00
LOOPCT= 0 , ARLXCC( 0)= 0.00000E+00, DRLXCC( 0)= 0.00000E+00

**** OUTPUT TEMPERATURES IN DEGREES ****
T 1= -3.7798 T 2= -3.7675 T 5= -4.9522 T 9= -3.7693 T 10= -4.9418 T 14= -4.9400
T 16= -3.7571 T 23= -4.9295 T 24=-273.1500
```

\*\*\*\*\*

TIME= 3.60000E+02, DTIMEU= 1.20000E+02, CSGMIN( 23)= 2.85972E+02, ATMPCC( 0)= 0.00000E+00, DTMPCC( 5)=  
2.47409E+00

LOOPCT= 0 , ARLXCC( 0)= 0.00000E+00, DRLXCC( 0)= 0.00000E+00

\*\*\*\* OUTPUT TEMPERATURES IN DEGREES \*\*\*\*

T 1 = -5.8712 T 2 = -5.8546 T 5 = -7.4263 T 9 = -5.8570 T 10 = -7.4122 T 14 = -7.4098  
T 16 = -5.8405 T 23 = -7.3957 T 24 = -273.1500

\*\*\*\*\*

TIME= 4.80000E+02, DTIMEU= 1.20000E+02, CSGMIN( 23)= 2.86182E+02, ATMPCC( 0)= 0.00000E+00, DTMPCC( 5)=  
2.31534E+00

LOOPCT= 0 , ARLXCC( 0)= 0.00000E+00, DRLXCC( 0)= 0.00000E+00

\*\*\*\* OUTPUT TEMPERATURES IN DEGREES \*\*\*\*

T 1 = -7.9428 T 2 = -7.9233 T 5 = -9.7416 T 9 = -7.9261 T 10 = -9.7250 T 14 = -9.7222  
T 16 = -7.9066 T 23 = -9.7056 T 24 = -273.1500

\*\*\*\*\*

TIME= 6.00000E+02, DTIMEU= 1.20000E+02, CSGMIN( 23)= 2.86376E+02, ATMPCC( 0)= 0.00000E+00, DTMPCC( 5)=  
2.17540E+00

LOOPCT= 0 , ARLXCC( 0)= 0.00000E+00, DRLXCC( 0)= 0.00000E+00

\*\*\*\* OUTPUT TEMPERATURES IN DEGREES \*\*\*\*

T 1 = -9.9694 T 2 = -9.9479 T 5 = -11.9171 T 9 = -9.9510 T 10 = -11.8987 T 14 = -11.8956  
T 16 = -9.9296 T 23 = -11.8773 T 24 = -273.1500

\*\*\*\*\*

TIME= 7.20000E+02, DTIMEU= 1.20000E+02, CSGMIN( 23)= 2.86554E+02, ATMPCC( 0)= 0.00000E+00, DTMPCC( 5)=  
2.05722E+00

LOOPCT= 0 , ARLXCC( 0)= 0.00000E+00, DRLXCC( 0)= 0.00000E+00

\*\*\*\* OUTPUT TEMPERATURES IN DEGREES \*\*\*\*

(C) COPYRIGHT 1982-2001 J.D.GASKI SINDA/G VERSION-2.20 NETWORK ANALYSIS ASSOCIATES, INC. - PAGE 2

T 1 = -11.9385 T 2 = -11.9157 T 5 = -13.9743 T 9 = -11.9190 T 10 = -13.9548 T 14 = -13.9515  
T 16 = -11.8962 T 23 = -13.9321 T 24 = -273.1500

\*\*\*\*\*

TIME= 8.40000E+02, DTIMEU= 1.20000E+02, CSGMIN( 23)= 2.86721E+02, ATMPCC( 0)= 0.00000E+00, DTMPCC( 5)=  
1.95602E+00  
LOOPCT= 0 , ARLXCC( 0)= 0.00000E+00, DRLXCC( 0)= 0.00000E+00

\*\*\*\* OUTPUT TEMPERATURES IN DEGREES \*\*\*\*

T 1 = -13.8442 T 2 = -13.8205 T 5 = -15.9303 T 9 = -13.8239 T 10 = -15.9101 T 14 = -15.9066  
T 16 = -13.8002 T 23 = -15.8864 T 24 = -273.1500

These results continue up to time = 5.0000 E +04 seconds. For complete SINDA  
Output files refer to CD.

## C Calculation of BLUEsat Surface Area and Optical Properties

### 1. NAKED STRUCTURE

- Calculated Total Area Solar Absorptivity and IR Emissivity for Top Plate, Bottom Plate and Side Panels.
- No applied Thermal Control Coatings

BLUEsat Surface Areas And Optical Properties					
	Area (cm <sup>2</sup> )	Solar Abs. ( $\alpha$ )	IR Emit ( $\epsilon$ )	Area. $\alpha$ (cm <sup>2</sup> )	Area. $\epsilon$ (cm <sup>2</sup> )
<b>Microsatellite Face</b>					
+Z (TOP PLATE)					
Total Area	556.96	0.57486449	0.660396	320.176529	367.814419
Solar Cell	374.3712	0.61	0.81	228.366432	303.240672
Exposed PCB	62.352	0.72	0.89	44.89344	55.49328
Connecting Tabs	6.31	0.04	0.02	0.2524	0.1262
Antenna Mounts	6	0.96	0.87	5.76	5.22
Exposed Top Plate	107.9268	0.379	0.0346	40.9042572	3.73426728
X & Y SIDES (EACH)					
Total Area	523.92	0.58578841	0.697897	306.906267	365.642688
Solar Cell	374.3712	0.61	0.81	228.366432	303.240672
Exposed PCB	62.352	0.72	0.89	44.89344	55.49328
Connecting Tabs	6.31	0.04	0.02	0.2524	0.1262
Bolts	4.71238898	0.96	0.88	4.52389342	4.14690230
Exposed Side Panels	76.1744110			28.8701017	2.63563462
-Z (BOTTOM PLATE)					
Total Area	468.292036	0.53029851	0.522783	248.334573	244.815489
Solar Cell	233.982	0.61	0.81	142.72902	189.52542
Exposed PCB	54.8916	0.72	0.89	39.521952	48.853524
Connecting Tabs	6.31	0.04	0.02	0.2524	0.1262
Antenna Mounts	38.4	0.96	0.87	0.36864	0.33408
Exposed Bottom Plate	172.724436			65.4625615	5.97626551
	7	0.379	0.0346	2	1

## 2. OSR COATED STRUCTURE

- Calculated Total Area Solar Absorptivity and IR Emissivity for Top Plate, Bottom Plate and Side Panels.
- Optical Solar Reflector (OSR) Thermal Control Coatings Applied
- OSR - 5 mm Silver Backing Teflon Pressure Sensitive Tape

BLUEsat Surface Areas And Optical Properties					
	Area (cm <sup>2</sup> )	Solar Abs. ( $\alpha$ )	IR Emit ( $\epsilon$ )	Area. $\alpha$ (cm <sup>2</sup> )	Area. $\epsilon$ (cm <sup>2</sup> )
with OSR coating					
Microsatellite Face					
+Z (TOP PLATE)					
Total Area	556.96	0.57263606	0.799025	318.93538	445.025252
Solar Cell	374.3712	0.69	0.81	258.316128	303.240672
Exposed PCB	62.352	0.72	0.89	44.89344	55.49328
Connecting Tabs	6.31	0.04	0.02	0.2524	0.1262
Antenna Mounts	6	0.96	0.87	5.76	5.22
Exposed Top Plate	107.9268	0.09	0.75	9.713412	80.9451
X & Y SIDES (EACH)					
Total Area	523.92	0.60093441	0.801912	314.841558	420.137862
Solar Cell	374.3712	0.69	0.81	258.316128	303.240672
Exposed PCB	62.352	0.72	0.89	44.89344	55.49328
Connecting Tabs	6.31	0.04	0.02	0.2524	0.1262
Bolts	4.71238898	0.96	0.88	4.52389342	4.14690230
Exposed Side Panels	76.17441102	0.09	0.75	6.85569699	57.13080826
-Z (BOTTOM PLATE)					
Total Area	468.2920367	0.463675985	0.7866513	217.1357713	368.3825515
Solar Cell	233.982	0.69	0.81	161.44758	189.52542
Exposed PCB	54.8916	0.72	0.89	39.521952	48.853524
Connecting Tabs	6.31	0.04	0.02	0.2524	0.1262
Antenna Mounts	38.4	0.96	0.87	0.36864	0.33408

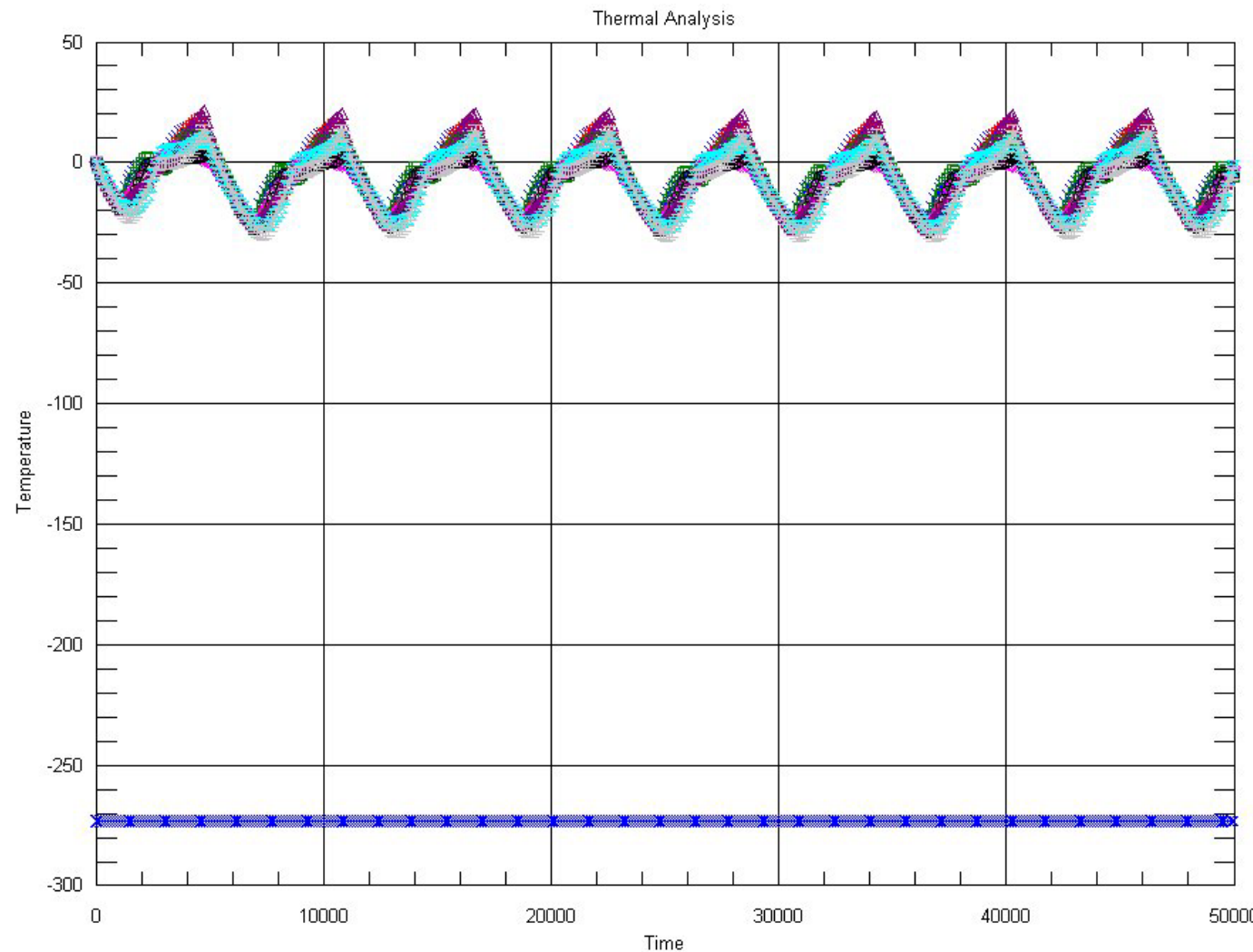
Exposed Bottom Plate	172.724436	7	0.09	0.75	15.5451993	129.543327	5
----------------------	------------	---	------	------	------------	------------	---

**D SINDAPLOTS**

## 1. Naked Structure

## 0 degree Beta Angle

DATA	LINETYPE
[1]T1	—x—
[1]T2	—+—
[1]T5	—□—
[1]T9	—◇—
[1]T10	—○—
[1]T14	—△—
[1]T16	—×—
[1]T23	—王—
[1]T24	—×—



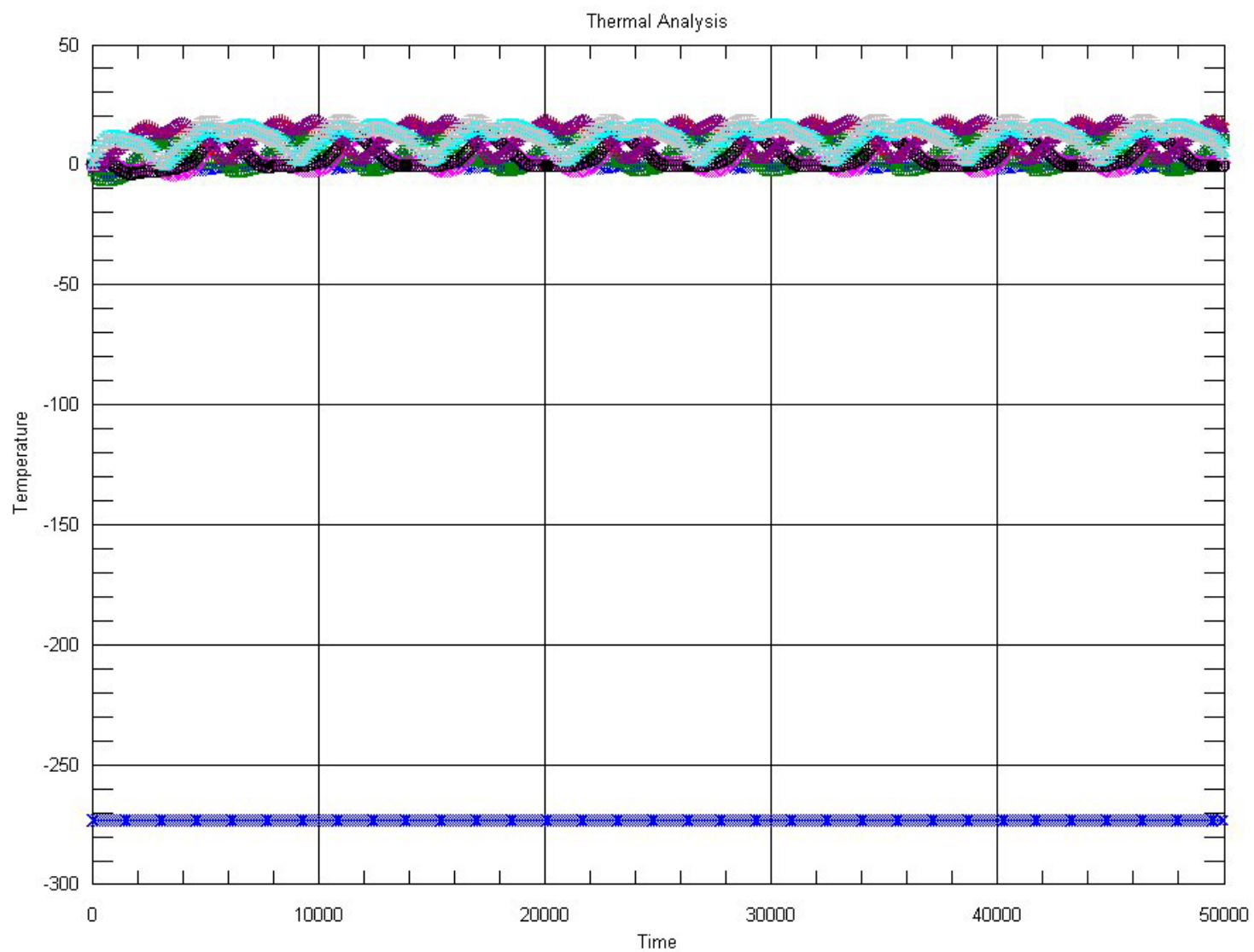
## SINDAPLOTS

## 2. Naked Structure

## 90 Degree Beta Angle

[1]model3\_90\_n.

DATA	LINETYPE
[1]T1	-x-
[1]T2	-+
[1]T5	-□-
[1]T9	-◇-
[1]T10	-○-
[1]T14	-△-
[1]T16	-x-
[1]T23	-I-
[1]T24	-·-x-·-

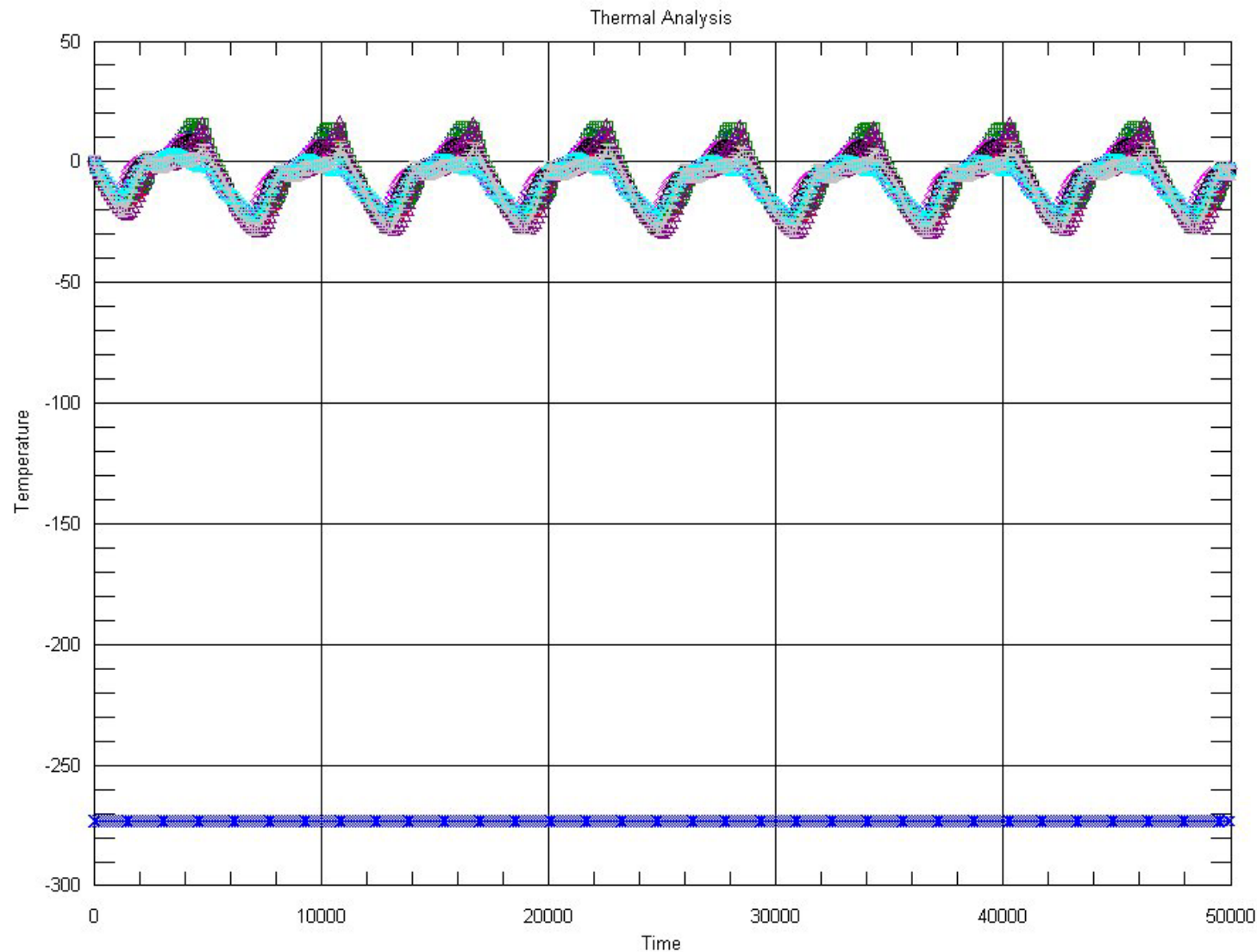


## SINDAPLOTS

## 3. OSR Coating

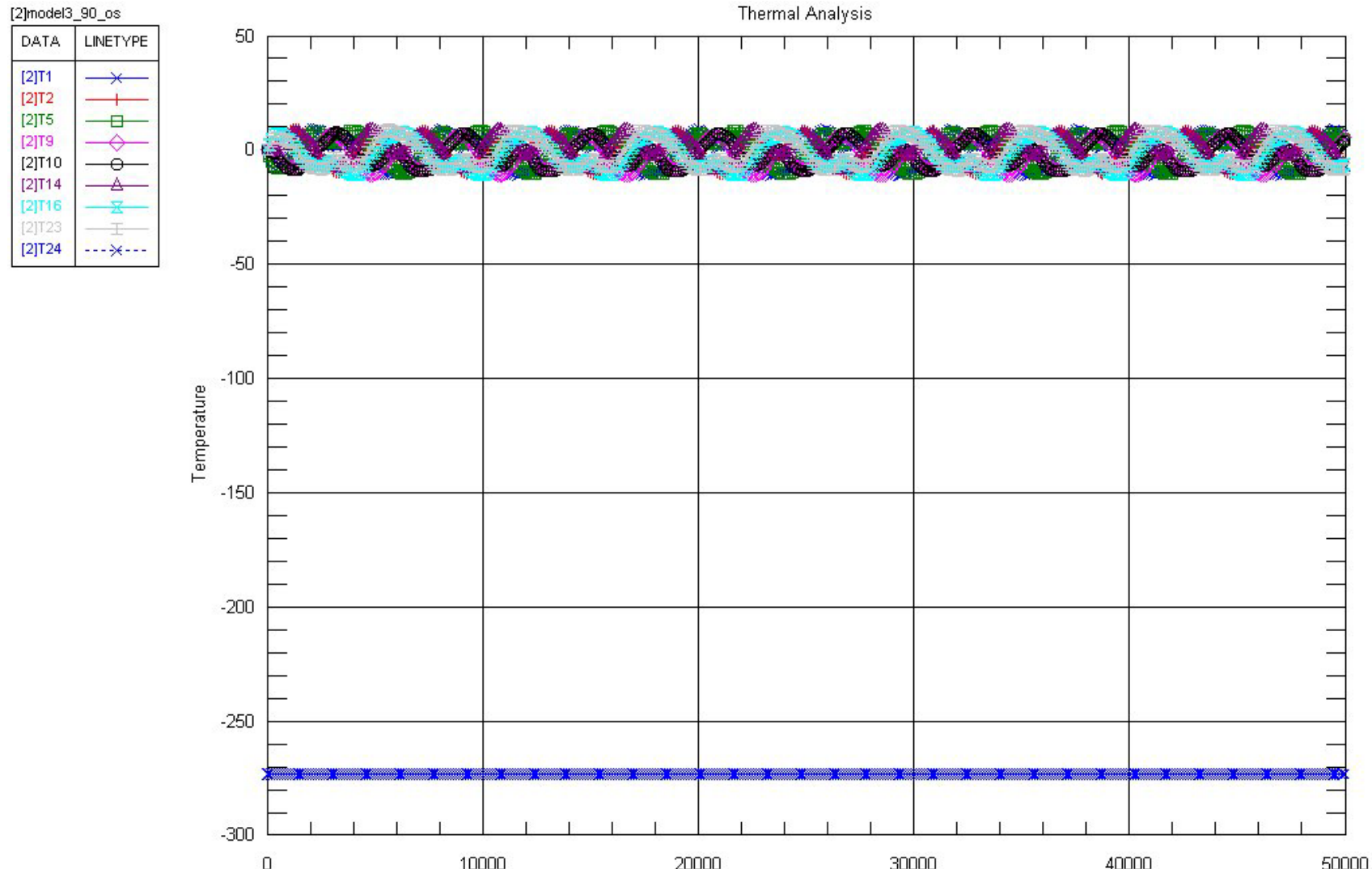
## 0 Degree Beta Angle

[1]model3_0_osr	
DATA	LINETYPE
[1]T1	—x—
[1]T2	—+—
[1]T5	—□—
[1]T9	—◇—
[1]T10	—○—
[1]T14	—△—
[1]T16	—×—
[1]T23	—█—
[1]T24	---*---



## 4. OSR Coating

## 90 Degree Beta Angle



## E Selected Materials Thermo-Optical Properties

The following lists the optical properties of common spacecraft materials and coatings. Information was provided courtesy of K & K Associates [26]

a= solar absorbtivity

e= normal emmitance

ESH=equivalent Sun Hours

Coating thickness is usually critical

NAME	SOLAR	NORMAL	Ratio
			a/e
<b>BLACK COATINGS</b>			
Anodize Black	0.88	0.88	1.00
Carbon Black Paint NS-7	0.96	0.88	1.09
Catalac Black Paint	0.96	0.88	1.09
Chemglaze Black Paint Z306	0.96	0.91	1.05
Delrin Black Plastic	0.96	0.87	1.10
Ebanol C Black	0.97	0.73	1.33
Ebanol C Black-384 ESH* UV	0.97	0.75	1.29
GSFC Black Silicate MS-94	0.96	0.89	1.08
GSFC Black Paint 313-1	0.96	0.86	1.12
Hughson Black Paint H322	0.96	0.86	1.12
Hughson Black Paint L-300	0.95	0.84	1.13
Martin Black Paint N-150-1	0.94	0.94	1.00
Martin Black Velvet Paint	0.91	0.94	0.97
3M Black Velvet Paint	0.97	0.91	1.07
Paladin Black Lacquer	0.95	0.75	1.27
Parsons Black Paint	0.98	0.91	1.08
Polyethylene Black Plastic	0.93	0.92	1.01
Pyramil Black on Beryllium Copper	0.92	0.72	1.28
Tedlar Black Plastic	0.94	0.90	1.04
Velesat Black Plastic	0.96	0.85	1.13
<b>WHITE COATINGS</b>			
	a	e	a/e
Barium Sulphate with Polyvinyl Alcohol	0.06	0.88	0.07
Biphenyl-White Solid	0.23	0.86	0.27
Catalac White Paint	0.24	0.90	0.27
Dupont Lucite Acrylic Lacquer	0.35	0.90	0.39

Dow Corning White Paint DC-007	0.19	0.88	0.22
GSFC White Paint NS43-C	0.20	0.92	0.22
GSFC White Paint NS44-B	0.34	0.91	0.37
GSFC White Paint NS-74	0.17	0.92	0.18
GSFC White Paint NS-37	0.36	0.91	0.40
Hughson White Paint A-276	0.26	0.88	0.30
Hughson White Paint A-276+1036 ESH UV	0.44	0.88	0.50
Hughson White Paint V-200	0.26	0.89	0.29
Hughson White Paint Z-202	0.25	0.87	0.29
Hughson White Paint Z-202+1000 ESH UV	0.40	0.87	0.46
Hughson White Paint Z-255	0.25	0.89	0.28
Mautz White House Paint	0.30	0.90	0.33
3M-401 White Paint	0.25	0.91	0.27
Magnesium Oxide White Paint	0.09	0.90	0.10
Magnesium Oxide Aluminium Oxide Paint	0.09	0.92	0.10
Opal Glass	0.28	0.87	0.32
OSO-H White Paint 63W	0.27	0.83	0.33
P764-1A White Paint	0.23	0.92	0.25
Potassium Fluorotitanate White Paint	0.15	0.88	0.17
Sherwin Williams White Paint (A8W11)	0.28	0.87	0.32
Sherwin Williams White Paint (F8WJ2030)	0.39	0.82	0.48
Sherwin Williams F8W2030 w Polasol V6V241	0.36	0.87	0.41
Sperex White Paint	0.34	0.85	0.40
Tedlar White Plastic	0.39	0.87	0.45
Titanium Oxide White Paint with Methyl Silicone	0.20	0.90	0.22
Titanium Oxide White Paint with Potassium Silicate	0.17	0.92	0.18
Zerlauts S-13G White Paint	0.20	0.90	0.22
Zerlauts Z-93 White Paint	0.17	0.92	0.18
Zinc Orthotitanate with Potassium Silicate	0.13	0.92	0.14
Zinc Oxide with Sodium Silicate	0.15	0.92	0.16
Zirconium Oxide with 650 Glass Resin	0.23	0.88	0.26

CONDUCTIVE PAINT	a	e	a/e
<hr/>			
Brilliant Aluminum Paint	0.30	0.31	0.97
Epoxy Aluminum Paint	0.77	0.81	0.95
Finch Aluminum Paint 643-1-1	0.22	0.23	0.96
Leafing Aluminum in Epon 828	0.37	0.36	1.03
Leafing Aluminum (80-U)	0.29	0.32	0.91
NRL Leafing Aluminum Paint	0.24	0.24	1.00
NRL Leafing Aluminum Paint	0.28	0.29	0.97
Silicone Aluminum Paint	0.29	0.30	0.97

Dupont Silver Paint 4817	0.43	0.49	0.88
Chromeric Silver Paint 586	0.30	0.30	1.00
GSFC Yellow NS-43-G	0.38	0.90	0.42
GSFC Green NS-53-B	0.52	0.87	0.60
GSFC Green NS-43-E	0.57	0.89	0.64
GSFC White NS-43-C	0.20	0.92	0.22
GSFC Green NS-55-F	0.57	0.91	0.63
GSFC Green NS-79	0.57	0.91	0.63

**ANODIZED ALUMINUM SAMPLES****a****e****a/e**

Black	0.65	0.82	0.79
Black	0.86	0.86	1.00
Blue	0.67	0.87	0.77
Blue	0.53	0.82	0.65
Brown	0.73	0.86	0.85
Chromic	0.44	0.56	0.79
Clear	0.27	0.76	0.36
Clear	0.35	0.84	0.42
Green	0.66	0.88	0.75
Gold	0.48	0.82	0.59
Plain	0.26	0.04	6.50
Red	0.57	0.88	0.65
Sulphuric	0.42	0.87	0.48
Yellow	0.47	0.87	0.54
Blue Anodized Titaniuml Foil	0.70	0.13	5.38

**METALS AND  
CONVERSION COATINGS****a****e****a/e**

Alzac A-2	0.16	0.73	0.22
Alzac A-5	0.18	-	
Black Chrome	0.96	0.62	1.55
Black Copper	0.98	0.63	1.56
Black Iridite	0.62	0.17	3.65
Black Nickel	0.91	0.66	1.38
Buffed Aluminum	0.16	0.03	5.33
Buffed Copper	0.30	0.03	10.00
Constantan-Metal Strip	0.37	0.09	4.11
Copper Foil Tape			
Plain	0.32	0.02	16.00
Sanded	0.26	0.04	6.50
Tarnished	0.55	0.04	13.75
Dow 7 on Polished Magnesium	0.49	-	

Dow 7 on Sanded Magnesium	0.65	-	
Dow 9 on Magnesium	0.87	-	
Dow 23 on Magnesium	0.62	0.67	0.93
Ebanol C Black	0.97	0.77	1.26
Electroplated Gold	0.23	0.03	7.67
Electroless Nickel	0.39	0.07	5.57
Irridite Aluminum	-	0.11	
Inconel X Foil (1 mil)	0.52	0.10	5.20
Kannigen-Nickel Alloy	0.45	0.08	5.63
Plain Beryllium Copper	0.31	0.03	10.33
Platinum Foil	0.33	0.04	8.25
Stainless Steel			
Polished	0.42	0.11	3.82
Machined	0.47	0.14	3.36
Sandblasted	0.58	0.38	1.53
Machine Rolled	0.39	0.11	3.55
Boom-Polished	0.44	0.10	4.40
1-mil 304 Foil	0.40	0.05	8.00
Tantalum Foil	0.40	0.05	8.00
Tungsten Polished	0.44	0.03	14.67

VAPOR DEPOSITED COATINGS	a	e	a/e
<hr/>			
Aluminum	0.08	0.02	4.00
Aluminum on Fiberglass	0.15	0.07	2.14
Aluminum on Stainless Steel	0.08	0.02	4.00
Chromium	0.56	0.17	3.29
Chromiumlon 5-mil Kapton	0.57	0.24	2.38
Germanium	0.52	0.09	5.78
Gold	0.19	0.02	9.50
Iron Oxide	0.85	0.56	1.52
Molybdenum	0.56	0.21	2.67
Nickel	0.38	0.04	9.50
Rhodium	0.18	0.03	6.00
Sliver	0.04	0.02	2.00
Titanium	0.52	0.12	4.33
Tungsten	0.60	0.27	2.22

Spacecraft Solar Arrays	a	e	a/e
<hr/>			
AE	0.78	0.82	0.95
AMSAT	0.82	0.85	0.96
ATN Black	0.77	0.80	0.96
ATN Blue	0.86	0.85	1.01

ATSF	0.85	0.85	1.00
COMSAT	0.82	0.85	0.96
DE	0.77	0.81	0.95
ETS/GOES	0.82	0.80	1.02
GOES	0.91	0.81	1.12
GPS-Conductive Coating	0.81	0.80	1.01
HELIOS	0.80	0.82	0.98
IME-Conductive Coating	0.75	0.79	0.95
IMP-H	0.78	0.82	0.95
IMP-I	0.78	0.81	0.96
ISEE-Conductive Coating	0.91	0.79	1.15
IUE	0.86	0.84	1.02
OAO	0.85	0.81	1.05
PAC	0.77	0.81	0.95
SMS-B	0.81	0.80	1.01
Spanish INTASAT	0.86	0.86	1.00
SSS	0.79	0.82	0.96

MISC	a	e	a/e
<hr/>			
Aluminum Oxide (Al <sub>2</sub> O <sub>3</sub> ) - (12/4) on Buffed Alum			
Initial	0.13	0.23	0.57
2560 ESH UV + P+	0.13	0.23	0.57
Aluminum Oxide (Al <sub>2</sub> O <sub>3</sub> ) (12/4) on Fused Silica	0.12	0.24	0.50
Silver Beryllium Copper (AgBeCu)	0.19	0.03	6.33
Kapton Overcoating	0.31	0.57	0.54
Parylene C Overcoating	0.22	0.34	0.65
Teflon Overcoating	0.12	0.38	0.32
GSFC DArk Mirror Coating-SiO-Cr-Al	0.86	0.04	21.50
GSFC Composite SiO <sub>x</sub> -Al <sub>2</sub> O <sub>3</sub> -Ag	0.07	0.68	0.10
Helios Second Surface Mirror/Silver Backing			
Initial	0.07	0.79	0.09
24 Hours at 5 Suns	0.07	0.80	0.09
48 Hours at 11 Suns + P+	0.08	0.79	0.10
Inconel with Teflon Overcoating-1mil	0.55	0.46	1.20
Vespel Polyimide SP1	0.89	0.90	0.99
Aclar Film (Aluminum Backing)			
1 mil	0.12	0.45	0.27
2 mil	0.11	0.62	0.18
5 mil	0.11	0.73	0.15
Kapton Film (Aluminum Backing)			
0.08 mil	0.23	0.24	0.96
0.15 mil	0.25	0.34	0.74
0.25 mil	0.31	0.45	0.69
0.50 mil	0.34	0.55	0.62

1.0 mil	0.38	0.67	0.57
1.5 mil	0.40	0.71	0.56
2.0 mil	0.41	0.75	0.55
3.0 mil	0.45	0.82	0.55
5.0 mil	0.46	0.86	0.53
Kapton Film (Chromium-Silicon Oxide-Aluminum Backing (Green))			
1.0 mil	0.79	0.78	1.01
Kapton Film (Aluminum-Aluminum Oxide Overcoating)-1 mil			
Initial	0.12	0.20	0.60
1800 ESH UV	0.12	0.20	0.60
Kapton Film (Aluminum-Silicon Oxide Overcoating)-1 mil			
Initial	0.11	0.33	0.33
2400 ESH UV	0.22	0.33	0.67
Kapton Film (Silver-Aluminum Oxide Overcoating)-1 mil			
Initial	0.08	0.19	0.42
2400 ESH UV	0.08	0.21	0.38
Kapton Film (Aluminum-Silicon Oxide Overcoating)-0.5 mil			
Initial	0.12	0.18	0.67
4000 ESH UV	0.28	0.24	1.17
Kimfoil-Polycarbonate Film (Aluminum Backing)			
0.08 mil	0.19	0.23	0.83
0.20 mil	0.20	0.30	0.67
0.24 mil	0.17	0.28	0.61
Mylar Film			
Aluminum Backing			
0.15 mil	0.14	0.28	0.50
0.25 mil	0.15	0.34	0.44
3.0 mil	0.17	0.76	0.22
5.0 mil	0.19	0.77	0.25
Skylab Sail			
Initial	0.15	0.35	0.43
1900 ESH UV	0.19	0.36	0.53
Skylab Parasol Fabric (Orange)			
Initial	0.51	0.86	0.59
2400 ESH UV	0.65	0.86	0.76
Teflon (Gold Backing)			
0.5 mil	0.30	0.49	0.61
1.0 mil	0.26	0.58	0.45
Teflon Aluminum Backing			
2 mil	0.08	0.66	0.12
5 mil	0.13	0.81	0.16
10 mil	0.13	0.87	0.15
Gold Backing			
0.5 mil	0.24	0.43	0.56

1.0 mil	0.22	0.52	0.42
5.0 mil	0.22	0.81	0.27
10 mil	0.23	0.82	0.28
<b>Silver Backing</b>			
2 mil	0.08	0.68	0.12
5 mil	0.08	0.81	0.10
10 mil	0.09	0.88	0.10
<b>Tefzel (Gold Backing)</b>			
0.05 mil	0.29	0.47	0.62
1.0 mil	0.26	0.61	0.43

<b>Tapes</b>	<b>a</b>	<b>e</b>	<b>a/e</b>
<hr/>			
235-3M Black	0.95	0.90	1.06
425-3M Aluminum Foil	0.20	0.03	6.67
850-3M Mylar-Aluminum Backing	0.15	0.59	0.25
7361-Mystic Alummized Kapton	0.09	0.03	3.00
7452- Mystic Aluminum Foil	0.14	0.03	4.67
7800-Mystic Aluminum Foil	0.21	0.03	7.00
Y9360-3M Aluminized Mylar	0.19	0.03	6.33

## F BLUESat Material Properties

### Aluminium Alloy 7075 –T6

Physical Properties	Metric	Imperial	Comments
Density	2.81 g/cc	0.102 lb/in <sup>3</sup>	
Mechanical Properties			
Hardness, Brinell	150	150	500 kg load with 10 mm ball
Hardness, Knoop	191	191	Converted from Brinell Hardness Value
Hardness, Rockwell A	53.5	53.5	Converted from Brinell Hardness Value
Hardness, Rockwell B	87	87	Converted from Brinell Hardness Value
Hardness, Vickers	175	175	Converted from Brinell Hardness Value
Tensile Strength, Ultimate	570 MPa	82700 psi	
Tensile Strength, Yield	505 MPa	73200 psi	
Elongation at Break	11 %	11 %	In 5 cm; Sample 1.6 mm thick
Modulus of Elasticity	72 GPa	10400 ksi	Average of Tension and Compression. In Aluminum alloys, the compressive modulus is typically 2% greater than the tensile modulus
Poisson's Ratio	0.33	0.33	
Fatigue Strength	160 MPa	23200 psi	500,000,000 Cycles
Fracture Toughness	20 MPa-m <sup>1/2</sup>	18.2 ksi-in <sup>1/2</sup>	K(IC) in S-L direction.
Fracture Toughness	25 MPa-m <sup>1/2</sup>	22.8 ksi-in <sup>1/2</sup>	K(IC) for T-L orientation
Fracture Toughness	29 MPa-m <sup>1/2</sup>	26.4 ksi-in <sup>1/2</sup>	K(IC) in L-T direction
Machinability	70 %	70 %	0-100 Scale of Aluminum Alloys
Shear Modulus	26.9 GPa	3900 ksi	
Shear Strength	330 MPa	47900 psi	
Thermal Properties			
CTE, linear 20°C	23.6 $\mu\text{m}/\text{m}^{\circ}\text{C}$	13.1 $\mu\text{in}/\text{in}^{\circ}\text{F}$	20-100°C
CTE, linear 250°C	25.2 $\mu\text{m}/\text{m}^{\circ}\text{C}$	14 $\mu\text{in}/\text{in}^{\circ}\text{F}$	Average over the range 20-300°C
Heat Capacity	0.96 J/g-°C	0.229 BTU/lb-°F	
Thermal Conductivity	130 W/m-K	902 BTU-in/hr-ft <sup>2</sup> -°F	
Melting Point	477 °C	891 °F	Eutectic for nonhomogeneous material that has not been heat treated
Melting Point	532 °C	990 °F	For homogeneous wrought material
Solidus	532 °C	990 °F	For homogeneous wrought material
Liquidus	635 °C	1170 °F	

## Aluminium Alloy 6061 – T6

Physical Properties			
Density	2.7 g/cc	0.0975 lb/in <sup>3</sup>	
Mechanical Properties			
Hardness, Brinell	95	95	500 kg load with 10 mm ball
Hardness, Knoop	120	120	Converted from Brinell Hardness Value
Hardness, Rockwell A	40	40	Converted from Brinell Hardness Value
Hardness, Rockwell B	60	60	Converted from Brinell Hardness Value
Hardness, Vickers	107	107	Converted from Brinell Hardness Value
Tensile Strength, Ultimate	310 MPa	45000 psi	
Tensile Strength, Yield	275 MPa	39900 psi	
Elongation at Break	12 %	12 %	In 5 cm; Sample 1.6 mm thick
Modulus of Elasticity	69 GPa	10000 ksi	Average of Tension and Compression. In Aluminum alloys, the compressive modulus is typically 2% greater than the tensile modulus
Notched Tensile Strength	324 MPa	47000 psi	2.5 cm width x 0.16 cm thick side-notched specimen, Kt = 17.
Ultimate Bearing Strength	607 MPa	88000 psi	Edge distance/pin diameter = 2.0
Bearing Yield Strength	386 MPa	56000 psi	Edge distance/pin diameter = 2.0
Poisson's Ratio	0.33	0.33	Estimated from trends in similar Al alloys.
Fatigue Strength	95 MPa	13800 psi	500,000,000 Cycles
Fracture Toughness	29 MPa-m <sup>1/2</sup>	26.4 ksi-in <sup>1/2</sup>	K <sub>IC</sub> ; TL orientation.
Machinability	50 %	50 %	0-100 Scale of Aluminum Alloys
Shear Modulus	26 GPa	3770 ksi	Estimated from similar Al alloys.
Shear Strength	205 MPa	29700 psi	
Thermal Properties			
CTE, linear 20°C	23.6 $\mu\text{m}/\text{m-}^{\circ}\text{C}$	13.1 $\mu\text{in}/\text{in-}^{\circ}\text{F}$	20-100°C
CTE, linear 250°C	25.2 $\mu\text{m}/\text{m-}^{\circ}\text{C}$	14 $\mu\text{in}/\text{in-}^{\circ}\text{F}$	Estimated from trends in similar Al alloys. 20-300°C.
Heat Capacity	0.896 J/g- $^{\circ}\text{C}$	0.214 BTU/lb- $^{\circ}\text{F}$	
Thermal Conductivity	166.9 W/m-K	1160 BTU-in/hr-ft <sup>2</sup> - $^{\circ}\text{F}$	
Melting Point	582 - 652 °C	1080 - 1210 °F	
Solidus	582 °C	1080 °F	
Liquidus	652 °C	1210 °F	

## Aluminium Alloy 5052

Physical Properties			
Density	2.68 g/cc	0.0968 lb/in <sup>3</sup>	
Mechanical Properties			
Hardness, Brinell	77	77	500 kg load with 10 mm ball
Hardness, Knoop	100	100	Converted from Brinell Hardness Value
Hardness, Vickers	87	87	Converted from Brinell Hardness Value
Tensile Strength, Ultimate	290 MPa	42100 psi	
Tensile Strength, Yield	255 MPa	37000 psi	
Elongation at Break	7 %	7 %	In 5 cm; Sample 1.6 mm thick
Modulus of Elasticity	70 GPa	10200 ksi	Average of Tension and Compression. In Aluminum alloys, the compressive modulus is typically 2% greater than the tensile modulus
Ultimate Bearing Strength	538 MPa	78000 psi	Edge distance/pin diameter = 2.0
Bearing Yield Strength	386 MPa	56000 psi	Edge distance/pin diameter = 2.0
Poisson's Ratio	0.33	0.33	Estimated from trends in similar Al alloys.
Fatigue Strength	140 MPa	20300 psi	500,000,000 Cycles
Machinability	50 %	50 %	0-100 Scale of Aluminum Alloys
Shear Modulus	25.9 GPa	3760 ksi	Estimated from similar Al alloys.
Shear Strength	140 MPa	290300 psi	
Thermal Properties			
CTE, linear 20°C	23.8 $\mu\text{m}/\text{m-}^{\circ}\text{C}$	13.2 $\mu\text{in}/\text{in-}^{\circ}\text{F}$	20-100°C
CTE, linear 250°C	25.7 $\mu\text{m}/\text{m-}^{\circ}\text{C}$	14.3 $\mu\text{in}/\text{in-}^{\circ}\text{F}$	Estimated from trends in similar Al alloys. 20-300°C.
Heat Capacity	0.88 J/g-°C	0.21 BTU/lb-°F	
Thermal Conductivity	137 W/m-K	1120 BTU-in/hr-ft <sup>2</sup> -°F	
Melting Point	607 - 649 °C	1120 - 1200 °F	
Solidus	607 °C	1120 °F	
Liquidus	649 °C	1200 °F	

## Kapton K271 One-Sided Thermal Tape

<b>Physical Properties</b>			
Density	1.41 g/cc		
<b>Mechanical Properties</b>			
Tear Strength	2.8kN/m	16pli	Initial Tear Strength
<b>Thermal Properties</b>			
Heat Capacity	1.080 J/g- °C		
Thermal Conductivity	0.16 W/m- K	1160 BTU- in/hr-ft <sup>2</sup> -°F	

## Delrin Acetal homopolymer, unfilled, extruded

<b>Physical Properties</b>			
Density	1.41 g/cc	0.0509 lb/in <sup>3</sup>	ASTM D792
<b>Mechanical Properties</b>			
Tensile Strength, Ultimate	75.8 MPa	11000 psi	ASTM D638
Elongation at Break	30 %	30 %	ASTM D638
Poisson's Ratio	0.35	0.35	
Fatigue Strength	32 MPa	4641 psi	Flexural fatigue endurance limit, 50% RH
Shear Strength	66 MPa	9573 psi	ASTM D732
<b>Thermal Properties</b>			
CTE, linear 20°C	108 µm/m- °C		Linear 20°C
CTE, linear 100°C	149.4 µm/m- °C		Linear 100°C
Heat Capacity	1.4644 J/g- °C	0.35 BTU/lb- °F	
Thermal Conductivity	0.36 W/m-K	2.5 BTU- in/hr-ft <sup>2</sup> -°F	
Melting Point	175 °C	347 °F	

(Courtesy of Matweb [19])



### **Description**

HexWeb™ 5052 is a hexagonal cell honeycomb material used principally as a shear carrying core in light weight adhesively bonded sandwich structures.

The HexWeb™ 5052 aluminium alloy used is a fully hard H191 temper 2.5% magnesium alloy conforming to MIL-A-81596. Except where indicated, the 5052 foil is treated against corrosion using a chromate conversion coating process.

HexWeb™ 5052 is available in a wide range of cell sizes and densities allowing versatility in design of sandwich structures and other applications.

### **Key Features**

- High strength and stiffness to weight ratio.
- High fatigue resistance.
- Good vibration damping characteristics.
- Non-combustible.
- Good retention of properties at elevated temperatures.
- Can be machined to complex profiles.
- Exhibits uniform crushing characteristics.
- Compatible with a wide range of materials providing a good bonding surface for Redux® adhesives.

### **Typical Applications**

- Helicopter blades
- Aircraft engine structures and nacelles
- Aircraft doors and hatches
- Aircraft floor panels
- Racing car structures and aerofoils
- Energy absorbers





#### Typical Mechanical Properties

Honeycomb Designation	Stabilised Compression		Plate Shear				Maximum Thickness mm
	Strength (MPa)	Modulus (MPa)	Strength "L Direction" (MPa)	Modulus "L Direction" (MPa)	Strength "W Direction" (MPa)	Modulus "W Direction" (MPa)	
1.8-3/4-25	0.95	215	0.74	182	0.46	96	150
2.3-1/4-10	1.35	310	0.96	220	0.58	112	150
3.0-3/8-20	2.10	485	1.35	295	0.85	145	150
3.1-3/16-10	2.30	517	1.45	310	0.90	152	150
3.4-1/4-15	2.60	620	1.60	345	1.10	166	150
3.7-3/8-25	2.95	725	1.80	380	1.17	180	150
3.9-1/2-40	3.30	820	1.94	405	1.25	190	150
4.3-1/4-20	3.75	965	2.20	455	1.45	205	150
4.4-3/16-15	4.10	1000	2.25	470	1.48	210	150
4.5-1/8-10	4.20	1034	2.30	483	1.50	214	150
5.2-1/4-25	5.20	1310	2.80	565	1.80	245	150
5.4-3/8-40	5.35	1380	2.90	590	1.95	250	150
5.7-3/16-20	5.80	1520	3.15	620	2.05	265	150
6.9-3/16-25	8.00	1965	4.04	785	2.50	320	75
7.9-1/4-40	10.00	2345	4.80	896	2.90	364	75
8.1-1/8-20	11.00	2414	5.00	930	3.00	372	50

† See Typical dimensions and tolerances section opposite

#### Material Properties

##### Fire Properties

Classified as non-combustible when tested to IMO resolution A.472(XII).

##### Elevated Temperature Performance

HexWeb™ 5052 honeycomb employs a node bond adhesive which retains a high proportion of its strength at temperatures up to 200°C.

##### Machining

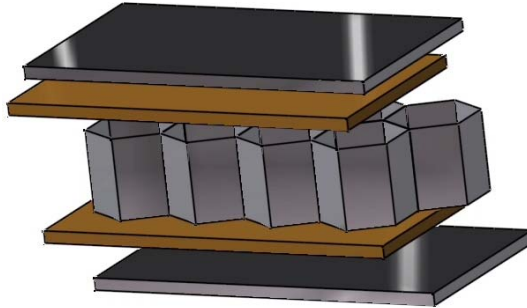
HexWeb™ 5052 honeycomb can be machined to form complex surfaces with the use of high speed routers. Some single curvature contours can be machined on to an un-expanded slice before expansion.

##### Bonding

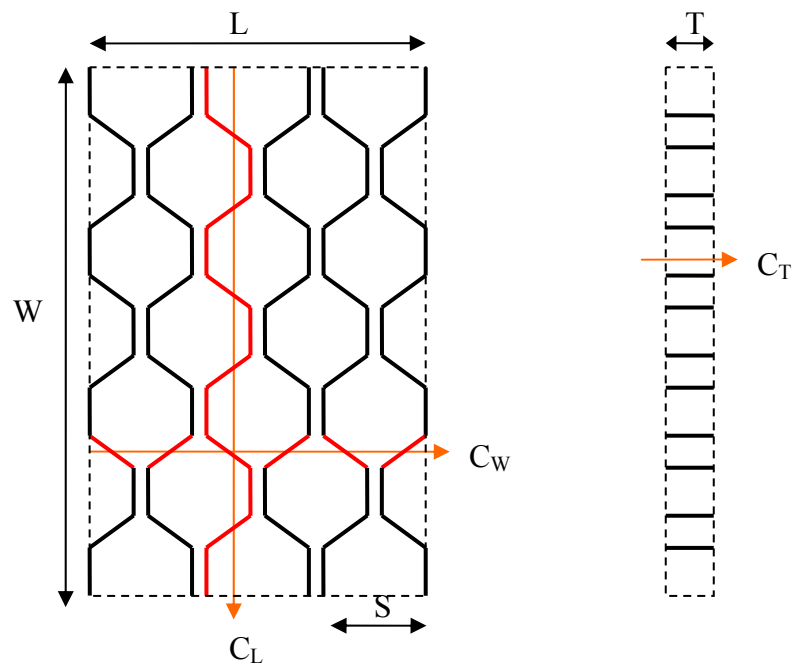
Non-volatile adhesives should be used for bonding skins to the honeycomb to prevent possible build up of volatiles during cure. This may be alleviated by using perforated honeycomb.



## G Calculation of Honeycomb Effective Conductivities



The aluminium honeycomb panels on BLUEsat exhibit 3D orthotropic thermal properties. Excluding the lateral conductivity of the skins, an aluminium honeycomb core will have directional conductance dependency. It is also proper to consider that a small percentage of heat transfer through a core will be radiation, but for this purpose, will be considered relatively negligible. Gilmore [3] describes the following method.



Calculation of the conductivities on the core have has been separated onto three components  $C_L$ ,  $C_W$  and  $C_T$ , where L, W and T represent the panel length, width and thickness respectively. To determine the global panel conductivity, each ribbons, conductivity is initially determined and then using cell geometries we calculate for the whole panel.

### L Direction Conductivity

Ribbons are positioned ‘up-down’ in the core and are glued together adjacently and stretched out to form the honeycomb pattern. The conduction through one ribbon is:

$$C_L = kA / x$$

k is the material thermal conductivity, in which case is 137 W/m K, A the cross-sectional area and x the total length of ribbon. Therefore applying geometrical relationships to get the total ribbon length gives the ribbon conductivity

$$C_L = \frac{k\delta T}{\sigma L}$$

Where  $\delta$ =film thickness

$$\begin{aligned} \sigma &= \text{extension factor of } 2/(1+\cos 60^\circ) \\ &= 4/3 \quad (60^\circ \text{ is the cell angle}) \end{aligned}$$

This is then formulated for the n (= Width / cell width S) number of ribbons that comprise of the width of the honeycomb panel which gives

$$CL = C_L \cdot n$$

$$= \frac{k\delta T}{\sigma L} \cdot \frac{2W}{S} \cdot L$$

Gives the conductance of the whole panel in the L direction. Therefore the equivalent honeycomb conductivity is

$$k_L = \frac{2k\delta}{\sigma S}$$

Solving for the following data on BLUESat's honeycomb panels gives:

$$k = 137 \text{ W / m K}$$

$$\delta = 0.0000508 \text{ m}$$

$$S = 0.00635 \text{ m}$$

$$k_L = 1.644 \text{ W / m K}$$

### W Direction Conductivity

Ignoring the glue effects of each joined ribbon the width conductivity is similarly:

$$C_W = kA / x$$

Where  $x$  = stretched path

$$= W / \sin \theta$$

$$A = \delta T$$

$$K = 137 \text{ W/m K}$$

Solving for m number of paths to get total conductance in the W direction:

$$m = L / (h + h \cos \theta) = \sigma L / 2h = \sigma L \sin \theta / S$$

gives

$$C_w = \frac{k \delta \sigma \sin^2 \theta}{S} \frac{LT}{W}$$

Therefore the equivalent honeycomb conductivity is:

$$k_w = \frac{k \delta \sigma \sin^2 \theta}{S}$$

Solving for the following data on BLUEsat's honeycomb panels gives:

$$k = 137 \text{ W / m K}$$

$$\delta = 0.0000508 \text{ m}$$

$$S = 0.00635 \text{ m}$$

$k_w = 1.096 \text{ W / m K}$

T Direction Conductivity

For one ribbon conduction through the core (transverse conductance) is:

$$C_T = k \frac{\sigma \delta L}{T}$$

For n number of ribbons in the length direction we get

$$n = 2W/S$$

And thus conductance in the t direction:

$$C_T = k \frac{\sigma \delta L}{T} \frac{2W}{S}$$

And honeycomb conductivity is:

$$k_T = \frac{2k\sigma\delta}{S}$$

Solving for the following data on BLUEsat's honeycomb panels gives:

$$k = 137 \text{ W / m K}$$

$$\delta = 0.0000508 \text{ m}$$

$$S = 0.00635 \text{ m}$$

$$k_T = 2.922 \text{ W /m K}$$